TAMPEREEN TEKNILLINEN YLIOPISTO
TAMPERE UNIVERSITY OF TECHNOLOGY

Seppo Turunen

Weak Signal Acquisition in Satellite Positioning

Julkaisu 906 • Publication 906

Tampere 2010

Tampereen teknillinen yliopisto. Julkaisu 906
Tampere University of Technology. Publication 906

Seppo Turunen

Weak Signal Acquisition in Satellite Positioning

Thesis for the degree of Doctor of Science in Technology to be presented with due permission for public examination and criticism in Tietotalo Building, Auditorium TB224, at Tampere University of Technology, on the 10th of September 2010, at 12 noon.

Tampereen teknillinen yliopisto - Tampere University of Technology
Tampere 2010

ISBN 978-952-15-2408-0 (printed)
ISBN 978-952-15-2425-7 (PDF)
ISSN 1459-2045

ABSTRACT

This thesis discusses the acquisition of Global Navigation Satellite System (GNSS) signals that are attenuated in propagation and proposes a receiver independent method of characterizing the acquisition performance of the signals. It then applies the proposed method to several GNSS signals with different assumptions about available acquisition assistance. Two receiver improvements are proposed, one to increase success rate in parallel acquisition and another to enhance sensitivity in serial acquisition. In the remaining part of the thesis, two techniques are presented for making satellite signals easier to acquire, one involving a novel family of ranging sequences and another involving a special symbol sequence for transmitting time information over a heavily attenuating propagation channel.

PREFACE

The work presented in this thesis has been carried out in connection with satellite positioning research in Nokia Corporation during the years 2004-2009.

My sincerest thanks are due to my supervisor, Professor *Jarmo Takala*, for his guidance, support, and valuable observations that have been of immeasurable benefit to me. I would also like to thank the reviewers of the publications and the reviewers of this thesis, Professor *Letizia Lo Presti* and Doctor *Thomas Pany* for their constructive feedback and helpful comments.

I would like to express my gratitude to Nokia Corporation for offering the environment and tools necessary for the research and to my colleagues for a pleasant working atmosphere. In particular, I would like to thank the members of the Tampere positioning team for innumerable stimulating discussions over the years. My warmest thanks also to my co-authors, Professor *David Akopian*, Professor *Qin Zhengdi*, and Doctor *Phani Sagiraju*.

Finally, I would like to thank my wife *Kaisa* for her support and understading.

Tampere, June 2010

Seppo Turunen

TABLE OF CONTENTS

LIST OF PUBLICATIONS

This thesis is based on the following publications. In the text, these publications are referred to as [P1], [P2],. . . , and [P9].

[P1] S. Turunen, "Acquisition of satellite navigation signals with dynamically chosen measurements." *IET Radar, Sonar & Navigation*, vol. 4, no. 1, pp. 49–61, Feb. 2010.

[P2] D. Akopian, P.K. Sagiraju and S. Turunen, "Performance of two-stage massive correlator architecture for fast acquisition of GPS signals," in *Proc. 2006 IEEE Region 5 Technical, Professional and Student Technical Conference*, San Antonio, TX, USA, Apr. 7–9 2006, 4 p.

[P3] S. Turunen, "Combinatorial loss in satellite acquisition," in *Proc. ION GNSS 18th International Technical Meeting of the Satellite Division*, Long Beach, CA, USA, Sept. 13–16 2005, pp. 890–895.

[P4] S. Turunen, "Network assistance - what will new GNSS signals bring to it?" *Inside GNSS*, vol. 2, no. 3, pp. 35–41, Spring 2007.

[P5] S. Turunen, "Acquisition performance of assisted and unassisted GNSS receivers with new satellite signals," in *Proc. ION GNSS 20th International Technical Meeting of the Satellite Division*, Fort Worth, TX, USA, Sept. 25–28 2007, pp. 211–218.

[P6] S. Turunen, "Acquisition sensitivity limits of new civil GNSS signals," *Coordinates*, vol. 3, no. 1, pp. 14–19, Jan. 2007.

[P7] Q. Zhengdi and S. Turunen, "Nearly orthogonal codes in GNSS using unequal code lenghts," in *Proc. ION 60th Annual Meeting*, Dayton, OH, USA, June 7–9 2004, pp. 666–670.

[P8] S. Turunen and Q. Zhengdi, "Shift register generated pilot codes with good cross-correlation properties," in *Proc. 2004 International Symposium on GNSS/GPS*, Sydney, Australia, Dec. 6–8 2004, Article ID 22, 8 p.

[P9] S. Turunen, "A robust time labeling mechanism for GNSS data frames," in *Proc. European Navigation Conference GNSS 2005*, Munich, Germany, July 19–22 2005, Session: Software and Algorithms 1, 5 p.

LIST OF FIGURES

LIST OF TABLES

LIST OF ABBREVIATIONS

A-GNSS	Assisted GNSS
AWGN	Additive White Gaussian Noise
BOC	Binary Offset Carrier
bps	Bits per Second
BPSK	Binary Phase-Shift Keying
C/A	Coarse Access
cdf	Cumulative Distribution Function
CDMA	Code Division Multiple Access
dB	Decibel
DC	Direct Current
DS-SS	Direct-Sequence Spread Spectrum
EVT	Extreme Value Theory
FEC	Forward Error Correction
FFT	Fast Fourier Transform
FSS	Finite Sample Size

GMLC	Gateway Mobile Location Centre
GLONASS	GLObal'naya NAvigatsionnaya Sputnikovaya Sistema
GNSS	Global Navigation Satellite System
GPS	Global Positioning System
HP	High Precision
IGSO	Inclined Geosynchronous Satellite Orbit
I/NAV	Integrity Navigation Message
IP	Internet Protocol
IRNSS	Indian Regional Navigational Satellite System
L1C	L1 Civil Signal
L2C	L2 Civil Signal
LEO	Low Earth Orbit
LOS	Line-of-Sight
m-sequence	Maximum Length Sequence
MCB	Massive Correlator Bank
MEO	Medium Earth Orbit
MLC	Mobile Location Center
MSPRT	Multi-Hypothesis Sequential Probability Ratio Test
NP-hard	Nondeterministic Polynomial Time Hard
NRZ	Non-Return-to-Zero

pdf	Probability Density Function
POMDP	Partially Ordered Markov Decision Problem
QZSS	Quasi-Zenith Satellite System
RF	Radio Frequency
ROC	Receiver Operating Characteristic
RTCM	The Radio Technical Commission For Maritime Services
SBAS	Satellite Based Augmentation System
SCB	Supplementary Correlator Bank
SET	SUPL Enabled Mobile Terminal
SLP	SUPL Location Platform
SNR	Signal to Noise Ratio
SP	Standard Precision
SPRT	Sequential Probability Ratio Test
SUPL	Secure User Plane Location
TCP	Transmission Control Protocol
TDM	Time-Division Multiplex
TDMA	Time-Division Multiple Access
TOT	Time of Transmission
TOW	Time of Week
WCDMA	Wide-Band CDMA
WWRN	World-Wide Reference Network

LIST OF SYMBOLS

B	Frequency uncertainty range
c_i	A sequence of elements
c_i^n, $c_n\left(i\right)$	Element i of sequence n
$C\left(t\right)$	Ranging code modulation
C/N_0	Signal power to single-sided noise power spectral density ratio
d_i^n	Fourier series coefficient i of satellite signal n
$D\left(t\right)$	Data modulation
E	Squared signal amplitude at integrator output
E_b	Bit energy
$E_{\boldsymbol{\gamma}}\left(\cdot\right)$	Expectation conditioned on policy $\boldsymbol{\gamma}$
$f\left(\cdot\right)$	pdf of measurement distribution in the absence of object
f_0	Carrier frequency
f_k	Doppler shift of satellite signal k
F_N	Noise factor, the power ratio corresponding to noise figure

$F_n(\cdot)$	cdf of the maximum of n noise cells
$g_k(t)$	Satellite signal k at receiver base-band input
$g(\cdot)$	pdf of measurement distribution in the presence of object
$\boldsymbol{\gamma}$	Search policy, $\boldsymbol{\gamma} = \{\gamma_k \mid k = 0, \ldots, K-1\}$,
γ_k	Rule in a search policy, $\gamma_k : \boldsymbol{\pi}(k) \rightarrow \{1, \ldots, N\}$
$h(t)$	Base-band pulse waveform
H_0	Hypothesis 0: object not present in search space
$H_j,\ j \neq 0$	Hypothesis j: object present in location j
$H(k)$	Shannon entropy of vector $\boldsymbol{\pi}(k)$
$H(\cdot)$	Fourier transform of $h(\cdot)$
I_i	i:th coherent integration result of in-phase signal
$\mathrm{I}_k(\cdot)$	Modified Bessel function of the first kind of order k
$\lambda_n(y_1, \ldots, y_n)$	Likelihood ratio based on samples $y_1, \ldots, y_n$
L, L_k	Sequence length
m	Number of coherent integrations
$n(t)$	Noise amplitude
n, N_u	Size of uncertainty region
N_c	Number of delay search options
N_f	Number of frequency search options
ν_i	Period length of sequence i

ν	Product of period lengths
N	Number of ranging sequences
N_0	Single-sided noise power spectral density
ω_0	Carrier radian frequency
$\Delta\omega$	Carrier radian frequency offset
$\hat{\omega}$	Carrier radian frequency hypothesis
$p_0(\cdot)$	pdf of an observation under H_0
$p_1(\cdot)$	pdf of an observation under H_1
ϕ_0	Carrier phase
$\mathrm{P}(\cdot,\cdot)$	Lower regularized (incomplete) gamma function
P_{fa}	Single cell false alarm probability
P_{FA}^{a}	System false alarm probability in the absence of signal
P_d	Single cell detection probability
P_D	System detection probability
π_0	Prior probability of H_0
π_j	Prior probability of H_j
$\pi_j(k)$	Probability of finding an object in cell j prior to k:th measurement
$\pi_{i(k)}$	Probability of finding an object in cell $i(k)$ visited at step k
$\pi_j(y_1,\ldots,y_n)$	Posterior probability of H_j based on samples $y_1,\ldots,y_n$

$\boldsymbol{\pi}(k)$	Vector of probabilities $\pi_i(k), i = 0, \ldots, N$
q	Detection threshold
Q_i	i:th coherent integration result of quadrature phase signal
$r(t)$	Signal at receiver input
$R_{m,n}$	Normalized even periodic cross-correlation function of sequences m and n
σ^2	Noise variance at integrator output
τ_d	Dwell time
θ_{max}	Maximum pairwise correlation of a set of sequences
$\theta^e_{m,n}(\cdot)$	Even periodic correlation function of sequences m and n
$\theta^o_{m,n}(\cdot)$	Odd periodic correlation function of sequences m and n
$\hat{t}$	Delay hypothesis
T	Signal observation time
T_c	Chip duration
T_{acq}	Acquisition time
U	Signal power at receiver input
$\mathbb{Z}$	Set of integer Numbers

1. INTRODUCTION

Personal navigation devices and location based services have gained considerable popularity among consumers during the past few years. This has led to a situation where the production volumes of global navigation satellite system (GNSS) [71] receivers are dominated by portable battery-powered units [19, 149]. In most cases, the GNSS receiver is combined with a mobile telephone and used to enable various local and networked applications, such as route finding and emergency call positioning. There is, therefore, a great demand for GNSS receivers that fulfill the strict power conservation requirements of battery-powered electronics and work in built environments where, unfortunately, satellite signal reception can be very unreliable. The receivers also have to meet regulatory performance requirements due to their role in emergency call positioning. The requirements are particularly concerned with signal acquisition, because reliable and fast acquisition is vital in an emergency situation. Experience has shown that good acquisition performance is an essential quality factor also in other location based services.

As an initial step of its operation, a GNSS receiver performs signal acquisition. Satellite signals are direct-sequence spread spectrum (DS-SS) signals with a wide Doppler frequency range and their acquisition therefore involves a two-dimensional search. The task is computationally intensive and creates a processing load that significantly exceeds the load from steady-state receiver operation, which mainly involves tracking of signals with relatively slowly changing parameters. Acquisition algorithms are sensitive to signal quality and typically require

a stronger signal than the algorithms used for the steady-state operation. For this reason, acquisition constitutes a primary performance bottleneck in portable consumer receivers that are frequently used in areas where signal propagation is obstructed.

The past few years have seen a flurry of research activity related to GNSS system design as existing American and Russian systems are being modernized and new satellite fleets are being planned by the European Union, India, China, and Japan. One of the main goals of signal design has been to improve resistance against interference from external sources and from other navigation satellites. The latter type of interference is potentially going to be more troublesome due to plans to share frequency bands between satellite fleets. Interference from other satellites is particularly harmful during acquisition because it easily misleads the receiver to lock onto a false signal. To address the problem, designers have adopted longer spreading sequences, but this approach is not without side-effects since it makes the acquisition uncertainty region larger and thus harder to search. Unfortunately, informed discussion about this serious side-effect has been more or less missing, presumably for two reasons. Firstly, there has been a lack of fresh ideas for sequence design and secondly, there has been a lack of commonly accepted methodology for assessing the impact of sequence design on acquisition performance.

The sequence design problem is challenging due to large Doppler shifts that require the sequences to have low cross-correlation both in time and frequency domains. Unfortunately, no systematic approaches for combating frequency domain cross-correlation have been suggested by this time. Designers have therefore resorted to long sequences from families that are known to have good correlation properties in the absence of Doppler shift. The sequences have exhibited acceptable correlation properties also when a Doppler shift is present, but this is probably due to statistical reasons attributable to sequence length rather than due to design.

A pervasive theme in recent signal design is the use of pilot signals to improve the stability of time and position estimates. The pilot signals lack data modulation and can therefore be tracked with narrowband phase or frequency locked loops, which reduces noise in the estimates. The signals have long spreading codes and they are therefore not particularly useful for acquisition, which is also generally understood. However, the advent of assisted GNSS (A-GNSS) [95, 139, 147] makes direct acquisition of pilot signals a realistic option. The stable time estimate obtained from an acquired pilot signal can then be utilized to retrieve frame timing under conditions where noise prevents direct timing retrieval from the data signal.

Integration of GNSS receivers with mobile telephones in the early 1990's led to the introduction of A-GNSS, a technique where the cellular network provides satellite information that would be difficult or time-consuming for the GNSS receiver to obtain directly from the satellites. Currently, A-GNSS information is standardized and widely available, even though its composition varies depending on the network. The main benefit of A-GNSS is that receivers can operate well below nominal satellite signal levels. This is possible because the receivers do not have to detect data bits and because the acquisition uncertainty range is greatly reduced by the assistance information. While the benefit of having a separate access to ephemeris and clocks is trivially understood, the benefit of the reduced uncertainty range is more difficult to quantify in terms of observable performance improvement and has not been thoroughly analyzed in the literature.

It is often difficult to provide a receiver with an accurate time reference in an A-GNSS system due to unknown delays in the assistance chain. A cellular network, for example, may not be able to provide chip timing or even frame timing. Some means of retrieving frame timing, or frame sequence identifiers, would be useful in circumstances where satellite signals are too weak for the detection of data bits but still sufficiently strong for the detection of sequence timing. The frame sequence identifiers together with satellite orbit information obtained from the

assistance network would then allow the receiver to solve navigation equations and to start tracking satellites normally, relying on the assistance network only for infrequent orbit information updates.

Power conservation has become one of the foremost design challenges for mobile devices as the number of features and subsystems continues to rise. To some extent, reduction of semiconductor feature sizes has lowered the power consumption of digital logic and, to a lesser extent, that of radio frequency electronics. In parallel with this development, GNSS receivers have been equipped with massively parallel acquisition accelerators, largely negating the savings. The situation cannot be expected to become any easier in future when multi-constellation receivers are introduced and wider bandwidths, higher front-end linearity, and more parallel processing are required. It is therefore of vital importance to have efficient receiver algorithms available, especially during acquisition when the digital and RF sections typically need to work at full power.

In early receivers, acquisition was performed by tracking correlators that operated in sequential search mode. This was time consuming and, when satellite signals were weak, even prohibitively so. Towards the end of the 1990's parallel correlator banks became available in consumer receivers and made their use practical in built environments by dramatically accelerating the acquisition process. However, a correlator bank consumes a substantial amount of power and its time of usage in a portable unit must therefore be minimized. The normal practice is to pre-empt its operation before the required level of certainty is reached and to verify the preliminary acquisition result so obtained with a tracking correlator. The downside of this procedure is that a negative verification result leads to a complete restart and a long delay.

In addition to verification of acquisition results, tracking correlators are also used independently for acquisition when the initial uncertainty area is narrow, as is the case in reacquisition and assisted acquisition. The reason for such usage could be power conservation or unavailability of a parallel correlator bank. The tracking

correlators would then be used to perform a fixed order sequential search, typically starting from locations of high prior success probability. Several ad-hoc ways of organizing the search have been proposed, but little is known about their optimality.

1.1 Scope and Objective of Research

The scope of this thesis is the signal acquisition process of weak open access GNSS signals in consumer receivers in the presence and in the absence of external assistance. Existing GPS and GLONASS signals, modernized GPS signals, and Galileo signals are explicitly discussed. Receiver operation is discussed on algorithmic level only; implementation details and imperfections are omitted. A simple path loss model is assumed for signal propagation and effects of multipath propagation are not discussed.

The objective of this thesis is to identify and analyze factors that impede weak signal acquisition in GNSS systems and to make improvements that accelerate the acquisition process and allow receivers to acquire signals that are attenuated by obstacles in natural and built environments. The analysis and the improvements pertain to receiver operation and to the ranging sequences and frame structures of satellite broadcast signals.

1.2 Main Contributions

This research is concerned with weak signal acquisition in stand-alone and assisted GNSS receivers and it divides into three main parts: evaluation of satellite signals for their acquisition properties, improvements to satellite signals and improvements to receiver operation. Its main contributions can be summed up as follows:

- Showing that acquisition sensitivity is related to the dimension of uncertainty region in a manner that is independent of receiver architecture. Deriving analytic expressions for this relationship and showing that the expressions have a simple asymptotic approximation that is consistent with a known result from extreme value theory.

- Based on the expressions referred to above, proposing metrics and criteria for the evaluation and comparison of acquisition properties of existing and planned GNSS signals. Providing evaluation results for GNSS signals under different assistance assumptions.

- Proposing a design methodology for satellite ranging sequences to obtain short sequences with good cross-correlation properties in channels with high Doppler frequency shifts.

- Proposing a modification to GNSS frame structures to allow retrieval of absolute frame timing from weak satellite signals.

- Proposing a modification to receiver operation to improve acquisition success rate in receivers that use parallel correlator banks and a separate verification stage.

- Proposing a novel sequential acquisition algorithm to improve acquisition sensitivity and to expedite acquisition.

1.3 Author's Contribution

The author has acted as the sole author of publications [P1], [P3], [P4], [P5], [P6], and [P9], and as the first author of publication [P8].

The author has contributed to publication [P7] by providing derivations for the satellite signal cross-correlation function and for the lower limit of cross-correlation

magnitude. In addition, he has shown that flatness of signal spectrum is a necessary and sufficient condition for reaching the limit.

The author's contribution to publication [P8] has been to propose the idea of using a single high-order primitive generator polynomial for a full set of sequences and to write the software for the numerical example.

The author's contribution to publication [P2] has been to participate in the concept development.

1.4 Thesis Outline

To start with, navigation satellite systems and their operating principles are reviewed in chapter 2. Chapter 3 provides an overview of satellite signal acquisition techniques and presents the new sequential acquisition strategy and the proposed receiver modification for improved success rate in parallel acquisition. Some background of search theory is introduced as required in the discussion of sequential acquisition. In chapter 4, an overview of present and planned satellite signals is first provided with emphasis on ranging sequences. The proposed measure for signal acquisition performance, referred to here as the attenuation margin, is then presented followed by an argumentation of its validity. In chapter 5, the new family of ranging sequences is introduced and an algorithm for practical construction of signal sets presented. Chapter 6 starts with an overview of time transfer and receiver synchronization techniques in satellite positioning and then proceeds to introduce the new time transfer mechanism. Chapter 7 concludes the thesis.

2. SATELLITE POSITIONING

The term Global Navigation Satellite System (GNSS) [71, 160] refers to a totality of satellites and their supporting ground infrastructures that collectively, with or without mutual coordination, provide a radio positioning service with global coverage. The only fully operational member of the GNSS is the United States Navstar global positioning system (GPS) that currently has 30 operational satellites. Other global members are the Russian GLONASS that is being replenished to full operational capability and the European Galileo that is in its early deployment phase. Additionally, there is a plan to extend the coverage area of Chinese regional BeiDou / Compass navigation test system to global as shown in Table 1. The Indian regional satellite system (IRNSS), the Japanese Quasi-Zenith satellite system (QZSS), and the so called satellite-based augmentation systems (SBAS) have regional coverage.

2.1 Operating Principles

The GNSS uses radio signal propagation delays to determine receiver position. Its operating principle is to transmit accurately timed signals from the satellites, to measure the arrival times of the signals at a receiver, to inform the receiver about the trajectories of the satellites in a navigation message modulated on the signals, and to solve a set of geometric equations for the coordinates of the receiver. As a fourth unknown, system time is resolved. To measure the arrival times, the receiver observes the phase and/or frequency of the RF carrier and the

timing of a modulating sequence. The modulating sequence, referred to as the ranging sequence, renders the transmitted signal into a carrier-synchronous DS-SS signal. The sequence also serves the purpose of multiplexing several satellite signals onto a single frequency band. GLONASS is an exception in that it applies frequency division multiplexing for signal isolation and uses a ranging sequence only for timing. Present GNSS ranging sequences are based on algebraic or computer generated binary pseudorandom codes consisting of 511 (GLONASS) to 36,828,000 (GPS L1C) chips.

The GNSS offers a multitude of services with different performance characteristics and usage restrictions. Each service is provided either using a single type of signal or using multiple types of signals in a redundant manner. In the latter case, the redundant signals are transmitted in different frequency bands. Some of the bands are dedicated to one GNSS member system while others are shared between several member systems. A single member system may transmit multiple signals on a single frequency band, relying on code division multiplexing for separation. Ideally, each satellite would be transmitting the complete set of signals provided by its member system, but this is not necessarily the case with new signals that are incompatible with existing satellites. The present and planned globally available GNSS signals and their frequency bands are listed in Table 2 [64,72,74]. The signals are classified as open if they are freely accessible or as restricted if their access is limited to a closed user group.

Fig. 1 shows schematically how a GNSS signal is generated in a satellite. The signal consists of a data component and an optional pilot component. The data component carries a so called navigation message, a serialized collection of parameters with information about satellite trajectories, satellite availability, satellite clock errors, and signal propagation in the atmosphere. The navigation message undergoes an optional error correction coding, after which its symbols are BPSK modulated onto a binary ranging sequence. The resulting spread-spectrum signal is optionally further modulated onto one or two binary or quaternary signals, referred to as subcarriers. The pilot component consists of a different rang-

Table 1. *Current and future GNSS satellite systems [45]*

	GPS	GLONASS	Galileo	Compass
	USA	Russia	EU	China
Operational satellites (as of June 2010)	29 MEO	23 MEO	1 MEO	1 MEO, 4 GEO
Nominal constellation	24 MEO	24 MEO	30 MEO	27 MEO, 5 GEO, 3 IGSO
Full operation capability	1995-	2011	2016-2018	2010-2015

Table 2. *Current and future GNSS signals*

Band	Frequency	GPS		GLONASS		Galileo	
	MHz	Open	Restricted	Open	Restricted	Open	Restricted
E1	1559-1591					L1F	L1P
G1	1593-1610			SP	HP		
L1	1563-1587	C/A, L1C	P/Y, M				
G2	1240-1256			SP	HP		
L2	1216-1240	L2C	P/Y, M				
E5A	1164-1188					E5a	
E5B	1188-1215					E5b	
L5	1164-1188	L5					
E6	1260-1300						E6C, E6P

ing sequence that is optionally modulated onto one or two subcarriers. After the modulations, the data and pilot components are combined into a real or complex baseband signal that is finally modulated onto a radio frequency carrier and transmitted. In some cases, the combining simply means interpreting the components as the real and imaginary parts of the complex baseband signal, while in other cases it means multiplication with a time-invariant or time-variant weighing matrix, or even a combination of linear and non-linear operations [55]. The subcarrier modulation, referred to as binary offset carrier (BOC) modulation [23], is used as a form of pulse shaping to improve receiver tracking accuracy or as a form of spectral shaping to reduce crosstalk with signals of other GNSS member systems.

Fig. 2 shows the block diagram of a generic GNSS receiver. The incoming antenna signal is amplified and band-pass filtered in an RF front-end and demodulated in a mixer into a complex baseband signal. The baseband signal, dominated by thermal noise at this stage, is sampled at a rate a few times higher than the chip rate of the signal and converted to digital form in an analog-to-digital converter. The digitized samples are passed to a parallel acquisition unit and to tracking correlators. The sample stream going into the acquisition unit is usually decimated to keep the complexity of the often massively parallel unit at a reasonable level. The acquisition unit detects a satellite signal and provides a coarse estimate of its carrier frequency and timing to the tracking correlators. A set of correlators is then connected to form a feedback loop that starts tracking the signal, yielding refined estimates of sequence timing, carrier frequency and carrier phase. The navigation message is also decoded by the feedback loop and provided along with the estimates to the navigation processor. The acquisition unit continues its operation until a sufficient number of satellite signals is detected to make a set of navigation equations determined, thereby allowing the navigation processor to estimate the position, time and velocity of the receiver. If required, additional satellite signals can be searched by using the acquisition unit or by substituting the previously obtained time and position estimates into

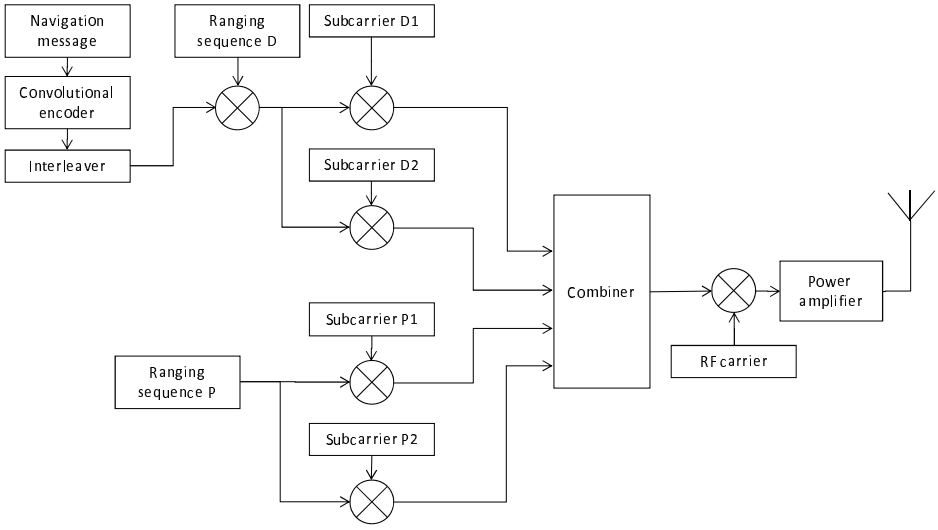

Fig. 1. *GNSS signal generator.*

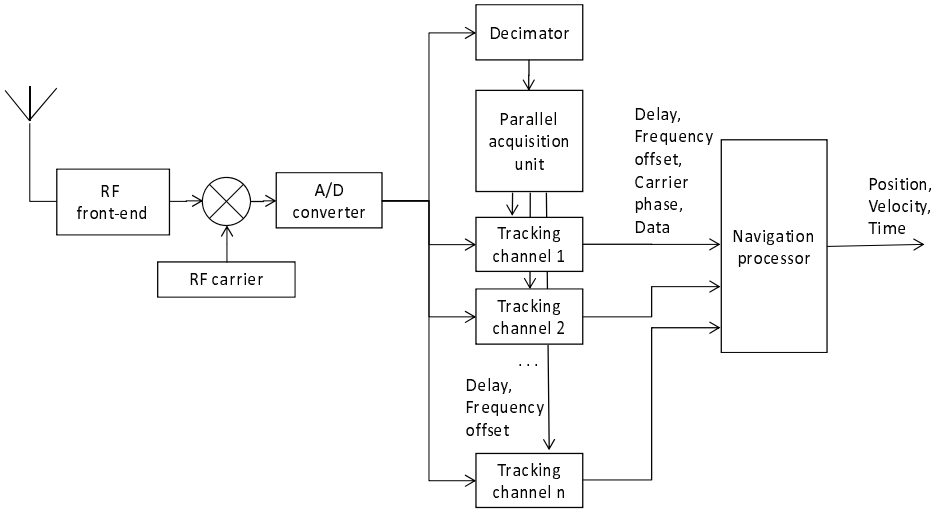

Fig. 2. *GNSS receiver.*

further navigation equations.

2.2 The GNSS Propagation Channel

A GNSS signal propagating from a satellite to a ground-based receiver experiences a Doppler frequency shift, a geometric path loss, an ionospheric dispersion, and a tropospheric refraction. The Doppler shift varies with satellite elevation and has a typical range of ± 6 kHz. The ionospheric and tropospheric effects cause variable group and phase delays equivalent to a path length deviation of up to a few tens of meters. The Doppler shift due to satellite movement and the atmospheric effects are well understood and accounted for in GNSS navigation messages and standard receiver algorithms [100].

Besides the line-of-sight (LOS) component, the receiver input signal may contain later arriving multipath components [69, 134]. Such reflected components are in principle useless for the basic GNSS operation because their propagation delays are unpredictable. A multipath component with an excess delay shorter than chip length distorts the correlation properties of the LOS component, potentially leading to an error in the position estimate. A multipath component with an excess delay longer than the chip length is uncorrelated with the LOS component but may be erroneously interpreted as such, leading to a crude error in the position estimate. Recently, a class of serial search acquisition strategies has been proposed that attempt to turn multipath propagation into benefit by making use of its statistical characteristics [136].

In indoor areas, satellite signals are obstructed by building materials that cause attenuation, diffraction, and reflections. In various measurements campaigns [61, 103, 145], signal attenuations ranging from 15 dB to 50 dB have been observed. Due to structural inhomogeneity, the attenuation of a building wall depends heavily on the direction of signal arrival, leading to a disparity in signal strength between satellites. There is some evidence that reflections from wall surfaces create standing wave patterns that change due to satellite movement, giving rise to fading phenomena similar to those known from mobile radio communications [127]. It would seem, however, that the LOS component mostly

dominates the multipath components that are more heavily attenuated [53, 154]. The delay spread of the indoor signal has been found to be small, in the order of 30 ns [80], which further supports the notion that the reflected components are heavily attenuated. Unfortunately, presently available characterizations of the satellite-to-indoor propagation channel are inconclusive due to difficulties in measuring the heavily attenuated signals. To circumvent the difficulties, sounder measurements have recently been used to characterize the channel [79, 99] and to confirm the applicability of a previously known channel model [125].

2.3 Assisted GNSS

Assisted GNSS [63, 95, 137, 138, 146, 147], originally proposed in [140], refers to a technique where explicit or implicit information about the timing, Doppler shifts, and navigation messages of satellite signals is provided from a terrestrial source to a GNSS receiver to expedite acquisition and to parametrize navigation equations. It has recently been proposed that also carrier phase information should be included in the assistance information [158] to enable real time kinematic positioning in the same sense as specified in the RTCM standard [118].

Should explicit and accurate information about the locally valid timing and Doppler shift of a satellite signal be available, a receiver could omit the acquisition step and start tracking the signal immediately. Such ideal assistance is difficult to provide, however, since assistance is location and time specific, and the receiver location and clock offset are usually unknown. Another option is to provide implicit assistance that allows the receiver to derive the satellite signal timing and Doppler shift internally. Implicit assistance typically consists of satellite trajectory information, a coarse location estimate, a more or less accurate reference time, and a reference frequency for oscillator calibration. Due to the uncertainties in receiver location and due to inaccuracies in implementation, neither type of assistance normally reduces the timing and frequency uncertainties sufficiently to allow a receiver to start tracking signals directly without an initial acquisition

step. In any case, however, at least the frequency uncertainty is significantly reduced.

Assistance for GPS L1 C/A receivers is included in standards that govern mobile telephony [1, 2] and location based mobile services [98]. The standard [98], which specifies the so-called secure user-plane location (SUPL) architecture, has provisions for Galileo, QZSS, GLONASS, and future GPS signals, and similar provisions may later be included also in the actual telephony standards [159]. Minimum performance requirements and test specifications for receivers are also standardized [111]. The standards recognize quality differences between networks, in particular regarding the accuracy of reference time.

Fig. 3 shows the assistance information flow in a cellular network using the SUPL architecture. A world wide reference network (WWRN) tracks the GPS satellite constellation and stores raw satellite data. The data is passed in periodical updates to an A-GPS server residing in a cellular network element, referred to as the mobile location center (MLC), where the data is formatted (steps 1 and 2). The formatted data is then provided to SUPL enabled mobile terminals (SETs) on a transaction basis (steps 3 through 9).

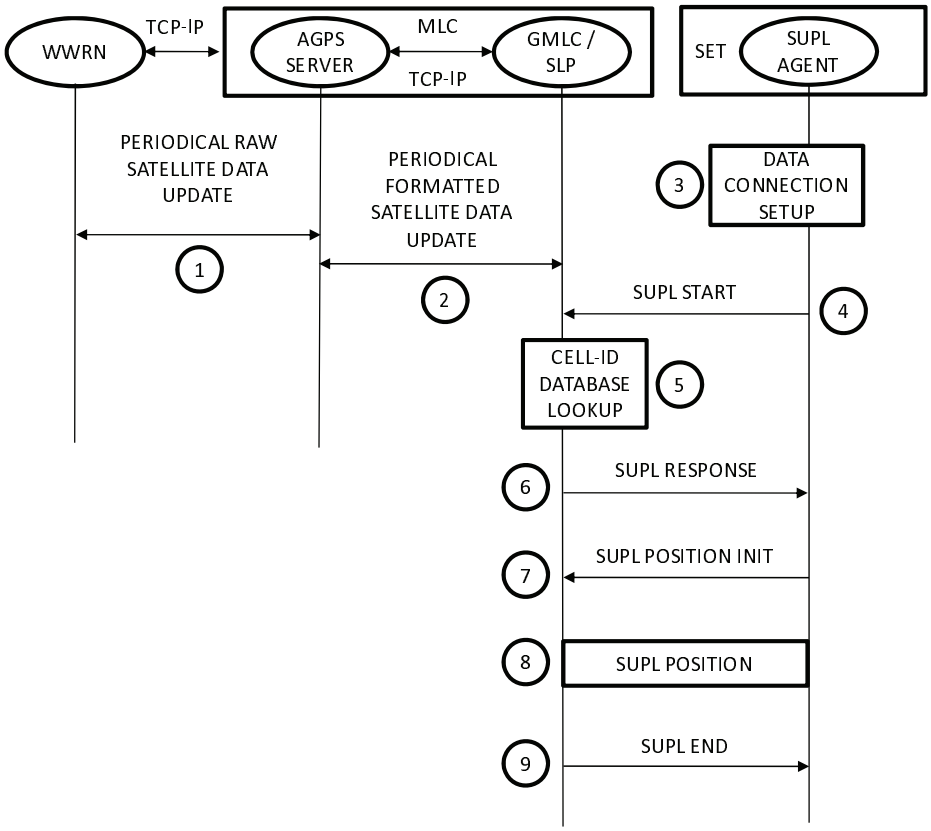

Fig. 3. *Assistance information flow in the SUPL architecture according to [63].*

3. SIGNAL ACQUISITION TECHNIQUES

This chapter discusses acquisition techniques and their performance metrics, reviews related work, and presents two original contributions. The acquisition problem is stated in section 3.1 and receiver performance metrics discussed in section 3.2. Related work is reviewed in two parts: section 3.3 deals with signal processing and section 3.4 with search and decision strategies. In section 3.5, a decision theoretic interpretation of serial search and sequential verification is presented. The interpretation has recently attained attention in the GNSS community and is also the basis of a novel sequential acquisition strategy that is introduced in section 3.6. In section 3.7, a new two-stage parallel acquisition strategy is presented. Section 3.8 concludes the discussion.

3.1 System Model and Problem Statement

Assuming that the propagation channel is free of multipath and fading disturbances and assuming that man-made interference can be ignored, a satellite signal at receiver input can be expressed as [100]

$$r(t) = \sqrt{2U}C(t-\Delta t)\,D(t-\Delta t)\cos\left(\left(\omega_0+\Delta\omega\right)t+\phi_0\right)+n(t), \qquad (1)$$

where U is the signal power, $C(\cdot)$ is the ranging sequence modulation, $D(\cdot)$ is the data modulation, Δt is a time delay including propagation delay, ω_0 is the

carrier radian frequency, $\Delta\omega$ is the radian frequency offset including Doppler frequency and oscillator bias, ϕ_0 is the carrier phase, and $n(t)$ is stationary AWGN with two-sided power spectral density $N_0/2$. A more accurate model would additionally include the effect of the relative radial movement between the satellite and the receiver on the perceived modulation rate of the signal, referred to as code Doppler or code-chip slipping [36].

The RF and base-band sections of a GNSS receiver are responsible for the synchronization of the receiver to the satellite signal and for the decoding of the navigation message. The synchronization consists of the estimation [85] of Δt, $\Delta\omega$, and eventually ϕ_0 and is further divided into acquisition and tracking. Acquisition discretizes the region of uncertainty in time and frequency into a finite number of cells, thus transforming the estimation problem into a detection problem [35, 84, 89]. Based on the coarse initial values of Δt and $\Delta\omega$ obtained from acquisition, the receiver refines and maintains their estimates by signal tracking.

3.2 Performance Metrics

A traditional measure for acquisition performance is the mean acquisition time. Unfortunately, it is not compatible with performance requirements that are given in terms of hard time limits, which is the case in mobile telephony [2], where such practice has been in force since the early 1990's, when it became mandatory to integrate GPS receivers into mobile phones for emergency call purposes. In the context of hard time limits, receiver performance specifications are stated in terms of probabilities of success and failure. The classical probabilities of detection and false alarm pertain to a dual hypothesis problem and need to be suitably generalized to make them applicable to signal acquisition that constitutes a multihypothesis problem. Of the possible generalizations [28, 105], referred to as system probabilities or global probabilities, the 'System false alarm probability in the absence of signal', P_{FA}^{a}, and 'System detection probability', P_D, as defined in [28] and discussed in more detail in section 4.1, would seem to be the

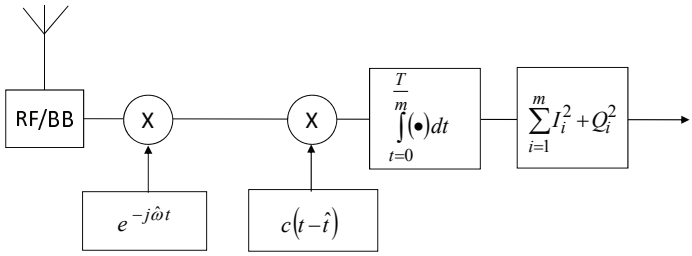

Fig. 4. *Model of cell processing.*

most widely used.

Two common diagramming conventions are to plot the detection probability against signal-to-noise ratio (SNR) at a fixed false alarm rate, obtaining what is called the power function curve [148], and to plot the detection probability against false alarm probability at a fixed SNR, obtaining what is referred to as the receiver operating characteristic (ROC) curve [128]. The utility of the ROC curve as a convenient instrument for receiver performance comparisons is argued in [40].

3.3 Related Work on Signal Processing

In a typical GNSS receiver, the antenna signal is down-converted to baseband, frequency shifted to eliminate a hypothesized frequency offset, and correlated with a replica signal suitably timed to account for a hypothesized time delay. Circuitry for eliminating data modulation may also be present if prior information about the data is available. The processing of one delay-frequency cell is shown conceptually in Fig. 4. In the figure, T denotes the total observation time, $\hat{\omega}$ denotes the radian frequency hypothesis and $\hat{t}$ denotes the delay hypothesis. A stream of complex-valued base-band samples from the receiver RF section is multiplied with a complex sinusoid and with a delayed replica sequence to eliminate Doppler frequency and ranging sequence modulation, leaving a complex-

valued DC signal. The signal is integrated to yield a complex variate, the modulus of which is stored as a test statistic, often in squared form, as shown in the figure. The test statistic is free of the variable ϕ_0. If the SNR of the integration result is insufficient, it may be improved by making the integration time longer or by combining several squared test statistics additively to generate an alternative test statistic [96]. The former approach is more efficient but not always applicable since the integration time cannot be usefully extended beyond a limit determined by data modulation, oscillator instability, or receiver movement. If squaring is used and the number of integrations is denoted by m, as indicated in the figure, the test statistics have a chi-squared distribution with $2m$ degrees of freedom, characterized by the pdf [P3] [110]

$$f_x(x) = \begin{cases} \left(\frac{m}{2\sigma^2}\right)^m \frac{x^{m-1}}{\Gamma(m)} \exp\left(-\frac{mx}{2\sigma^2}\right) & \text{if } E = 0 \\ \frac{m}{2\sigma^2}\left(\frac{mx}{E}\right)^{\frac{m-1}{2}} \exp\left(-\frac{E+mx}{2\sigma^2}\right) \mathrm{I}_{m-1}\left(\frac{\sqrt{mxE}}{\sigma^2}\right) & \text{if } E > 0, \end{cases} \quad (2)$$

where σ^2 denotes the noise variance at both real and complex integrator outputs in absence of signal and E denotes the squared modulus of the integrator output in absence of noise. These definitions assume that $m = 1$. $\mathrm{I}_k(\cdot)$ denotes the modified Bessel function of the first kind of order k [3]. The manner of calculating the statistics entitles the receiver to be called a quadratic receiver. It is well known that for small values of SNR the quadratic receiver approximates the more ideal likelihood ratio receiver [93].

So-called differential correlation techniques [161] have recently attained attention in the GNSS community [129]. They aim to reduce noise by multiplying successive coherent integration results with each other, but have the shortcoming of being more sensitive to residual frequency offset than the squaring technique discussed above.

To acquire a satellite signal, a GNSS receiver conducts a search over an uncertainty region in time-frequency domain to detect the cell that corresponds to the

frequency offset and sequence timing of the satellite signal. Before testing a cell, the receiver evaluates its statistic as explained above. Since the operations up to and including the integration are linear, their order of execution is immaterial for the result. The execution order may, however, have an impact on word lengths, dynamic ranges of variables, storage of intermediate results, and parallelization of operations, thus potentially influencing the economy of receiver design.

Joint evaluation of cell statistics has gained popularity due to the advent of hardware accelerators with parallel correlator banks or matched filters [6, 7, 51, 52, 145]. Typically, all cells with the same frequency hypothesis are processed in a single run that covers all timing hypotheses. It is not uncommon that the accelerator is also capable of handling several frequency offsets simultaneously [117]. Another common parallel technique is correlation processing with the fast Fourier transform (FFT) [5, 10, 88, 122–124, 143]. It is also possible to do the correlation processing in time domain and to compensate the frequency offset with FFT processing [31]. An example of a technique where both the correlation processing and the frequency offset compensation are implemented with FFT is presented in [8] and schematically depicted in Fig. 5. The technique uses two matrices of intermediate results, one for storing coherent integration results and another for accumulating their squared moduli. In the latter matrix, the row index corresponds to the time delay and the column index to the frequency offset.

For several reasons, the size of the uncertainty region varies within wide limits, as is discussed in more detail in section 4.2. While acquisition under full uncertainty typically requires a joint evaluation facility to proceed at an acceptable speed, acquisition under limited uncertainty may be better performed with stand-alone correlators due to their lower processing overhead and power consumption. Stand-alone correlators have the additional advantage that they can be used for signal tracking after the acquisition. Battery powered portable receivers in particular can benefit by judicious use of both stand-alone correlators and parallel processing accelerators since the receivers need to conserve power and since they often experience short signal outages that do not cause them to

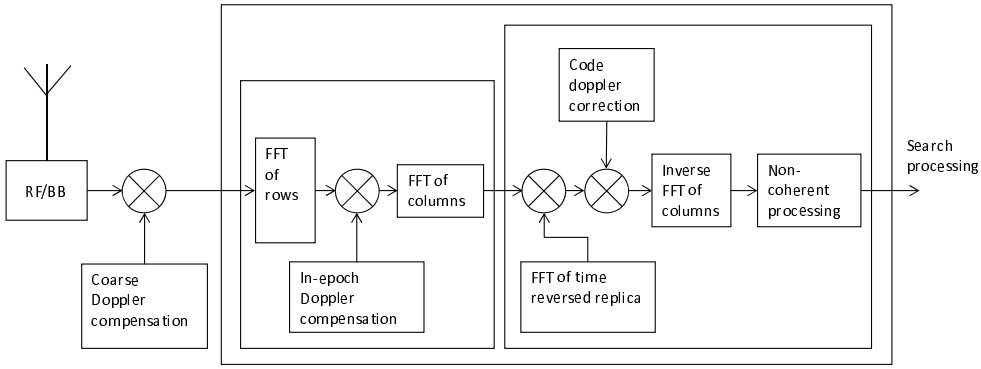

Fig. 5. *FFT based evaluation of cell statistics [8].*

entirely lose track of satellite signals.

3.4 Related Work on Search and Decision Strategies

To find a signal in the uncertainty region, a receiver has to visit the time-frequency cells in a serial, parallel, or block-parallel order, as defined by a search strategy [82], and to apply threshold detection [78], maximum search, or some other suitable decision strategy to conclude if and where in the uncertainty region a signal is present. The search and decision strategies are chosen so as to optimize a performance measure, such as mean acquisition time, probability of false acquisition, probability of detection, energy consumption, or a combination thereof. The preferred strategy also depends on the available memory, available processing resources, and on the size of the uncertainty region. Search and decision strategies are further classified according to time horizon that can be infinite, allowing the processing to proceed for an unlimited time, or finite, forcing a decision after a fixed delay.

Early work [47, 107, 108, 114] on the acquisition of DS-SS signals centered around serial search strategies. In a basic serial acquisition scheme, test statistics are examined cyclically one cell at a time until a decision criterium is met [100]. A serial search strategy can be implemented without a large memory, because a cell can be visited as soon as its statistics are available, and the statistics discarded immediately afterwards. Some serial search strategies, such as the expanding window search [32, 106], which is depicted in Fig. 6, can make limited use of prior information about success probabilities by visiting cells in the order of descending prior probability.

Serial search is often followed by verification to avoid costly false alarms. The arrangement is referred to as multiple dwell detection [37, 48]. The Tong detection algorithm [153] compares a decision variable with a threshold and advances a counter downwards or upwards depending on the result. The process is re-

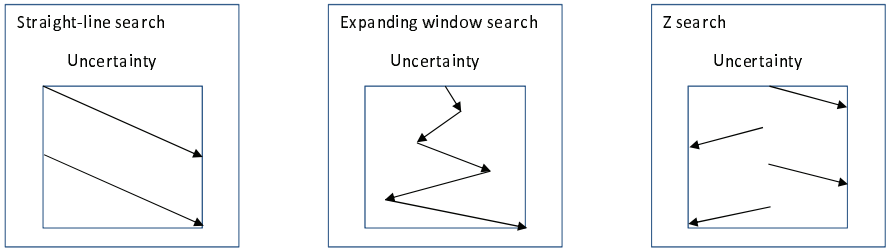

Fig. 6. *Three serial-search strategies.*

peated until a set lower or upper limit is reached. The M of N algorithm [87] makes N test trials and compares the N decision variables so obtained against a pre-defined threshold. If M or more variables exceed the threshold, a signal is declared present. In the dual dwell approach, a potentially successful serial search is followed by a verification step where a second sample with a longer integration time is taken and compared with a threshold. The value of the separate verification step has recently been questioned by pointing out that it does not necessarily shorten the mean acquisition time of the serial search [90]. In any case, it may be noted that verification can only reduce false alarm probability but not improve detection probability.

Parallel or hybrid search strategies can be applied if the statistics of all or a group of cells are simultaneously available in memory. Hybrid strategies [16] typically apply a parallel decision criterium on a group of cells at a time, sieving out a set of cells that are then subjected to serial search. A parallel strategy based on maximum search outperforms hybrid strategies which, again, outperform serial strategies in terms of P_D when P_{FA}^a is given [28] [27]. In fact, the fully parallel maximum search fulfils the maximum likelihood criterium for frequency non-selective fading channels [105] [116].

In likeness to serial search, parallel search can also be followed by verification. In [43], a maximum search followed by verification with a Tong detector is studied. In [82], a thresholding step followed by maximum search and a verification

by majority decision is investigated. In [117], a strategy is proposed where six cells, instead of one, are passed over to verification by thresholding and majority decision making. In [102], a strategy is discussed where a predefined number of cells is passed over to verification by thresholding and ambiguity resolution by mutual comparison of decision variables.

3.5 Serial Search and Sequential Verification as Decision Problems

In search and decision theories [21, 25], a detector that decides when to stop sampling based on what has been sampled is referred to as a sequential detector. In contrast, if the number of samples is predefined, the detector is referred to as a finite sample size (FSS) detector. The sample size of a sequential detector is determined by a stopping rule that should be chosen appropriately to guarantee desired performance.

A basic sequential detector uses the sequential probability ratio test (SPRT) [33, 150] to test a simple null hypothesis H_0 against a simple alternative hypothesis H_1. In its Bayesian form [109], SPRT uses as test variable the posterior probability

$$\pi_1\left(y_1,\ldots,y_n\right)=\frac{\pi_1\lambda_n\left(y_1,\ldots,y_n\right)}{\pi_0+\pi_1\lambda_n\left(y_1,\ldots,y_n\right)} \tag{3}$$

of H_1 given the samples $y_1,\ldots,y_n$ that are assumed to be independent.

In (3), λ_n is the likelihood ratio based on n samples given by

$$\lambda_n\left(y_1,\ldots,y_n\right)=\prod_{k=1}^{n}\left[p_1\left(y_k\right)/p_0\left(y_k\right)\right], \tag{4}$$

π_0 and π_1 are the prior probabilities of H_0 and H_1, respectively, and $p_0\left(\cdot\right)$ and $p_1\left(\cdot\right)$ are the probability densities of the observations under H_0 and H_1, respectively. For consistency, it is defined that $\lambda_0=1$. The test is continued until the

posterior probability (3) reaches a pre-defined lower or upper limit, confirming either H_0 or H_1. SPRT is optimal in the sense that it has the shortest expected stopping time for specified levels of false alarm and detection probabilities [17]. This makes it an interesting candidate for a verification algorithm in GNSS acquisition, but it has only recently attained attention for this purpose [97].

Baum and Veeravalli provide a generalization of SPRT to multihypothesis testing, termed MSPRT [17]. In likeness to SPRT, the problem setting of MSPRT is that of deciding when a scalar measurement has been repeated enough times that additional measurements are not needed. Kadane [81] investigates the whereabouts search problem, a multihypothesis testing problem where measuring a specific location gives a binary result indicating if an object is present in that location. He assumes that no false alarms occur, which leads to a considerable simplification of the problem and allows him to show that only open-loop strategies have to be considered as candidates for an optimal search strategy. Unfortunately, this simplification is not available in the GNSS signal acquisition problem where false alarms do occur.

Castañon [34] discusses a more general whereabouts search problem where the measurements are continuous-valued and false alarms are possible. The problem can be viewed as a generalization of MSPRT where the measurement space is multidimensional. He shows that an optimal search strategy has a closed-loop structure where the search order is determined by previous measurements. He further shows that in the case of symmetrical (e.g. normal) measurement distributions an optimal rule for choosing a measurement has the Markov property so that only a state vector, rather than the complete measurement history, needs to be preserved in the receiver. The state vector consists of the success probabilities of the search locations, referred to as $\pi_j\,(k)$, that are maintained up-to-date using the equations [34] (for a derivation, see [P1], appendix)

$$\pi_j(k+1) = \begin{cases} \frac{\pi_j(k) f(y(k))}{p(y(k)|i(k))} & j \neq i(k) \\ \frac{\pi_j(k) g(y(k))}{p(y(k)|i(k))} & j = i(k) \end{cases} \tag{5}$$

and

$$p(y(k) \mid i(k)) = \left(1 - \pi_{i(k)}(k)\right) f(y(k)) + \pi_{i(k)}(k)\, g(y(k)) , \tag{6}$$

where j, $j = 1, \ldots, n$, denotes the index of a search location, $i(k)$ denotes the search location that is measured at step k, $f(\cdot)$ is the pdf of the measurement distribution when the search object is not present in the search location, and $g(\cdot)$ is the pdf of the measurement distribution when the search object is present in the search location. It may be noted that (5) is equivalent to (3) in the special case where $n = 1$. The optimal strategy in the case of symmetrical $f(\cdot)$ and $g(\cdot)$ is to measure at step k the location j that has the highest or, alternatively, the second highest posterior probability $\pi_j(k+1)$.

3.6 New Sequential Acquisition Algorithm

In [P1], we present an FSS serial search acquisition algorithm that relies on the decision theoretic framework presented in section 3.5 and has the following novel features. The algorithm performs sequential verification as an integral part of its operation and therefore does not need a separate verification stage. This integration of operational stages is achieved by abandoning fixed order search in favor of a dynamical search where correlator resources are re-allocated at the end of each correlation interval on the basis of freshly updated probabilities of acquisition hypotheses. Additive combining of correlation results as a means of improving SNR is abandoned in favor of statistically more universal Bayesian probability updates. The algorithm also accepts an arbitrary prior distribution for the probabilities, which follows naturally from their use as state variables. Using probabilities as state variables has the additional benefit of separating the

operational logic of the algorithm from noise and signal models, making the latter changeable, even during operation. This makes it possible, for example, to adjust coherent integration times dynamically. Since the state variables can be understood outside the receiver context, they can also be conveniently used to monitor the quality of the acquisition process. Finally, the state update equations are independent of the chosen stopping time which can therefore be altered at a late stage.

The algorithm is based on the observation that sequential acquisition can be viewed as a partially ordered Markov decision problem (POMDP) [115], where the state vector consists of the conditional success probabilities of acquisition hypotheses given past measurements [22]. The receiver has a single correlator that is set to execute a total of K coherent integrations. Based on the modulus of each integration result, the probability vector is updated, and a next cell to be visited chosen by applying a search policy on the updated probability vector. Finally, a decision is made in favor of the hypothesis that has the highest posterior probability. Finding an optimal search policy is a special case of the general test sequencing problem that is known to be NP-hard [119] and, in our case, computationally very expensive to solve due to the continuous-valued state vector [115]. We have studied and evaluated by Monte Carlo simulations two sub-optimal search policies, one based on maximizing one-step posterior probability and another based on maximizing information [130] gain. The policies have representations as index rules and they are therefore computationally inexpensive. In choosing the policies we have followed a recommendation in [34] for the probability maximizing policy and recommendations in [20,41,44,101,119] for the information gain maximizing policy.

3.6.1 Simple Example

In this section, the algorithm of [P1] is discussed in the light of a simple example. The example considers elementary sample distributions and a small search

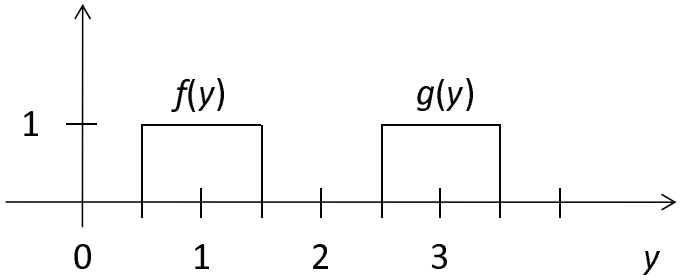

Fig. 7. *Measurement distributions.*

space with just three cells. Of the two alternative search policies, the probability maximizing search policy is applied.

Assume that the measurements are evenly distributed over the interval $(0.5, 1.5)$ when the signal is absent and over the interval $(2.5, 3.5)$ when the signal is present. The corresponding probability distribution functions $f\,(y)$ and $g\,(y)$ are shown in Fig. 7. The functions have disjoint supports, which is a crude simplification but serves the example. Let the cells be numbered 1, 2, and 3 and let there be a signal in cell number 3.

Four hypotheses are examined. Hypothesis H_0 corresponds to the case where no signal at all is present and each hypothesis H_i, $i \in \{1, 2, 3\}$, to the case where a signal is present in cell i. Prior probabilities are assigned to the hypotheses as shown in Table 3.

The search policy tells the receiver to visit the cell with the second highest probability. Consequently, cell number 2 is measured in the first round. Since there is no signal in that cell, the measurement result belongs to the support of $f\,(y)$, which yields $f\,(y) = 1$ and $g\,(y) = 0$ for the choice of $f\,(y)$ and $g\,(y)$ used here. These values are substituted to (5) and (6) to obtain the posterior probabilities shown in the table. Applying the search policy to the posterior probabilities now directs the receiver to measure cell number 1 and, after yet another probability update, cell number 3. Since there is a signal present in cell number 3, the result

Table 3. *Simple example*

Hypothesis	H0	H1	H2	H3	$f(y)$	$g(y)$
Cell		1	2	3		
Signal		absent	absent	present		
Prior probability	0.5	0.15	0.3	0.05		
Measurement 1	-	-	$y = 1.12$	-	1	0
Posterior probability	0.71	0.21	0	0.07		
Measurement 2	-	$y = 0.85$	-	-	1	0
Posterior probability	0.91	0	0	0.09		
Measurement 3	-	-	-	$y = 2.9$	0	1
Posterior probability	0	0	0	1		

of the latter measurement belongs to the support of $g(y)$, which yields $f(y) = 0$ and $g(y) = 1$. After one further probability update, the algorithm converges to a state where the posterior probability of H_3 is unity. If the decision rule of [P1] is applied at this stage by choosing the hypothesis with the highest posterior probability, the correct decision is taken. The decision is also known to the receiver to be correct with probability one. Alternatively, one or more additional measurements could be performed, but these would no longer change the probabilities, as can easily be seen.

3.6.2 Performance

In [P1], ROC and power function curves from Monte Carlo simulations have been presented for the proposed algorithm. Parallel search with additive noncoherent combining has been used as a reference strategy due to the fact that it represents an upper performance limit for serial search strategies, as was noted in section 3.4. The reference strategy and the new strategy with both alternative search policies have been evaluated with an equal number of coherent integration results of equal post-integration SNR. The ROC and power function curves for the reference strategy have been evaluated numerically. All results are reported in terms of P_{FA}^a and P_D. The simulation range for the number of cells is from 5 to 60 and for the number of coherent integrations from 20 to 70. To verify the robustness of the algorithm, an SNR estimation error ranging from -6 dB to 6 dB has been introduced.

The simulations demonstrate the superiority of the proposed algorithm over the reference strategy for the whole range of P_{FA}^a values from 0 to 1. The SNR advantage of the new algorithm is greater than 1.5 dB and exceeds 3 dB for the important range $0\% \leq P_{FA}^a \leq 5\%$. Expressed in different terms, the performance of the new algorithm is approximately equal to that of the reference strategy if the new algorithm is put at a disadvantage by doubling or tripling the size of its uncertainty range or, alternatively, by doubling or tripling the number of coher-

ent integration results available for the reference strategy. As a further finding, no significant performance difference between the two search policies has been observed.

3.6.3 Receiver Implementation

In [P1], the computational load of the proposed algorithm is assessed and compared to that of the reference strategy. A numerical example in [P1] shows that the excess load of the new algorithm in comparison with the reference strategy is marginal.

Two approaches are identified in [P1] for extending the new acquisition strategy to the case where multiple correlators are available. One approach is to partition the uncertainty region into as many sections as there are correlators and to apply the single correlator strategy to each section separately. The probability vectors so obtained are then concatenated for decision making. Another approach is to have several correlators operate in parallel in the full uncertainty region and to use one of the proposed policies to allocate new cells to the correlators as they become vacant. In this variant the probability updates and the decision making are no different from the basic strategy, because the probability update equations (5) and (6) are idempotent.

3.7 Improved Two-Stage Parallel Acquisition Strategy

In [9], we claim a generalized parallel acquisition unit where a massive correlator bank (MCB) passes information about multiple time-frequency cells to a supplementary correlator bank (SCB) for verification. Such a two-stage unit has two potential benefits in comparison with one that only passes information about a single cell to verification. Firstly, the risk of omitting the signal can obviously be reduced if more cells are verified. Secondly, in a case where implementation

difficulties limit the flexibility of the MCB, the smaller SCB may more easily be equipped with capabilities that allow high quality verification processing. In general, structural separation of the two units allows them to be better optimized for their respective tasks.

In [P2], we study the performance improvements available from combining an MCB with an SCB. We first identify alternative operating modes. For example, the SCB can either be allowed to run to completion or be pre-empted when new candidate cells are found by the MCB. We further identify different structural embodiments for the SCB depending on what type of statistics, coherent or noncoherent, are passed between the two units.

In the numerical part of [P2], we evaluate cases where different numbers of candidate cells are passed from an MCB to an SCB for verification. A power function plot (Fig. 4 in [P2]) of a Monte Carlo simulation shows that increasing the number from one to twelve provides a sensitivity improvement in the order of 3 dB. Another power function plot (Fig. 5 in [P2]) shows that the advantage is preserved across different combinations of coherent integration and noncoherent combining.

3.8 Discussion

In this chapter, an overview of algorithms used in GNSS signal acquisition has been presented and two new acquisition strategies proposed, one to improve detection rate in two-stage parallel acquisition and another to improve ROC performance in serial search acquisition. We have also reviewed the results of decision theory that were the starting point for the latter strategy.

In [P1], a completely new fixed sample-size sequential acquisition strategy for GNSS signals has been presented where the order of visiting cells is steered dynamically during the acquisition process. Two policies for choosing the visiting order have been derived from statistical considerations and they have been

shown to have implementations as simple index rules. Unlike previous methods, the state of the acquisition process is maintained as a vector of probabilities. This novel approach has been shown to have several operational advantages, and Monte Carlo simulations indicate a significant performance advantage over a reference strategy for a wide range of parameters.

In [P2], an improved two-stage parallel acquisition strategy has been presented that is based on a massive correlator bank cascaded with a supplementary correlator bank. Monte Carlo simulations show that using the supplementary correlator bank for verification instead of a single correlator significantly improves system detection rate. Before our original filing [9], the idea of passing several cells from a parallel acquisition accelerator to subsequent verification by tracking correlators had been discussed without evaluation in [117]. We have expanded the idea by discussing alternative structures and operational modes and provided verification by Monte Carlo simulation. After our paper, a similar idea has been discussed in [102] for use in terrestrial TDM/TDMA communication systems.

Our system model makes the simplifying assumptions that the search cells are uncorrelated and that the satellite signal is not present in multiple cells. In practice, the satellite signal can leak into adjacent cells due to a short sampling interval, due to off-peak sampling, or due to multipath propagation. The error from omitting the leakage is discussed in [29] and found to be small. Multipath signal components have been measured in areas of heavy GNSS signal attenuation and they have been found to be largely dominated by the LOS component [53, 154].

We have not discussed the acquisition of BOC modulated signals separately. The autocorrelation main lobes of BOC modulated signals have multiple peaks, which makes their acquisition difficult and a subject of continual research. One of the proposed approaches [91] is to use single sideband processing to obtain a signal that has a BPSK-like autocorrelation function and can be acquired with standard techniques.

4. ACQUISITION PERFORMANCE OF GNSS SIGNALS

During the past few years, several families of satellite signals with long ranging sequences have been proposed. One purpose of using long sequences is to mitigate interference by reducing autocorrelation function minor peaks and cross-correlation [24, 49]. Several authors have expressed their concern that the long sequences are difficult to acquire [56, 70, 112], but it is not clear to what extent the difficulty is due to limitations of current receiver technology and to what extent it is inherent to the signals. Answering this question and providing a method for comparing satellite signals for their ease of acquisition are the main topics of this chapter. Our approach is to assume an idealized receiver that is free of technology limitations, which allows us to confine ourselves to the study of fully parallel search. We show that there is a functional dependency between acquisition sensitivity and the size of the uncertainty range which, again, is dependent on the availability of acquisition assistance and on signal parameters, in particular on sequence length. To complement the theoretical discussion, we provide numerical results for several GNSS signals.

The chapter begins with a review of related work in section 4.1. In section 4.2, the acquisition uncertainty range and its dependence on available acquisition assistance are discussed. A new performance measure, attenuation margin, is then introduced in section 4.3. Section 4.4 summarizes the discussion.

4.1 Related Work

Acquisition strategies for modern and modernized GNSS signals are still under intensive research and few comparative studies have been published about the signals, their acquisition, and the effect of assistance on their acquisition. Studies on individual signals are available, however, and the old GPS L1 C/A signal has understandably been somewhat more extensively investigated. Unfortunately, lack of common performance measures makes a comparison of results difficult.

The acquisition performance of the Galileo E1 OS pilot signal at a fixed C/N_0 is evaluated in [39] by Monte Carlo simulation. The results are reported in the form of ROC curves and mean acquisition times that are plotted against false alarm rate. The mean acquisition times are evaluated by assuming single dwell serial search with a threshold crossing criterion [107]. In [92], four acquisition techniques for the data and pilot channels are analyzed in terms of probabilities of false alarm and detection. The mean acquisition times are plotted against penalty time, a parameter of an assumed serial search algorithm. In [75], detection probabilities and mean acquisition times are plotted against C/N_0 for five acquisition algorithms. None of the publications discuss parallel acquisition, and the probabilities of false alarm and detection are defined in the context of a single cell, not in the context of the complete acquisition process.

The acquisition of the GPS L2C signal data component is discussed in [164], where a few pointwise simulation results are given for the acquisition time at two C/N_0 levels. The acquisition of the data component is also discussed in [58], where four algorithms for the joint acquisition of the GPS L1 C/A and GPS L2C signals are evaluated and the results presented as ROC curves. The assisted acquisition of the L2C pilot signal using long coherent integration times is discussed in [13] and simulations presented for the probability of detection as a function of C/N_0. Three acquisition strategies for the data component are discussed in [142], and the lowest acceptable C/N_0 derived theoretically for two combinations of detection and false alarm probabilities and two combinations of

coherent and non-coherent integration times.

The Galileo E5 and GPS L5 signals are often discussed jointly since they have identical symbol rates and similar concatenated ranging sequences. In [15], the mean acquisition times and the probabilities of false alarm and detection are plotted against C/N_0 for different numbers of coherent integrations. Two strategies are considered, one based on a single signal component and another based on both data and pilot components. Single-dwell serial acquisition is assumed with idealizations regarding receiver front-end filtering and off-peak sampling. Three different uncertainty regions are considered and acquisition times plotted. In a continuation paper [14], Monte Carlo simulation results for acquisition time distributions are provided. Monte Carlo simulations for the ROC characteristics of five acquisition strategies are presented in [30] at two C/N_0 levels for a fixed number of coherent integrations. One of the strategies uses a single signal component and the other strategies use both data and pilot components. In [131] and [132], the theoretical and simulated mean acquisition times of the Galileo E5 signals are plotted against C/N_0 for four different acquisition strategies, all based on single dwell serial search. Some of the strategies involve simultaneous acquisition of the E5a and E5b signals.

In the publications referred to above, the mean acquisition times of the serial search strategies are derived from single cell false alarm and detection probabilities P_{fa} and P_d by using some variant of the equation

$$\overline{T_{acq}} = \frac{(2 - P_d)\,(1 + K_p P_{fa})}{2P_d} N_u \tau_d \tag{7}$$

due to Holmes [77], where N_u is the size of the uncertainty region, τ_d is the dwell time, and K_p is a penalty factor, so that $K_p \tau_d$ corresponds to the time lost when a false alarm occurs. The parameters of the equation are heavily dependent on several aspects of the acquisition procedure, such as the estimation of signal parameters, the evaluation of cells, the detection of satellites, the verification of acquisition results, and the technique of reacquisition used in the case of a false

alarm. The metric represented by the equation therefore has to be modified or newly derived if the acquisition engine is changed, which makes it ill-suited for comparing GNSS signals for their acquisition performance.

The probability of acquisition error in a parallel acquisition GPS L1 C/A receiver is plotted against signal power in [156] for several numbers of coherent integrations. In a continuation paper [155], a more generic and extensive set of plots is presented for several sizes of uncertainty regions. The plots are obtained by Monte Carlo simulation. In both publications, acquisition error is defined as an erroneous outcome in a situation where a signal is present and is known to the receiver to be present. Analytical expressions for the same problem are derived and numerical results reported in [P3].

Borio [28, 29] generalizes the single cell detection and false alarm probabilities by introducing the notion of system probabilities. 'System false alarm probability in the absence of signal', P_{FA}^{a}, is defined as the probability of getting an indication of signal presence when no signal is present, and 'System detection probability', P_D, is defined as the probability of getting an indication of signal presence, combined with correct information of its timing and frequency offset, when a signal is present. He also plots P_D against P_{FA}^{a} for serial, parallel and hybrid search strategies and demonstrates that the P_D of the parallel strategy surpasses those of the two other strategies uniformly over the whole range of P_{FA}^{a} values when an AWGN channel and a single coherent integration are assumed. Analytical expressions for the parallel strategy in the case of multiple coherent integrations are derived in [P4] and [P5] and discussed below in section 4.3.

Konovaltsev [87] discusses serial, parallel, and hybrid acquisition strategies and proposes to use the complexity and duration of the acquisition process as performance measures. As a reference algorithm he uses a 'maximum likelihood algorithm' where all search cells are examined in parallel and the cell with the maximum search statistic, if it exceeds a predefined threshold, is singled out as the one containing a signal. The process is followed by a separate verification

stage and a possible re-initialization of the algorithm. The coherent integration time and the single-cell false alarm and detection probabilities are given as design parameters and the decision threshold and the number of coherent integrations chosen accordingly. As acceptable outcomes for the parallel search, correct detection in the presence of signal and lack of alarm in the absence of signal are defined. These conditions are identical to those defined by Borio and their probabilities can likewise be obtained from the analytical expressions derived in [P4] and [P5].

4.2 Size of Uncertainty Region with and without Assistance

The size of the acquisition uncertainty region is the product of the numbers of search options in frequency domain, N_f, and in time domain, N_c. The number N_f has been given the expression [83]

$$N_f = 1.5BT/m\,, \tag{8}$$

where B is the frequency uncertainty range, T is the total observation time, and m is the number of coherent integrations. Equation (8) reflects the fact that the width of a frequency search band is inversely proportional to the coherent integration time T/m. Slightly different values have been suggested by other writers for the numerical factor 1.5 that is a tradeoff between speed and sensitivity requirements and receiver qualities such as frequency resolution and signal tracking capability. For FFT based methods, a factor of 1 is commonly used [143]. When no assistance is available, B is determined by the worst case receiver clock bias and the maximum Doppler shift and is typically in the order of 10 kHz. The number N_c is the product of time uncertainty range and receiver oversampling rate. Equation (8) shows that an attempt to improve sensitivity by increasing the coherent integration time results in a larger uncertainty region.

Acquisition assistance includes frequency and time references. The frequency reference usually allows the receiver to significantly reduce B while the time

reference in some cases allows it to reduce N_c. Three factors contribute to the accuracy of the frequency reference: the accuracy of the basestation oscillator, user movement with respect to the basestation, and the accuracy of the Doppler estimate, usually calculated in the receiver. A typical accuracy of a frequency reference is ± 200 Hz [P5]. In most cellular networks, a time reference is available at an accuracy of 2–3 s, which is longer than the period of a satellite ranging sequence and therefore does not help to reduce N_c. In some networks, however, a time reference accurate to within a few tens of microseconds is available, allowing a significant reduction of N_c. In 3GPP WCDMA networks in particular, a so called fine time assistance is available if basestations are equipped with optional GNSS reference receivers. The specified error range of the fine time assistance for terminal conformance testing [111] is ± 10 µs [1, 2].

Publications [P3], [P4], [P5], and [P6] discuss the size of the acquisition uncertainty region of open access Galileo, GPS, and GLONASS signals when assuming different levels of cellular assistance. Two types of assistance are assumed in [P5]: pure frequency assistance, referred to as coarse assistance, and combined frequency and time assistance, referred to as fine assistance. The study reveals a wide variability in the size of the uncertainty region, ranging from 130 cells for the Galileo E1 data channel with fine assistance to 5.5×10^{11} cells for the GPS L1C pilot channel without assistance.

4.3 Attenuation Margin as a Performance Measure

In publications [P4], [P5], and [P6], a new performance measure, referred to as attenuation margin, is proposed for GNSS signals to indicate their susceptibility to path loss during acquisition. Attenuation margin is defined as the highest attenuation that permits an idealized receiver to detect a signal or absence of signal at a specified level of reliability. The idealization is chosen so as to minimize the number of arbitrary parameters and the influence of receiver technology on the performance measure, but still to take into account essential signal char-

acteristics, such as the length of ranging sequence. The measure is based on the observation in [P3] that the dependency of acquisition sensitivity on the size of uncertainty region can be expressed in a receiver independent manner if suitable simplifying assumptions are made about the acquisition process and receiver structure. More specifically, by assuming unconstrained processing and memory capacities, it is possible to obtain a functional relationship between the size of the uncertainty region and the minimum signal strength required to achieve a given acquisition performance in the sense of section 3.2. By further assuming an AWGN channel, unlimited receiver bandwidth, synchronized sampling, absence of quantization effects, and uncorrelated cells, we are able to reduce the arbitrary parameters to three: P_{FA}^{a}, P_D, and T. With such a small number of optional parameters, the performance measure is universal enough for comparing GNSS signals for their acquisition performance in a technology independent manner.

To evaluate the attenuation margin, the global detection and false alarm probabilities are expressed as [P5]

$$P_{FA}^{a}\left(q\right) = 1 - \left[\mathrm{P}\left(m, \frac{mq}{2\sigma^2}\right)\right]^{n} \tag{9}$$

and as

$$P_D\left(q\right) = \tfrac{1}{2}\int_{\frac{mq}{\sigma^2}}^{\infty}\left(\frac{u}{E/\sigma^2}\right)^{\frac{m-1}{2}} e^{-\frac{E/\sigma^2+u}{2}}\mathrm{I}_{m-1}\left(\sqrt{\frac{uE}{\sigma^2}}\right)\mathrm{P}\left(m, \frac{u}{2}\right)^{n-1} du\,, \tag{10}$$

respectively.

Here, n denotes the size of the uncertainty region, q denotes a detection threshold, and $\mathrm{P}\left(\cdot,\cdot\right)$ denotes the lower regularized (incomplete) gamma function as defined in [3]. The expressions are derived from the distributions (2) of cell statistics.

Equations (9) and (10) lend themselves for evaluation with standard numerical

software packages even for large values of m and n, but it is still instructive to study their asymptotic behavior, especially as a simple relationship between acquisition sensitivity and search space dimension can thereby be found. As a first observation, the second term of (9) is proportional to q^{mn} for small values of q, so that for a large uncertainty region P_{FA}^{a} rapidly tends to unity when the threshold q is lowered to zero. In [P3], (10) is studied for its asymptotic behavior when $n \to \infty$, $q = 0$, and $P_D = 1/2$. For $m = 1$, the following approximate relationship is obtained:

$$\frac{E}{2\sigma^2} \approx \ln(n-1) - 1 \approx \ln n \,. \tag{11}$$

Another approach to study the asymptotic behavior of (10), yielding essentially the same results, is taken in [P6] by evoking extreme value theory (EVT) [42,67]. It is shown in [P6] that for $m = 1$, the mean value and standard deviation of the maximum of the magnitudes of n noise cells, denoted here by F_n, obtain the expressions

$$\overline{F_n} = 2\sigma^2 (\ln n + \gamma) \tag{12}$$

and

$$\sqrt{\overline{\left(F_n - \overline{F_n}\right)^2}} = \pi\sqrt{\frac{2}{3}}\sigma^2 \,, \tag{13}$$

respectively, where γ is the Euler constant with the approximate value of 0.5772. It follows that to meet some given error rate requirements, detection thresholds have to be tied to the logarithm of the size of the uncertainty range. Consequently, a larger uncertainty region results in a lower acquisition sensitivity, and the dependency is logarithmic.

4.3.1 Numerical Results

In [P3] and [P6], the complement of P_D when $q = 0$, denoted as P_{fa} in the publications, is plotted against $E/\left(2\sigma^2\right)$ for a wide range of combinations of parameters n and m. Some of the combinations are motivated by examples from Galileo and GPS signal acquisition. The variable P_{fa} represents the acquisition error probability in the idealized case where a signal is present and is known to the receiver to be present. The plots clearly demonstrate the logarithmic dependency of acquisition sensitivity on the size of uncertainty region.

In [P4], P_D is plotted against $E/\left(2\sigma^2\right)$ for several GNSS signals by solving (9) for q when $P_{FA}^a = 0.01$ and inserting the result into (10). Two cases are discussed, acquisition without assistance and acquisition with fine assistance. Results are also shown for single cell acquisition ($n = 1$). Attenuation margin is tabulated under the conditions $P_{FA}^a = 0.01$ and $P_D = 0.99$[1]. In [P5], the GLONASS L1 SP signal and coarse assistance are additionally analyzed. In both publications, the total signal observation time is taken to be one second, leading to multiple coherent integrations for the data channels. For the pilot channels, a single one-second coherent integration is assumed, which in some cases means integration over several code cycles and in two cases (GPS L1C and GPS L2C) integration over a fractional code cycle.

The numerical analysis in [P4], [P5], and [P6] reveals that the data channels of modern and modernized satellite signals have low attenuation margins in comparison with those of GPS L1 C/A. This is especially true for signals whose coherent integration time is short due to their high symbol rate. Pilot signals in general offer attenuation margins that are 7 dB higher than those of the corresponding data signals. However, assistance would seem to be a precondition for their use in weak signal acquisition due to their otherwise extremely wide uncertainty regions. Reducing the uncertainty with assistance would seem to increase

[1] The single cell attenuation margin for the L1C pilot signal in Table 2 of [P4] is in error and should read 29.7 dB, not 39.7 dB.

the attenuation margins of the pilot signals by an additional 0.5 dB for coarse assistance and by an additional 2 dB for fine assistance. Following this line of argument, a sensitivity improvement of as high as 9 dB can be attributed to fine assistance, 7 dB of which is due to the difference between data and pilot signals and 2 dB due to the reduction of uncertainty space.

4.4 Discussion

A new performance measure, attenuation margin, has been introduced as a metric for comparing different GNSS signals for their acquisition properties when the signals are attenuated by obstacles in the propagation path. To make the performance measure applicable in practice despite the often large uncertainty regions involved, analytical expressions for its evaluation have been derived. The expressions have been used to calculate the attenuation margins of several old, modern, and modernized GNSS signals under different assumptions about acquisition assistance. The results have been discussed and conclusions drawn about the significance of acquisition assistance and various signal parameters for the acquisition properties of the signals. Additionally, a simple asymptotic functional relationship between acquisition sensitivity and the size of uncertainty region has been established for large uncertainty regions.

The idea of comparing the acquisition properties of satellite signals using a common performance measure is new in the GNSS literature where the problem setting has usually been one of comparing receiver architectures and algorithms. In particular, the idea of attributing acquisition sensitivity quantitatively to the size of the uncertainty region is new. The derived expressions are also new, although a special case has been published earlier. The asymptotic study has been done both on the basis of known theory and by using a new, alternative approach that gives additional insight into the functional relationship established.

5. RANGING SEQUENCES

The topic of this chapter is to provide a method of constructing families of ranging sequences that are both short and have good cross-correlation properties. The method is based on using sequences of unequal lengths, first proposed by one of us for terrestrial CDMA wireless networks in [162] and then jointly by us for GNSS in [163], [P7], and [P8]. The method is particularly well suited for the design of GNSS ranging sequences because it provides for the first time a systematic method for reducing cross-correlation in the time-frequency domain as opposed to earlier approaches that have only addressed cross-correlation in the time domain.

In section 5.1, general requirements and performance metrics for CDMA spreading sequences are reviewed and the specific requirements for GNSS ranging sequences highlighted. Related work is reviewed in section 5.2 and our method presented in section 5.3. The chapter is summarized in section 5.4.

5.1 Requirements for Ranging Sequences

A GNSS system is akin to a terrestrial CDMA communication network in that transmissions from several transmitters are separated by code multiplexing. The Russian GLONASS system currently relies on frequency multiplexing, but is reported to introduce code multiplexing in the next generation K-series satellites [59]. The similarity of GNSS with communication networks extends to the so-called near-far effect, a phenomenon where a weaker signal is masked by a

stronger one due to an imperfection in the multiplexing scheme. In GNSS systems, this phenomenon mainly manifests itself in urban locations where some satellite signals are attenuated more than others. If the signals are not fully orthogonal, a receiver trying to receive a weaker signal may erroneously react to a stronger one and subsequently malfunction. In code multiplexed systems, lack of orthogonality is mostly caused by cross-correlation between ranging sequences. Minimizing pairwise cross-correlation is therefore a central objective in the design of GNSS ranging sequences.

Unlike the terrestrial CDMA communication channel, the GNSS channel introduces a large Doppler shift that may have a significant impact on the cross-correlation properties of the signals. Consider, for example, a GPS L1 C/A correlation receiver tuned to the nominal carrier frequency and subjected to a satellite signal with a Doppler shift of 4 kHz. The incoming signal experiences four $360\,^{\circ}$ complex phase rotations with respect to a local reference during a 1 ms code cycle, yielding a correlation result that is likely to differ significantly from what would have been obtained if the Doppler shift had been absent. Indeed, it is known that a 4 kHz Doppler difference increases the worst-case cross-correlation between GPS L1 C/A signals by more than 2 dB [100].

Some further objectives for GNSS sequence design are avoidance of high spectral peaks, minimization of minor autocorrelation peaks, and minimization of a DC component. Ease of signal acquisition is also an important consideration, especially for portable receivers. High peaks in the signal frequency spectrum make receivers vulnerable to narrowband interference [133]. Although such interference should be uncommon in the strictly regulated GNSS frequency bands, locally generated in-band spurious signals are still present in mobile phones and other integrated electronic devices [144]. Narrowband interference mitigation therefore plays an important role in achieving high sensitivity GNSS reception in such devices. Minor autocorrelation peaks are a concern in sequential acquisition where the correlation function between the satellite signal and its local replica is often only partially evaluated. If the main peak is not present in the seg-

ment evaluated, it is possible that the receiver accepts a minor peak for the main peak. This is less of a concern for parallel acquisition where the entire correlation function is typically evaluated. A GNSS ranging sequence should normally be free of a DC component to allow AC coupling in signal paths. In practice, a small DC component is often present and is not considered harmful [73]. Ease of acquisition is inversely related to the size of uncertainty region and further to sequence length, as was discussed in chapter 4.

In early GNSS literature, orthogonality requirements were mainly expressed in terms of even correlation functions, but attention has recently also been given to odd correlation functions [121]. Even periodic correlation functions for a set of M sequences of length L and complex elements c_i^n, $n = 1, \ldots, M$ and $i = 0, \ldots, L-1$, are defined for $0 \leq l < L$ as [57, 113, 126]

$$\theta_{m,n}^{e}(l) = C_{m,n}(l) + C_{m,n}(l-L) \ , \tag{14}$$

where

$$C_{m,n}(l) = \begin{cases} \sum_{j=0}^{L-l-1} c_j^m c_{j+l}^{n*}, & 0 \leq l \leq L-1 \\ \sum_{j=0}^{L+l-1} c_{j-l}^m c_j^{n*}, & 1-L \leq l < 0 \\ 0, & |l| \geq L. \end{cases} \tag{15}$$

In (14), $m = n$ corresponds to the autocorrelation function and $m \neq n$ to the cross-correlation functions. Odd periodic correlation functions are similarly defined as

$$\theta_{m,n}^{o}(l) = C_{m,n}(l) - C_{m,n}(l-L) \ . \tag{16}$$

Odd periodic correlation functions reflect cross-correlation between DS-SS signals that have sign changes at sequence boundaries while even periodic correlation functions reflect cross-correlation between DS-SS signals that do not have

sign changes. The even functions are therefore applicable to GNSS signal pilot components while the even and odd functions are both applicable to GNSS signal data components that contain passages with and without sign changes. In a case where the modulation rate of the data component is low in comparison with the repetition rate of its ranging sequence, as is the case with the GPS L1 C/A signal, sign transitions are infrequent, and cross-correlation may be best reflected by the even correlation functions. Pilot components with composite ranging sequences (see section 5.2) are sometimes viewed as data components where the elements of the secondary code are interpreted as data symbols. This approach calls for the use of even and odd correlation functions. More specifically, it has been suggested that a weighted mean of even and odd correlation functions be used as a performance measure in this case [68].

Welch [157] considers the normalized case

$$\theta^e_{m,m}(0) = \sum_{i=0}^{L-1} |c_i^m|^2 = 1\,, \tag{17}$$

defines

$$\theta_{max} = \max\left(\max_{m\neq n}\left(\max_{0\leq l<L-1}\left|\theta^e_{m,n}(l)\right|\right), \max_{m}\left(\max_{1\leq l<L-1}\left|\theta^e_{m,m}(l)\right|\right)\right), \tag{18}$$

and derives the lower bound

$$\theta_{max} \geq \sqrt{\frac{M-1}{ML-1}}\,. \tag{19}$$

The bound gives the lowest possible maximum for even cross-correlation and minor peak autocorrelation magnitudes that can be obtained for a set of M sequences of length L. It is shown in [126] that (19) also holds for odd periodic correlation functions.

The vulnerability of a GNSS signal to narrowband interference is customarily assessed by inspecting its power spectral density for strong components. If a strong spectral component coincides with an interfering narrowband signal, the interfering signal is not efficiently suppressed when it is correlated with a replica sequence in a receiver [110]. To take an example, a GPS L1 C/A signal without data modulation has a line spectrum with lines separated by intervals of 1 kHz, the inverse period of the ranging sequence. The spectrum of the actual signal is not fully discrete since the signal is BPSK modulated with a 50 bps data stream, which causes some broadening of spectral lines. The spectrum has a $\sin x/x$ envelope due to the NRZ waveform of the signal. The amplitudes of the spectral lines do not accurately follow the the $\sin x/x$ envelope, however, since the power spectra of the ranging sequences are not flat, the largest upward deviation among spectral components being 8.8 dB [83]. If it is desired to reduce strong spectral components, either sequences with a flatter spectrum or sequences with a lower average spectral component power need to be chosen. The average spectral component power can only be reduced by using a longer ranging sequence.

5.2 Related Work

The GPS L1 C/A signals are based on a set of 1,023 long ranging sequences due to Gold [60]. The sequences are generated by modulo 2 addition of two m-sequences, one of which is selectively delayed to yield a set of sequences, 32 of which are assigned to satellites. The cross-correlation functions and minor peak autocorrelation functions of the sequences have an upper limit of 65 on a scale where the autocorrelation main peaks obtain the value of 1,023 [126]. This corresponds to a cross-correlation separation of 23.9 dB in the absence of Doppler shift.

The primary ranging sequences of the GPS L1C signal [66] were originally constructed by padding selected 10,223 long Weil sequences [120] to the desired length of 10,230 with pads chosen by exhaustive computer search to optimize

both even and odd correlation behavior of the sequences [121]. The search yielded 739 primary ranging sequences with a minimum even cross-correlation separation of 27.5 dB and with a minimum odd cross-correlation separation of 26.2 dB. From these sequences, 210 matched pilot–data pairs were chosen that have a zero DC component and a zero-lag cross correlation value of +2 or -2. A data symbol has a duration of 10 ms and is represented by one cycle of a primary ranging sequence. The pilot signal has a composite ranging sequence [18] that is constructed by representing a binary 1,800 long secondary ranging sequence in terms of a primary ranging sequence. Each pilot sequence has a unique secondary ranging sequence that is either a truncated m-sequence or a modulo-2 sum of two truncated m-sequences. To generate all the data and pilot sequences it is sufficient to store in memory a single 10,223 long Legendre sequence from which the sequences are derived with shift registers and modulo-2 adders.

The ranging sequences of the GPS L2C signals [65] are truncated m-sequences that have the same degree 27 generating polynomial but different initial phases. The data sequences have a length of 10,230 and a transmission time of 20 ms, which is also the symbol duration. The pilot channel sequences have a length of 767,250 and a transmission time of 1.5 seconds. The data and pilot channels are time multiplexed at chip level and the resulting stream transmitted at a chip rate of 1.023 MHz. The cross-correlation separation between any pair of ranging sequences and the separation between the main and minor peaks of autocorrelation functions are greater than 45 dB [56].

The GPS L5 primary ranging sequences [64] have a length of 10,230 and a chip rate of 10 MHz. The sequences are the modulo-2 sum of two polynomial degree 13 linear feedback shift register sequences, one of which is selectively delayed to generate a set of sequences. There are 37 pairs of sequences for use in the data and pilot components of satellite signals. The data and pilot components have composite ranging sequences formed by modulo-2 summing a secondary sequence onto a primary sequence. The main reason for using a secondary sequence here is to cause additional spreading of narrowband interference [49].

There is one 10 long secondary sequence for the data sequences and one 20 long secondary sequence for the pilot sequences. The data component is formed by modulo-2 summing a 100 Hz symbol stream onto the corresponding composite ranging sequence. The cross-correlation separation between sequences belonging to different pairs is 27 dB. The largest autocorrelation minor peak is 30 dB below the main peak. The correlation values are reported for zero Doppler difference only. Cross-correlation at other Doppler differences was considered unimportant by the signal designers due to the high chip rate which, in combination with a Doppler difference, makes the lifetime of an unfavorable sequence alignment short [50].

The design criteria of the Galileo E1 OS ranging sequences [55] are discussed in [133]. Five performance measures were established to take into account even and odd correlation functions and sensitivity to narrowband interference. The correlation functions were calculated both in absence and in presence of Doppler shift. Acquisition and tracking were addressed separately by calculating different weighted averages of the correlation functions. The Welch bound (19) was used to normalize the correlation functions and to discriminate poorly performing sequences from good ones. The sequence design itself is reported in [152]. Primary sequences, each 4.092 elements in length, were computer-searched by evaluating a set of initial sequences for their correlation properties, identifying the worst behaving sequences, changing elements randomly, and adopting the changes if they were for the better. The search yielded a set of 100 sequences, 50 each for the pilot and data components. The worst-case cross-correlation separation of the sequences is 21.49 dB. The transmission time of a primary sequence is 4 ms which is the same as the data symbol duration. A data symbol is represented by adding its binary value modulo-2 to one cycle of the primary sequence. The pilot sequence is a composite sequence obtained by adding the elements of a 25 long secondary sequence modulo-2 to 25 consecutive cycles of the primary sequence. The secondary sequence was obtained by computer search [54].

In [151], the design approach of the Galileo E1 OS sequences is compared to that

of the GPS L1C sequences by constructing new sequences of equal length and calculating their correlations at different Doppler differences. The established correlation magnitudes are mostly within one decibel from each other and the results are therefore inconclusive as to the superiority of either approach.

The Galileo E5a and E5b signals [55] have primary sequences 10,230 in length and one millisecond in duration. There are 200 sequences in total, 50 each for the data and pilot channels of the two signals. Two alternative sets of sequences are given, one based on computer search and another based on modulo-2 summing of two truncated Gold codes of polynomial order 14 [54]. In the E5a signal the data symbol and pilot sequence durations are 20 ms and 100 ms, respectively. In the E5b signal the durations are 4 ms and 100 ms. The pilot sequences are formed as composite sequences from the primary sequences and from secondary sequences that are unique to each satellite. A data symbol is represented by adding its binary value modulo-2 to a composite sequence that is formed using a fixed secondary sequence of length 4 for the E5a signal and of length 20 for the E5b signal. The secondary sequences were obtained by computer search [54]. Some correlation properties of the ranging sequences are evaluated in [68].

5.3 New Family of Ranging Sequences with Good Cross-Correlation Properties

In this section, we give the rationale behind our unequal length ranging sequences [P7] [163] and their use in GNSS pilot signals. In subsection 5.3.1 we show how worst-case cross-correlation can be reduced by using unequal sequence lengths and in subsection 5.3.2 we present an algorithm [P8] for practical sequence design.

5.3.1 General Case

We consider a set of M ranging sequences of pairwise relatively prime lengths L_k, $k = 1, \ldots, M$, that consist of binary elements c_i^k so that $c_i^k \in \{-1, +1\}$ and $i = 0, \ldots, L_k - 1$, and assume that a GNSS system employs pilot signals modulated with these sequences using a pulse waveform $h(t)$. Neglecting a multiplicative factor, the receiver baseband signals can then be expressed as

$$g_k(t) = \exp(j2\pi f_k t) \sum_{l=-\infty}^{\infty} \sum_{i=0}^{L_k-1} c_i^k h(t - (i + lL_k) T_c) , \tag{20}$$

where f_k is the Doppler shift and T_c is the chip period. It follows from the Chinese remainder theorem [46] that any pair of sequences of lengths L_m and L_n has a joint period of length $L_m L_n$. Equation (20) can be expressed in Fourier series form as

$$g_k(t) = \exp(j2\pi f_k t) \sum_{i=-\infty}^{\infty} d_i^k \exp\left(j2\pi \frac{it}{L_k T_c}\right) , \tag{21}$$

where the coefficients are given by

$$d_i^k = \frac{H\left(j2\pi \frac{i}{L_k T_c}\right)}{L_k T_c} \sum_{l=0}^{L_k-1} c_l^k \exp\left(-j2\pi \frac{il}{L_k}\right) . \tag{22}$$

In (22), $H(\cdot)$ denotes the Fourier transform of $h(\cdot)$. Defining the continuous time cross-correlation function between two pilot signals as

$$R_{m,n}(t) = \lim_{T\to\infty} \frac{1}{T} \int_{-\frac{T}{2}}^{\frac{T}{2}} g_m^*(u)\, g_n(u + t)\, du \tag{23}$$

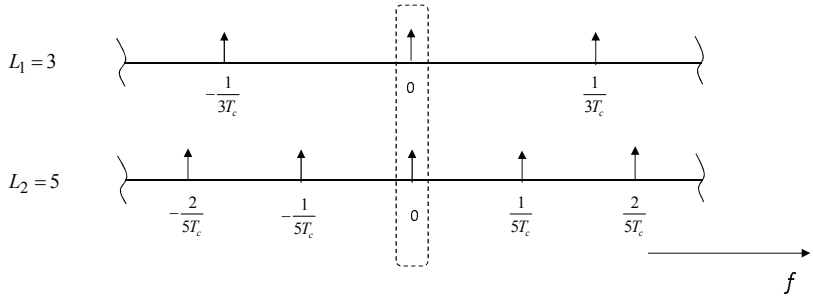

Fig. 8. *Alignment of spectral lines in the absence of Doppler difference.*

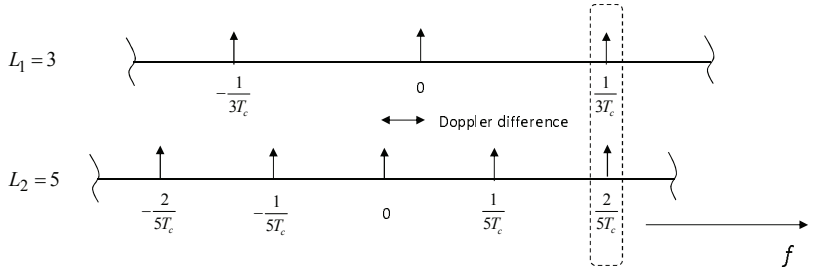

Fig. 9. *Alignment of spectral lines in the presence of Doppler difference.*

and substituting (21) into (23), it can be observed that only terms with identical frequency components in the signals contribute to $R_{m,n}(\cdot)$. Making the simplifying assumption that $H(\cdot)$ has a sharp cut-off at $f = 1/(2\,T_c)$, it is shown in [P7] that there is at most one pair of such components. The situation is illustrated schematically in Figs. 8 and 9 for the cases where a Doppler shift is absent or present, respectively. It is shown further in [P7] that, for $l \in \mathbb{Z}$,

$$|R_{m,n}(lT_c)| \leq \max_i |d_i^m| \max_j \left|d_j^n\right| . \tag{24}$$

The rhs of (24) represents the amplitude ratio of the highest possible cross-correlation component to the signal component in a perfect tracking situation where the desired and disturbing components have equal power. The tightest cross-correlation upper bound is obtained when the spectral power is evenly distributed among the spectral components of the signals. In this case,

$$|R_{m,n}(lT_c)| \leq \frac{1}{\sqrt{L_m L_n}} . \tag{25}$$

For a numerical example, assume that $L_m = 1,021$ and $L_n = 1,022$. The rhs of (25) then evaluates to 60.2 dB which is almost three times the worst-case cross-correlation separation of the GPS L1 C/A signals, which is 21.6 dB. This is quite a remarkable potential advantage considering the fact that the separation is achieved with sequences that are shorter than those of GPS L1 C/A.

Equation (20) assumes that the effect of code frequency offset can be neglected. The code frequency offset, also referred to as the code Doppler [36], and the carrier frequency offset, customarily referred to as the Doppler shift, represent the first and zeroth order baseband approximations, respectively, of a frequency dilatation or contraction caused by radial movement of transmitters and receivers with respect to each other. For channels with narrow bandwidth and slow movement the Doppler shift is often a sufficient approximation, while for wider bandwidths and faster movements the code frequency offset may also have to be con-

sidered. In the frequency domain, the effect of the Doppler shift is to move the origin, while the effect of the code frequency offset is to cause a scaling around the origin. The scaling constant is $(1 + f_k/f_0)$, where f_k is the Doppler shift and f_0 is the carrier frequency. For a signal with a spectral width of $1/T_c$, as is considered here, the scaling causes a mutual shift of frequency components that is shorter than or equal to $f_k/\left(f_0 T_c\right)$. Assume now that two signals with sequence lengths L_m and L_n have a mutual Doppler shift f_k such that they have a single pair of overlapping spectral components. Generalizing from Figs. 8 and 9 it can be seen, and further verified using the Chinese remainder theorem, that the frequency difference between any other pair of spectral components has a lower limit of $1/\left(L_m L_n T_c\right)$. In order for the code frequency offset not to cause a second pair of spectral components to overlap, it is necessary to require that

$$\frac{f_k}{f_0 T_c} < \frac{1}{L_m L_n T_c} \Leftrightarrow L_m L_n < \frac{f_0}{f_k}\,. \tag{26}$$

Assuming that $L_m \approx L_n$, it follows that (26) is satisfied when the sequences are shorter than $\sqrt{f_0/f_k}$. For longer sequences the cross-correlation performance can be expected to improve slower than (25) suggests. As a numerical example, for $f_0 = 1.57$ GHz and $f_k = 6$ kHz, the sequence lengths should be shorter than 511.

5.3.2 Sequence Design Using Truncated m-Sequences

Fig. 10 shows a flow diagram of a sub-optimal iterative algorithm for creating a set of N ranging sequences [P8]. A set of pairwise relatively prime numbers n_i, $i = 1, \ldots, N$, is first chosen and a long m-sequence then split into N non-overlapping segments that are chosen so as to minimize the strongest spectral component of the whole set. The splitting points found by the algorithm are stored for use as initialization values for sequence generators.

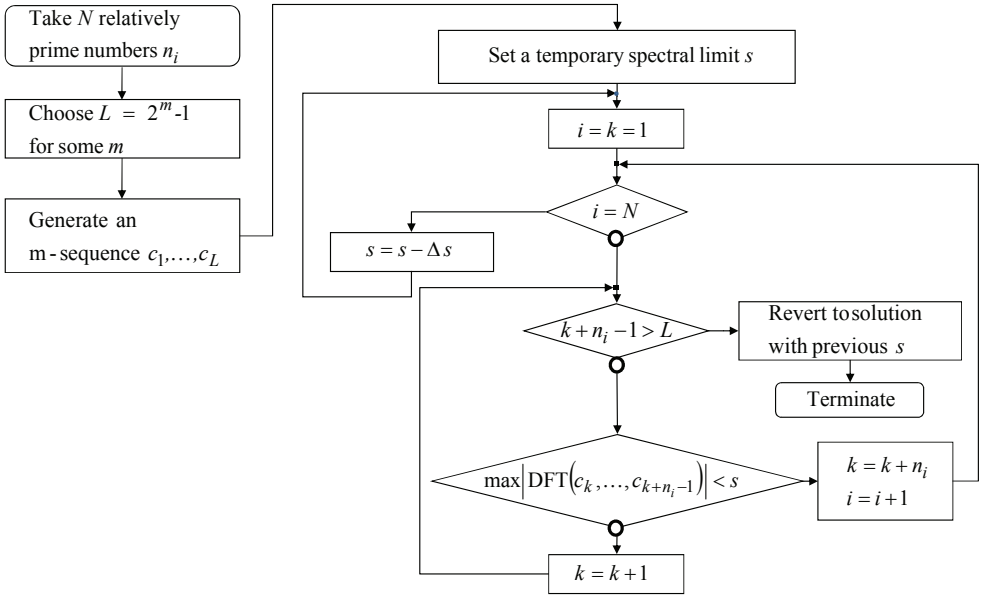

Fig. 10. *Algorithm for sequence family search.*

In [P8], a design example is given for a set of 40 balanced sequences that are obtained from an m-sequence based on the primitive generator polynomial $x^{24} + x^7 + x^2 + x + 1$ [104]. The sequence lengths were chosen from the range of 1,024 to 1,229 to achieve a resistance to narrowband interference equal or better than that of the GPS L1 C/A signals. The design resulted in a set of sequences with a cross-correlation separation of 47.7 dB. This figure is 12.5 dB below the theoretical maximum given by (25), but more than twice as high as that of the GPS C/A signals, and higher than that of the GPS L2C pilot signals that have much longer sequences.

5.4 Discussion

A new method of GNSS ranging sequence design has been presented that for the first time takes Doppler differences into account when minimizing cross-correlation. The method yields unprecedentedly short pilot sequences with cross-correlation maximums comparable to those of earlier proposals. The new sequences have a nearly flat spectrum by design, which is generally considered to give good resistance to narrowband interference. They also have a simple receiver implementation since a complete set of sequences can be generated with a single linear feedback shift register with fixed tap positions. Perhaps most importantly, however, the new sequences allow constructing pilot signals that have a short enough cycle time for direct acquisition. Direct acquisition of pilot components is attractive due to the fact that their coherent integration times are not limited by data bit transitions. To illustrate the proposed method, a design example has been presented where a set of sequences similar to those of GPS L1 C/A in length but with vastly better cross-correlation characteristics has been created.

Our key idea is to use unequal sequence lengths to achieve a worst-case cross-correlation magnitude that is typically tens of decibels lower than that achievable with previous methods. Additionally, practically zero cross-correlation can be achieved in the absence of Doppler difference if balanced sequences are used [P7]. Unequal sequence lengths are of decisive importance for the success of our method, while the choice of the sequences is less critical, because the required spectral smoothness can easily be achieved with computer search, as is seen from Table 1 in [P8]. The design example reported in the table also shows that constraining the design space to truncated m-sequences is not a serious limitation if a high enough polynomial order is chosen.

The idea of using several truncated m-sequences with a single generator polynomial has been proposed earlier for GPS L5 signals [50]. In that case, however, the sequence lengths were equal and Doppler differences were ignored when choosing the sequences. Another approach to computer optimized sequences, applied

in Galileo E1 and E5 signal design, is to conduct a computer search in an unconstrained design space and to store the resulting sequences verbatim in memory. The transmitter and receiver implementations of this approach are likely to be more expensive than those of the m-sequence based approach.

We have discussed our method in the context of pilot sequence design, which has allowed us to concentrate on even cross-correlation functions. However, GNSS signal design is not complete until also the data components meet system cross-correlation requirements. A full treatment of this problem would require a study of odd cross-correlation functions and the effects of modulation on spectral lines. The following observations can, however, be readily made. If the data and pilot sequences are the same length and their repetition rate is higher than the symbol rate, as is the case with the GPS L1 C/A signals, even correlation functions dominate cross-correlation. It may then be acceptable to optimize the signals for even cross-correlation only and ignore odd cross-correlation. Alternatively, one could use longer sequences for the data signals, which would provide more freedom for their optimization.

We have omitted the discussion of pulse waveforms and multipath propagation by assuming Nyquist pulses and chip-spaced sampling. Modern and modernized GNSS signals have complex pulse waveforms with multiple local maximums in their autocorrelation main peaks. Correctly resolving the related ambiguities in acquisition has proved to be a non-trivial problem in itself and has spawned several research programs that continue today [132] [76]. It has been pointed out [12] that the problems of ranging sequence and pulse waveform design are not entirely separable, and it is therefore thinkable that further progress can be made by joint optimization. A further complicating factor requiring more research is the RF envelope equalization scheme adopted by Galileo and shown to interfere with signal cross-correlation [152].

We have not addressed the impact of unequal code lengths on receiver design and complexity. The differences in code lengths would obviously require some

asymmetry to be introduced to acquisition electronics and tracking loops. How this can be accounted for in practical receiver design remains a matter of further research.

6. TIME TRANSFER AND RECEIVER SYNCHRONIZATION TECHNIQUES

In this section, a time transfer mechanism is proposed that allows a GNSS receiver to extract time information directly from a satellite signal that is too weak for bit detection. The information is determined from a new type of changing bit pattern embedded in the signal. The pattern is chosen so as to allow SNR improvement through coherent processing. The coherent processing requires good phase stability and the mechanism is therefore mainly suited for satellite signals that have a pilot component.

The chapter begins with an outline of related work in section 6.1. The proposed technique is presented in section 6.2. Section 6.3 concludes the discussion.

6.1 Related Work

6.1.1 Broadcasting of Time Information

A basic measurement made by a GNSS receiver is the apparent transit time of a signal from a satellite to the receiver, defined as the difference between signal reception time, as determined by the receiver clock, and the time of transmission (TOT) at the satellite, as marked on the signal [94]. To make it possible for a receiver to extract timing information from satellite signals, the signals are composed of blocks with an easily recognizable delimiter, referred to here as basic blocks. As an alternative to delimiters, a pilot signal can be provided that has its

periods synchronized with those of the basic blocks [66]. In GPS, GLONASS and Galileo the basic blocks are referred to as sub-frames [65], strings [38], and page parts [55], respectively. Some of the basic blocks contain TOT information that effectively establishes a sequence numbering for all of the blocks. The basic blocks are concatenated to form a nested hierarchy of signal structures that are transmitted cyclically at regular intervals. The highest level structure is called the navigation message. To illustrate the concept, the structure of the Galileo E1 navigation message is discussed in more detail below.

The Galileo E1 signal [55] consists of a data component and a pilot component that are code division multiplexed and modulated onto a carrier for transmission. The data component is formed of a sequence of navigation messages of type I/NAV that have the nested structure shown in Fig. 11. The structure allows satellites to broadcast information updates cyclically at three different repetition rates. There is no data content in the pilot signal that merely consists of a repeating sequence with a period of 100 ms. The pilot sequence is synchronized to the basic blocks of the data component.

The basic block of the I/NAV navigation message, shown in Fig. 12, is referred to as the page part, and has a duration of one second. It consists of a fixed synchronization pattern of ten symbols, 0101100000, and a changeable field of 240 symbols. The changeable field carries 114 bits of control, time, satellite, and atmospheric information that is subjected to FEC encoding and interleaving before transmission. The FEC encoding comprises rate 1:2, constraint length 7 convolutional encoding. The synchronization pattern is not encoded. Page parts always appear in pairs, referred to as pages.

A sub-frame consists of fifteen pages. In each sub-frame, TOT information is transmitted in part on the third page and in full on the thirteenth page. Full TOT information is thus transmitted once and partial TOT information twice every 30 seconds. The full TOT information consists of a 12 bit week number that has a roll-over period of 4096 weeks and a 20 bit time of week (TOW) indicator that

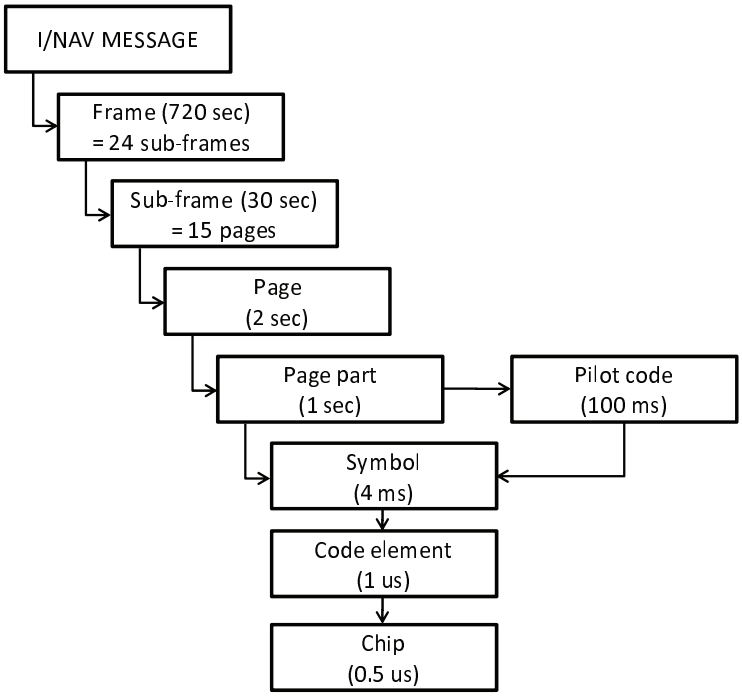

Fig. 11. *Galileo E1 navigation message.*

Sync.	I/NAV Page Part (even or odd symbols)
10	240

Total (symb)
250

I/NAV Word	Tail
114	6

Total (bits)
120

Fig. 12. *Galileo I/NAV page part layout.*

has a resolution of one second and a roll-over period of one week. The partial TOT information consists of the TOW indicator only.

6.1.2 Time Recovery from Nominal Signal

If a good quality satellite signal is available, time recovery can be based solely on its data component. If a receiver is able to process the pilot signal, it may benefit from the fact that the navigation message and its substructures, such as the page parts of the Galileo E1 data message, are synchronized to the pilot sequence. The receiver would presumably conduct the time recovery by proceeding along the following steps:

- Acquiring the satellite signal by synchronizing to the carrier frequency, carrier phase, and sequence timing of its data component. Optionally, synchronizing also to the sequence timing of its pilot component and using the pilot component to improve the synchronization to the carrier frequency and carrier phase.
- Observing the data signal until a synchronization pattern is detected. Using the pattern to establish synchronization to the boundaries of basic blocks. If available, using the sequence timing of the pilot signal to limit the search range.
- Receiving and decoding the contents of basic blocks until TOT information is encountered.

6.1.3 Time Recovery from Weak Signal

If the SNR of the satellite signal is significantly below nominal, the steps in 6.1.2 cannot be completed because bit errors prevent reliable decoding of signal contents. Due to the low modulation rates of GNSS signals, it may still be possible to

track their sequence timing. We then say that the SNR is above sequence tracking threshold but below data decoding threshold. For the GPS L5 data signal, for example, C/N_0 thresholds of 22.1 dB-Hz and 25.6 dB-Hz have been reported for sequence tracking and data decoding, respectively [15]. If the symbol rate of the signal is higher than its bit rate, as is the case with the GPS L1 C/A, GPS L5, and Galileo E5 signals, bit edge timing needs to be extracted before data decoding becomes possible. There are several ways to do this after the sequence timing has been established [11, 86], which suggests that also a third threshold, bit synchronization threshold, can be meaningfully defined.

Assume that the SNR of a satellite signal lies between the sequence tracking and data decoding thresholds and that the receiver is tracking both data and pilot signals. Assume further that the receiver has valid satellite trajectory information, either from an assistance network or from a recent successful download from a satellite. Due to the lack of data modulation in the pilot signal, the receiver is likely to obtain a relatively noiseless carrier phase estimate from the signal by using a narrowband tracking loop. Using the estimate, the receiver is able to demodulate the data channel coherently, but is not likely to detect ordinary data bits correctly due to the low SNR of the demodulation result. However, a cyclically repeating pattern, such as the Galileo E1 synchronization pattern, can be received multiple times and the SNR of the demodulation result improved by additive combining. As a consequence, the receiver may be able to synchronize to the pattern. In terms of Galileo E1 this means that the receiver is able to synchronize to page part boundaries and by so doing learn the TOT up to an integer number of page part durations. The full TOT remains unknown for the receiver, however, since it cannot identify the page parts by decoding the TOT information in their data fields. If the missing information were available, the receiver would be able to solve the navigation equations for its current position. It may be noted that the missing information is equivalent to having available any unique set of sequence identifiers for the page parts.

Three techniques, referred to as time stamp recovery techniques, have been pro-

posed for identifying the basic blocks of navigation messages in weak signal conditions [4]:

- Base station synchronization. A cellular network operator can synchronize base stations with GNSS time and include the timing information into assistance messages.

- Navigation data alignment. A cellular network operator can transmit navigation bits or symbols verbatim in assistance messages. By aligning them with a demodulated satellite signal, a receiver can determine the TOT of the latter [137].

- Enhanced triangulation. If the set of navigation equations is over-determined, it may be solvable even if TOT information is only available up to an integer number of basic block durations [138].

There are significant limitations to the use of these techniques. All of them require assistance information from outside the GNSS system. Such information is available only by using a separate radio transceiver, only for account holders, and only in a small fraction of the total GNSS coverage area. Base station synchronization incurs an additional cost from equipping cellular base stations with GNSS receivers. A prerequisite for navigation data alignment is that at least part of the navigation message can be predicted by the assistance network and that a reasonably accurate time estimate already exists in the receiver. This technique is also complicated by the FEC coding of some GNSS signals. Enhanced triangulation requires that the receiver is able to receive at least five satellite signals, which limits its applicability especially in areas where signal propagation is obstructed.

Synchronization Sequence	Time Label *i*	Navigation Data	...	Time Label *i*+ 9	Navigation Data
0101100000	$c_1(i)$, $c_2(i)$, $c_3(i)$	---		$c_1(i+9)$, $c_2(i+9)$, $c_3(i+9)$	---

Fig. 13. *Galileo basic block with proposed time tabels.*

6.2 New Time Transfer Technique for Weak Signals

6.2.1 Time Label

Consider a GNSS satellite signal with basic blocks as explained in section 6.1.1 and binary modulation symbols. Let $c_1(\cdot)$, $c_2(\cdot)$,...,$c_n(\cdot)$ be n maximum-length binary linear shift-register sequences [62], or m-sequences, with pairwise relatively prime periods ν_1, ν_2,...,ν_n. The choice of n will be discussed later. We propose to include the n–tuple $\{c_1(i), c_2(i),\ldots, c_n(i)\}$ at one or multiple fixed locations in the symbol sequence of each basic block. The index i denotes the sequence number of the n–tuple with an initial point known to the receiver. It follows from the Chinese remainder theorem [46] that the cycle length ν of the sequence of the n–tuples is the product of the cycle lengths of the m–sequences: $\nu = \prod_{i=1}^{n} \nu_i$.

Using an example discussed in [P9], where $n = 3$, $\nu_1 = 127$, $\nu_2 = 255$, and $\nu_3 = 511$, an n–tuple with three symbols, if included ten times in each Galileo E1 page part by eliminating some data content, would cover a period of 19.15 days, thus obviating the TOW indicator. The proposed structure of the basic block with its contained n–tuples, referred to here as time labels, is outlined in Fig. 13.

The technique proposed here was inspired by but is not identical with the so called rapid acquisition sequences that have been proposed for the synchronization of noisy signals by Titsworth [141], Stiffler [135], and Bluestein [26].

6.2.2 Time Recovery

To generate $c_i(\cdot)$, a k_i-bit shift register is needed such that $\nu_i = 2^{k_i} - 1$. If the satellite signal is strong enough for reliable symbol detection, it is sufficient to collect $\max_{i=1}^{n} k_i$ consecutive time labels to detect the phases of the m–sequences, since the phase of an m-sequence generated by a k-bit shift register is determined as soon as k consecutive bits are known. Evoking again the Chinese remainder theorem, we observe that the phases of the m–sequences fully determine the phase of the (much longer) sequence of n-tuples, thus allowing the receiver to resolve the sequence numbering of the basic blocks.

If the SNR of the satellite signal does not allow reliable detection of individual symbols, several symbol samples can be collected and coherently processed to detect the phases of the m–sequences. A prerequisite for the coherent processing is a stable phase reference that can, under favorable conditions, be obtained from the pilot component. An uncomplicated way of detecting the phase of an m–sequence is to collect samples over an integer number of cycles, to correlate them with a local replica of the sequence, and to detect the correlation maximum. Due to the low minor peaks of cyclic autocorrelation functions of m–sequences, a considerable processing gain and increase of sensitivity can be obtained by such processing.

6.2.3 Weak Signal Performance

Using the union bound approximation as in [26], it shown in [P9] that the probability of timing failure can be expressed as

$$P_e = \sum_{i=1}^{n} \frac{\nu_i}{\sqrt{2\pi}} \int_{\sqrt{\frac{E_b}{N_0} A_i \nu_i}}^{\infty} e^{-x^2/2}\, dx\,, \tag{27}$$

where A_i is the number of cycles of sequence $c_i(\cdot)$ that are received, E_b is the

symbol energy, and N_0 is the single-sided noise power spectral density. Continuing the example of section 6.2.1 by putting $n = 3$, $\nu_1 = 127$, $\nu_2 = 255$, $\nu_3 = 511$, $A_1 = 4$, $A_2 = 2$, and $A_3 = 1$, a success rate of 95% is achieved at an E_b/N_0 of -15.4 dB, a figure that is clearly below the data detection threshold. For Galileo in particular, the figure corresponds to a C/N_0 of 11.6 dB-Hz, which is far below the nominal level of 47 dB-Hz. The time needed to collect the timing information is 51 s, one complete cycle of $c_3(\cdot)$.

6.3 Discussion

The capacity of the GNSS broadcast channel is low and ought to be carefully allocated between time transfer and navigation data transmission. In earlier work, time information is embedded in data fields and cannot be received if the signal SNR is below the data detection threshold. This is unfortunate since the time information cannot easily be supplied from other sources due to the high timing accuracy required. To improve the situation, a novel time transfer mechanism has been presented that is tolerant of low SNR.

The proposed mechanism may require trading off some bits from data transmission, as is the case in the example discussed in 6.2.1. We believe that such a trade-off is well grounded since, in contrast to the time information, navigation data is long-lived and available from terrestrial sources for a growing number of GNSS receivers. Also, some more recent signal proposals (GPS L2C in [65]) show that a GNSS member system can be implemented with a low navigation data bit rate, further attesting to the feasibility of our proposal.

The amount of transmission power that needs to be allocated to the proposed mechanism depends on the required minimum roll-over period and on the allowed maximum latency for time retrieval. There are two central design parameters: the number of m-sequences and the density of time labels in the symbol stream. In the example above, 6 % of the combined data and pilot channel trans-

mission power was used to obtain a roll-over period of 19.15 days. Since this period exceeds that of the Galileo TOW indicator, the latter could be eliminated. Adding a fourth m-sequence of length 2047 would extend the roll-over period to 5610 weeks, allowing also the week number of the Galileo signal to be eliminated, thus making full time retrieval possible in weak signal conditions. Assuming that the density of time labels remains unchanged, the power allocation in this case would be 8 %.

7. CONCLUSIONS

In this thesis, the acquisition of weak GNSS signals has been studied with special attention to mobile receivers and acquisition assistance. Good performance with weak signals is important since mobile receivers are used for emergency calls, route guidance, and other purposes where time is premium and the available GNSS signals often heavily attenuated. Acquisition performance is attributable to both satellite signals and receiver algorithms. Signals and algorithms that enable fast and reliable acquisition also contribute to energy conservation in battery powered equipment.

New metrics have been proposed to characterize the acquisition performance of GNSS signals by quantifying their susceptibility to path loss due to obstructions. The metrics are independent of receiver design but take eventual network assistance into account. They should allow satellite operators and receiver designers to compare GNSS signals for their acquisition performance.

Two new methods for GNSS signal design have been introduced, one to obtain short ranging sequences with good cross-correlation properties irrespective of the high Doppler frequency shifts that are present in GNSS channels and another to encode system time into GNSS signal frames for time retrieval from heavily attenuated signals. The motivation for striving after short ranging sequences is ease of acquisition. Robust time labeling is needed immediately after acquisition to allow a receiver to solve its position in the frequently encountered situation where absolute time is missing and satellite signals are weak. In contrast with earlier approaches, the proposed ranging sequences address Doppler shifts by

design and not by blindly increasing sequence length. The novelty of the time labels is the possibility to exploit processing gain to improve signal to noise ratio.

Two acquisition algorithms have been presented, one to increase the success rate of parallel search and another to improve the operating characteristics of serial search. Both operational modes are common in mobile receivers. The former algorithm constitutes a structural improvement over previous approaches and has alternative embodiments, some of which have been evaluated in this thesis and shown to significantly increase the probability of signal detection. The latter algorithm is novel in that it traverses the acquisition uncertainty space in a dynamically adaptive order as opposed to a static order. It exhibits significant performance advantages over a reference algorithm for a wide range of parameters. It also offers several operational advantages that result from using Bayesian probability updates in the collection of signal statistics.

BIBLIOGRAPHY

[1] *Requirements for support of assisted global positioning system (A-GPS), FDD (release 8)*, 3rd generation partnership project, Dec. 2008, 3GPP TS 25.171 V8.0.0.

[2] *Terminal conformance specification – assisted global positioning system (A-GPS), FDD (release 8)*, 3rd generation partnership project, Mar. 2009, 3GPP TS 34.171 V8.1.0.

[3] M. Abramowitz and I. A. Stegun, Eds., *Handbook of Mathematical Functions*. Dover Publications, 1970.

[4] N. Agarwal et al., "Algorithms for GPS operation indoors and downtown," *GPS Solutions*, vol. 6, no. 3, pp. 149–160, Dec. 2002.

[5] D. Akopian, "Fast FFT based GPS satellite acquisition methods," *IEE Proc.-Radar Sonar Navig.*, vol. 152, no. 4, pp. 277–286, Aug. 2005.

[6] D. Akopian and S. Agaian, "Fast and parallel matched filters in time domain," in *Proc. ION GNSS 2004*, Long Beach, CA, USA, Sep. 21–24 2004, pp. 491–500.

[7] ——, "Fast-matched filters in time domain for global positioning system receivers," *IEE Proc.-Radar Sonar Navig.*, vol. 153, no. 6, pp. 525–531, Dec. 2006.

[8] D. Akopian, I. Kontola, H. Valio, and S. Turunen, *Method in a receiver and a receiver. US Patent No. US 6,909,738*, July 2005.

[9] D. Akopian, S. Turunen, S. Pietilä, and H. Valio, *Acquisition of a code modulated signal. US Patent No. US 7,336,696*, Feb. 2008.

[10] A. A. Alaqeeli, "Global positioning system signal acquisition and tracking using field programmable gate arrays," Ph.D. dissertation, Ohio University, Nov. 2002.

[11] M. Anghileri, T. Pany, J.-H. Won, and G. W. Hein, "An algorithm for bit synchronization and signal tracking in software GNSS receivers," in *Proc. ION GNSS 2006*, Fort Worth, TX, USA, Apr. 26–29 2006, pp. 1836–1848.

[12] J.-Á. Ávila-Rodríguez, S. Wallner, and G. W. Hein, "How to optimize GNSS signals and codes for indoor positioning," in *Proc. ION GNSS 2006*, Fort Worth, TX, USA, Apr. 26–29 2006, pp. 2418–2426.

[13] A. S. Ayaz, T. Pany, and B. Eissfeller, "Performance of assisted acquisition of the L2CL code in a multi-frequency software receiver," in *Proc. ION GNSS 2007*, Fort Worth, TX, USA, Sep. 25–28 2007, pp. 1830–1838.

[14] F. Bastide, "Galileo E5a/E5b and GPS L5 acquisition time statistical characterization and application to civil aviation," in *Proc. ION GNSS 2004*, Long Beach, CA, USA, Sep. 21–24 2004, pp. 2623–2635.

[15] F. Bastide, O. Julien, C. Macabiau, and B. Roturier, "Analysis of L5/E5 acquisition, tracking and data demodulation thresholds," in *Proc. ION GPS 2002*, Portland, OR, USA, Sep. 24–27 2002, pp. 2196–2207.

[16] C. Baum and V. Veeravalli, "Hybrid acquisition schemes for direct sequence CDMA systems," in *Proc. IEEE ICC 94*, New Orleans, LA, USA, May 1–5 1994, pp. 1433–1437 vol. 3.

[17] C. Baum and V. V. Veeravalli, "A sequential procedure for multihypothesis testing," *IEEE Trans. Inf. Theory*, vol. 40, no. 6, pp. 1994–2007, Nov. 1994.

[18] M. Beale and T. C. Tozer, "A class of composite sequences for spread-spectrum communications," *Computers and Digital Techniques*, vol. 2, no. 2, pp. 87–92, Apr. 1979.

[19] P. Bellavista, A. Küpper, and S. Helal, "Location-based services: back to the future," *IEEE Pervasive Comput.*, vol. 7, no. 2, pp. 85–89, Apr.-June 2008.

[20] M. Ben-Bassat, "Myopic policies in sequential acquisition," *IEEE Trans. Comput.*, vol. 27, no. 2, pp. 170–174, Feb. 1978.

[21] J. O. Berger, *Statistical decision theory and bayesian analysis*. Springer, 2006.

[22] D. P. Bertsekas, *Dynamic programming: Deterministic and stochastic models*. Prentice Hall, 1987.

[23] J. W. Betz, "The offset carrier modulation for GPS modernization," in *Proc. ION NTM 1999*, San Diego, CA, USA, Jan. 25–27 2005, pp. 639–648.

[24] J. W. Betz et al., "Description of the L1C signal," in *Proc. ION GNSS 2006*, Fort Worth, TX, USA, Apr. 26–29 2006, pp. 2080–2091.

[25] D. Blackwell and M. A. Girshick, *Theory of games and statistical decisions*. Wiley, 1954.

[26] L. I. Bluestein, "Interleaving of pseudorandom sequences for synchronization," *IEEE Trans. Aerosp. Electron. Syst.*, vol. 4, no. 4, pp. 551–556, July 1968.

[27] D. Borio, "A statistical theory for GNSS signal acquisition," Ph.D. dissertation, Politecnico di Torino, Mar. 2008.

[28] D. Borio, L. Camoriano, and L. L. Presti, "Impact of the acquisition searching strategy on the detection and false alarm probabilities in a CDMA receiver," in *Proc. IEEE/ION PLANS 2006*, San Diego, CA, USA, Apr. 25–27 2006, pp. 1000–1107.

[29] ——, "Impact of GPS acquisition strategy on decision probabilities," *IEEE Trans. Aerosp. Electron. Syst.*, vol. 44, no. 3, pp. 996–1011, July 2008.

[30] D. Borio, C. Mongrédien, and G. Lachapelle, "New L5/E5a acquisition algorithms: analysis and comparison," in *Proc. 10th IEEE International Symposium on Spread Spectrum Techniques and Applications*, Bologna, Italy, Aug. 25–28 2008, pp. 1–5.

[31] K. Borre, D. M. Akos, N. Bertelsen, P. Rinder, and S. H. Jensen, *A software-defined GPS and Galileo receiver*. Birkhäuser, 2007.

[32] W. R. Braun, "Performance analysis for the expanding search PN acquisition algorithm," *IEEE Trans. Comput.*, vol. 30, no. 3, pp. 424–435, Mar. 1982.

[33] J. Bussgang and D. Middleton, "Optimum sequential detection of signals in noise," *IRE Trans. Inform. Theory*, vol. 1, pp. 5–18, Dec. 1955.

[34] D. A. Castañon, "Optimal search strategies in dynamic hypothesis testing," *IEEE Trans. Syst., Man, Cybern.*, vol. 25, no. 7, pp. 1130–1138, 1995.

[35] K. K. Chawla and D. V. Sarwate, "Parallel acquisition of PN sequences in DS/SS systems," *IEEE Trans. Commun.*, vol. 42, no. 5, pp. 2155–2164, May 1994.

[36] U. Cheng, W. J. Hurd, and J. I. Statman, "Spread-spectrum code acquisition in the presence of Doppler shift and data modulation," *IEEE Trans. Commun.*, vol. 38, no. 2, pp. 241–250, Feb. 1990.

[37] G. M. Comparetto, "A generalized analysis for a dual threshold sequential detection PN acquisition receiver," *IEEE Trans. Commun.*, vol. 35, no. 9, pp. 956–960, Sep. 1987.

[38] *Glonass Interface Control Document*, Coordination Scientific Information Center, Moscow, 2002, version 5.0.

[39] G. E. Corazza, C. Palestini, R. Pedone, and M. Villanti, "Galileo primary code acquisition based on multi-hypothesis secondary code ambiguity elimination," in *Proc. ION GNSS 2007*, Fort Worth, TX, USA, Sep. 25–28 2007, pp. 2459–2465.

[40] G. E. Corazza and R. Pedone, "Generalized and average likelihood ratio testing for post detection integration," *IEEE Trans. Commun.*, vol. 55, no. 11, pp. 2159–2171, Nov. 2007.

[41] L. A. Cox, X. Sun, and Y. Qiu, "Optimal and heuristic search for a hidden object in one dimension," in *Proc. IEEE Int. Conf. on Humans, Information and Technology*, San Antonio, TX, USA, Oct. 1994, pp. 1252–1256 vol. 2.

[42] L. de Haan and A. Ferreira, *Extreme value theory: An introduction*. Springer, 2006.

[43] W. De Wilde et al., "Fast signal acquisition technology for new GPS/Galileo receivers," in *Proc. IEEE/ION PLANS 2006*, San Diego, CA, USA, Apr. 25–27 2006, pp. 1074–1079.

[44] M. H. DeGroot, *Optimal statistical decisions*. Wiley, 2004.

[45] Z. Deng, D. Zou, J. Huang, X. Chen, and Y. Yu, "The assisted GNSS boomed up location based services," in *Proc. IEEE WiCom 2009*, Beijing, China, Sep. 24–26 2009, pp. 1–4.

[46] W. E. Deskins, *Abstract Algebra*. Dover Publications, 1995.

[47] D. M. DiCarlo and C. L. Weber, "Statistical performance of single dwell serial synchronization systems," *IEEE Trans. Commun.*, vol. 28, no. 8, pp. 1382–1388, Aug. 1980.

[48] ——, "Multiple dwell serial search: performance and application to direct sequence code acquisition," *IEEE Trans. Commun.*, vol. 31, no. 5, pp. 650–659, May 1983.

[49] A. J. V. Dierendonck, C. Hegarty, W. Scales, and S. Ericson, "Signal specification for the future GPS civil signal at L5," in *Proc. IAIN World Congress and ION AM 2000*, San Diego, CA, USA, June 26–28 2000, pp. 232–241.

[50] A. J. V. Dierendonck and J. J. Spilker, Jr., "Proposed civil GPS signal at 1176.45 MHz: in-phase/quadrature codes at 10.23 MHz chip rate," in *Proc. ION AM 1999*, Cambridge, MA, USA, June 28–30 1999, pp. 761–770.

[51] V. Eerola, "Rapid parallel GPS signal acquisition," in *Proc. ION GPS 2000*, Salt Lake City, UT, USA, Sep. 19–22 2000, pp. 810–816.

[52] V. Eerola, S. Pietilä, and H. Valio, "A novel flexible correlator architecture for GNSS receivers," in *Proc. ION NTM 2007*, San Diego, CA, USA, Jan. 22–24 2007, pp. 681–691.

[53] H. A. El-Natour, A.-C. Escher, C. Macabiau, and M.-L. Boucheret, "Impact of multipath and cross-correlation on GPS acquisition in indoor environments," in *Proc. ION NTM 2005*, San Diego, CA, USA, Jan. 24–26 2005, pp. 1062–1070.

[54] "Galileo signal-in-space design," http://www.galileoic.org/la/files/SignalPresentation_MasterPolito_9thMay2005.pdf, ESA, May 2005.

[55] *European GNSS (Galileo) Open Service Signal in Space Interface Control Document*, European Union, Feb. 2010, OD SIS ICD, Issue 1.

[56] R. D. Fontana, W. Cheung, P. M. Novak, and T. A. Stansell, Jr., "The new L2 civil signal," in *Proc. ION GPS 2001*, Salt Lake City, UT, USA, Sep. 11–14 2001, pp. 617–631.

[57] H. Fukumasa, R. Kohno, and H. Imai, "Design of pseudonoise sequences with good odd and even correlation properties for DS/CDMA," *IEEE J. Sel. Areas Commun.*, vol. 12, no. 5, pp. 828–836, June 1994.

[58] C. Gernot, K. O'Keefe, and G. Lachapelle, "Comparison of L1 C/A and L2C combined acquisition techniques," in *Proc. ENC 2008*, Toulouse, France, Apr. 23–25 2008, pp. 1–9.

[59] G. Gibbons, "360 degrees - Russia dwells on GLONASS future," *Inside GNSS*, vol. 3, no. 2, pp. 12–27, Mar./Apr. 2008.

[60] R. Gold, "Optimal binary sequences for spread spectrum multiplexing," *IEEE Trans. Inf. Theory*, vol. 13, no. 5, pp. 619–621, Oct. 1967.

[61] J. Goldhirsh and W. J. Vogel, "Handbook of propagation effects for vehicular and personal mobile satellite systems," Johns Hopkins University, Tech. Rep. A2A-98-U-0-021, Dec. 1998.

[62] S. W. Golomb, *Shift Register Sequences*. Aegean Park Press, 1982.

[63] T. Göze, Ö. Bayrak, M. Barut, and M. O. Sunay, "Secure user-plane location (SUPL) architecture for assisted GPS (A-GPS)," in *Proc. IEEE ASMS 2008*, Bologna, Italy, Aug. 26–28 2008, pp. 229–234.

[64] *Navstar GPS Space Segment / User Segment L5 Interfaces*, GPS Navstar JPO, Sep. 2005, IS-GPS-705.

[65] *Navstar GPS Space Segment / Navigation User Interfaces*, GPS Navstar JPO, Mar. 2006, IS-GPS-200 Revision D.

[66] *Navstar GPS Space Segment / User Segment L1C Interfaces*, GPS Navstar JPO, Sep. 2008, IS-GPS-800.

[67] E. J. Gumbel, Ed., *Statistics of Extremes*. Dover Publications, 2004.

[68] M. Hadef, J. Reiss, and X. Chen, "Chaotic codes for satellite navigation systems," in *Proc. ION AM 2007*, Cambridge, MA, USA, Apr. 23–25 2007, pp. 213–219.

[69] B. M. Hannah, "Modelling and simulation of GPS multipath propagation," Ph.D. dissertation, Queensland university of technology, Mar. 2001.

[70] C. Hegarty and A. J. Van Dierendonck, "Civil GPS/WAAS signal design and interference environment at 1176.45 MHz: results of RTCA SC159 activities," in *Proc. ION GPS '99*, Nashwille, TN, USA, Sep. 14–17 1999, pp. 1727–1735.

[71] C. J. Hegarty and E. Chatre, "Evolution of the global navigation satellite system (GNSS)," *Proc. IEEE*, vol. 96, no. 12, pp. 1902–1917, Dec. 2008.

[72] G. W. Hein, "Towards a GNSS system of systems," in *Proc. ION GNSS 2007*, Fort Worth, TX, USA, Sep. 25–28 2007, pp. 22–30.

[73] G. W. Hein, J.-Á. Ávila-Rodríguez, and S. Wallner, "The ~~DaVinci~~ Galileo code and others," *Inside GNSS*, vol. 1, no. 6, pp. 62–74, Sep. 2006.

[74] G. W. Hein and S. Wallner, "Development and design of Galileo," in *Proc. ION AM 2005*, Cambridge, MA, USA, June 27–29 2005, pp. 94–104.

[75] V. Heiries, J.-Á. Ávila-Rodríguez, M. Irsigler, G. W. Hein, E. Rebeyrol, and D. Roviras, "Acquisition performance analysis of composite signals for the L1 OS optimized signal," in *Proc. ION GNSS 2005*, Long Beach, CA, USA, Sep. 13–16 2005, pp. 877–889.

[76] V. Heiries, D. Roviras, L. Ries, and V. Calmettes, "Analysis of non ambiguous BOC signal acquisition performance," in *Proc. ION GNSS 2004*, Long Beach, CA, USA, Sep. 21–24 2004, pp. 2611–2622.

[77] J. Holmes and C. C. Chen, "Acquisition time performance of PN spread-spectrum systems," *IEEE Trans. Commun.*, vol. 25, no. 8, pp. 778–784, Aug. 1977.

[78] J. H. J. Iinatti, "Threshold setting principles in code acquisition of DS-SS signals," *IEEE J. Sel. Areas Commun.*, vol. 18, no. 1, pp. 62–72, Jan. 2000.

[79] T. Jost, M. Khider, and E. A. Sanchez, "Characterization and modeling of the indoor pseudorange error using low cost receivers," in *Proc. ION ITM 2010*, San Diego, CA, USA, Jan. 25–27 2010, pp. 277–284.

[80] T. Jost and W. Wang, "Satellite-to-indoor broadband channel measurements at 1.51 GHz," in *Proc. ION ITM 2009*, Anaheim, CA, USA, Sep. 26–28 2009, pp. 777–783.

[81] J. B. Kadane, "Optimal whereabouts search," *Operations Research*, vol. 19, no. 4, pp. 894–904, 1994.

[82] B.-J. Kang and I.-K. Lee, "A performance comparison of code acquisition techniques in DS-CDMA system," *Wireless Personal Communications*, vol. 25, pp. 163–176, 2003.

[83] E. D. Kaplan, Ed., *Understanding GPS Principles and Applications*. Artech House Publishers, 1996.

[84] S. M. Kay, *Fundamentals of statistical signal processing: Detection theory*. Prentice Hall, 1993, vol. 2.

[85] ——, *Fundamentals of statistical signal processing: Estimation theory*. Prentice Hall, 1993, vol. 1.

[86] M. Kokkonen and S. Pietilä, "A new bit synchronization method for a GPS receiver," in *Proc. IEEE PLANS 2002*, Palm Springs, CA, USA, Apr. 15–18 2002, pp. 85–90.

[87] A. Konovaltsev, H. Denks, A. Hornbostel, M. Soellner, and M. Witzke, "General framework for acquisition performance analysis with application to GALILEO signals," in *Proc. ION GNSS 2006*, Fort Worth, TX, USA, Sep. 26–29 2006, pp. 1276–1287.

[88] N. F. Krasner, *GPS receiver and method for processing GPS signals. US Patent No. US 5,781,156*, July 1998.

[89] F. Liese and K.-J. Miescke, *Statistical decision theory*. Springer, 2008.

[90] E. S. Lohan, A. Burian, and M. Renfors, "Acquisition of Galileo signals in hybrid double-dwell approaches," in *ESA NAVITEC 2004*, Noordwijk, The Netherlands, Dec. 8–10 2004, pp. 1–6.

[91] ——, "Low-complexity unambiguous acquisition methods for BOC-modulated CDMA signals," *Int. J. Commun. Syst. Network*, vol. 26, no. 6, pp. 503–522, Oct. 2008.

[92] F. Macchi, D. Borio, M. G. Petovello, and G. Lachapelle, "New galileo L1 acquisition algorithms: Real data analysis and statistical characterization," in *Proc. ENC 2008*, Toulouse, France, Apr. 22–25 2008, pp. 1–10.

[93] R. N. McDonough and A. D. Whalen, *Detection of signals in noise*. Academic Press, 1995.

[94] P. Misra and P. Enge, *Global Positioning System*. Ganga-Jamuna Press, 2006.

[95] M. Monnerat, "AGNSS standardization," *Inside GNSS*, vol. 3, no. 5, pp. 22–33, July/Aug. 2008.

[96] C. O'Driscoll, "Performance analysis of the parallel acquisition of weak GPS signals," Ph.D. dissertation, National University of Ireland, Jan. 2007.

[97] N. O'Mahony, C. O'Driscoll, and C. C. Murphy, "Performance of sequential probability ratio test for GPS acquisition," in *Proc. IEEE ICC 2009*, Dresden, Germany, June 14–18 2009, pp. 1–6.

[98] *UserPlane location protocol: Draft version 2.0*, Open Mobile Alliance, Nov. 2009, OMA-TS-ULP-V2_0-20091118-D.

[99] M. Paonni, V. Kropp, A. Teuber, and G. W. Hein, "A new statistical model of the indoor propagation channel for satellite navigation," in *Proc. ION GNSS 2008*, Savannah, GA, USA, Sep. 16–19 2009, pp. 1748–1757.

[100] B. W. Parkinson and J. J. Spilker, Jr., Eds., *Global positioning system: theory and applications*. American institute of aeronautics and astronautics, Inc., 1996, vol. I, ch. GPS signal structure and theoretical performance.

[101] K. R. Pattipati and M. G. Alexandridis, "Application of heuristic search and information theory to sequential fault diagnosis," *IEEE Trans. Syst., Man, Cybern.*, vol. 20, no. 4, pp. 872–887, 1990.

[102] R. Pedone, M. Villanti, and G. E. Corazza, "MAX search with parallel verification for frame synchronization," in *Proc. IEEE GLOBECOM 2005*, St. Louis, MO, USA, Nov. 28–Dec. 2 2005, pp. 1299–1303.

[103] B. Peterson, D. Bruckner, and S. Heye, "Measuring GPS signals indoors," in *Proc. ION GPS 1997*, Kansas City, MO, USA, Sep. 16–19 1997, pp. 615–624.

[104] W. W. Peterson and E. J. Weldon, Eds., *Error-correcting codes*. The MIT Press, 1972.

[105] A. Polydoros and S. Glisic, "Code synchronization: a review of principles and techniques," in *Proc. IEEE ISSSTA '94*, Oulu, Finland, July 4–6 1994, pp. 115–137.

[106] A. Polydoros and M. K. Simon, "Generalized serial search code acquisition: the equivalent circular state diagram approach," *IEEE Trans. Commun.*, vol. 32, no. 12, pp. 1260–1268, Dec. 1984.

[107] A. Polydoros and C. L. Weber, "A unified approach to serial search spread-spectrum code acquisition–part I: General theory," *IEEE Trans. Commun.*, vol. 32, no. 5, pp. 542–549, May 1984.

[108] ——, "A unified approach to serial search spread-spectrum code acquisition–part II: A matched-filter receiver," *IEEE Trans. Commun.*, vol. 32, no. 5, pp. 550–560, May 1984.

[109] H. V. Poor, *An introduction to signal detection and estimation*. Springer, 1994.

[110] J. G. Proakis, Ed., *Digital communications*. McGraw-Hill, Inc., 1995.

[111] A. Proctor and R. Catmur, "Certification processes and testing of A-GPS equipped cellular phones," *Inside GNSS*, vol. 2, no. 8, pp. 38–44, Nov./Dec. 2007.

[112] M. L. Psiaki, "FFT-based acquisition of GPS L2 civilian CM and CL signals," in *Proc. ION GNSS 2004*, Long Beach, CA, USA, Sep. 21–24 2004, pp. 457–473.

[113] M. B. Pursley and D. V. Sarwate, "Evaluation of correlation parameters for periodic sequences," *IEEE Trans. Inf. Theory*, vol. 23, no. 4, pp. 508–513, July 1977.

[114] A. R. Raghavan, C. W. Baum, and D. L. Noneaker, "Analysis of a serial acquisition scheme for unslotted distributed direct-sequence packet radio networks," in *Proc. IEEE ICC 98*, Atlanta, GA, USA, June 7–11 1998, pp. 1248–1252 vol. 3.

[115] V. Raghavan, M. Shakeri, and K. Pattipati, "Test sequencing algorithms with unreliable tests," *IEEE Trans. Syst., Man, Cybern. A*, vol. 29, no. 7, pp. 347–357, 1999.

[116] R. R. Rick and L. B. Milstein, "Optimal decision strategies for acquisition of spread-spectrum signals in frequency-selective fading channels," *IEEE Trans. Commun.*, vol. 46, no. 5, pp. 686–694, May 1998.

[117] S. F. Rounds and C. Norman, "Combined parallel and sequential detection for improved GPS acquisition," in *Proc. ION AM 2000*, San Diego, CA, USA, June 26–28 2000, pp. 368–372.

[118] *RTCM standard for differential GNSS (global navigation satellite systems) services – version 3*, RTCM special committee No. 104, Oct. 2006, RTCM 10403.1.

[119] S. Ruan, F. Tu, R. Pattipati, and A. Patterson-Hine, "On a multimode test sequencing problem," *IEEE Trans. Syst., Man, Cybern. B*, vol. 34, no. 3, pp. 1490–1499, 2004.

[120] J. J. Rushanan, "Weil sequences: a family of binary sequences with good correlation properties," in *Proc. ISIT 2006, IEEE international symposium on Information Theory*, Seattle, USA, July 9–14 2006, pp. 1648–1652.

[121] ——, "The spreading and overlay codes for the L1C signal," *Journal of The Institution of Navigation*, vol. 54, no. 1, pp. 43–51, Spring 2007.

[122] P. K. Sagiraju, S. Agaian, and D. Akopian, "Reduced complexity acquisition of GPS signals for software embedded applications," *IEE Proc.-Radar Sonar Navig.*, vol. 153, no. 1, pp. 69–78, Feb. 2006.

[123] P. K. Sagiraju, D. Akopian, and G. V. S. Raju, "Performance study of reduced search FFT-based acquisition," in *Proc. ION NTM 2007*, San Diego, CA, USA, Jan. 22–24 2007, pp. 153–160.

[124] P. K. Sagiraju, G. V. S. Raju, and D. Akopian, "Fast acquisition implementation for high sensitivity global positioning systems receivers based on joint and reduced space search," *IET Radar Sonar Navig.*, vol. 2, no. 5, pp. 376–387, Oct. 2008.

[125] A. A. M. Saleh and R. A. Valenzuela, "A statistical model for indoor multipath propagation," *IEEE Trans. Commun.*, vol. 5, no. 2, pp. 128–137, Feb. 1987.

[126] D. V. Sarwate and M. B. Pursley, "Crosscorrelation properties of pseudorandom and related sequences," *Proc. IEEE*, vol. 68, no. 5, pp. 593–619, May 1980.

[127] S. Satyanarayana, D. Borio, and G. Lachapelle, "GPS L1 indoor fading characterization using block processing techniques," in *Proc. ION GNSS 2009*, Savannah, GA, USA, Sep. 22–25 2009, pp. 1742–1755.

[128] L. L. Scharf, *Statistical signal processing*. Addison–Wesley, 1991.

[129] A. Schmid and A. Neubauer, "Performance evaluation of differential correlation for single shot measurement positioning," in *Proc. ION GNSS 2004*, Long Beach, CA, USA, Sep. 21–24 2004, pp. 1998–2009.

[130] C. E. Shannon, "A mathematical theory of communication," *The Bell System Technical Journal*, vol. 27, pp. 379–423, 623–656, July, Oct. 1948.

[131] N. C. Shivaramaiah and A. G. Dempster, "An analysis of Galileo E5 signal acquisition strategies," in *Proc. ENC 2008*, Toulouse, France, Apr. 22–25 2008, pp. 1–11.

[132] N. Shivaramaiah and A. G. Dempster, "Galileo E5 signal acquisition strategies," *Coordinates Magazine*, vol. 4, no. 8, pp. 12–16, Aug. 2008.

[133] F. Soualle et al., "Spreading code selection criteria for the future GNSS Galileo," in *Proc. GNSS 2005*, Munich, Germany, July 19–22 2005, pp. 1–5.

[134] J. Soubielle, I. Fijalkow, P. Duvaut, and A. Bibaut, "GPS positioning in a multipath environment," *IEEE Trans. Signal Process.*, vol. 50, no. 1, pp. 141–150, Jan. 2002.

[135] J. J. Stiffler, "Rapid acquisition sequences," *IEEE Trans. Inf. Theory*, vol. 14, no. 2, pp. 221–225, Mar. 1968.

[136] W. Suwansantisuk and M. Z. Win, "Multipath aided rapid acquisition: optimal search strategies," *IEEE Trans. Inf. Theory*, vol. 53, no. 1, pp. 174–193, Jan. 2007.

[137] J. Syrjärinne, "Possibilities for GPS time recovery with GSM network assitance," in *Proc. ION GPS 2000*, Salt Lake City, UT, USA, Sep. 19-22 2000, pp. 955–966.

[138] ——, "Time recovery throught fusion of inaccurate network timing assistance with GPS measurements," in *Proc. Fusion 2000*, Paris, France, July 10–13 2000, pp. WeD5–3–WED5–10 vol. 2.

[139] J. Syrjärinne and L. Wirola, "Setting a new standard: assisting GNSS receivers that use wireless networks," *Inside GNSS*, vol. 1, no. 7, pp. 26–31, Oct. 2006.

[140] R. E. Taylor and J. W. Sennott, *Navigation system and method. US Patent No. US 4,445,118*, Apr. 1984.

[141] R. C. Titsworth, "Optimal ranging codes," *IEEE Trans. Space Electron. Telem.*, vol. 10, no. 1, pp. 19–30, Mar. 1964.

[142] M. Tran, "Performance evaluations of the new GPS L5 and L2 civil (L2C) signals," *Journal of The Institute of Navigation*, vol. 51, no. 3, pp. 199–212, Fall 2004.

[143] J. B. Tsui, *Fundamentals of global positioning system receivers - A software approach*. John Wiley & Sons, Inc., 2000.

[144] G. Turetzky, "Expanding the indoor location solution from GPS to multiple hybrid technologies," in *Proc. ION ITM 2010*, San Diego, CA, USA, Jan. 25–27 2010, pp. 1138–1160.

[145] F. van Diggelen, "Global locate indoor GPS chipset & services," in *Proc. ION GPS 2001*, Salt Lake City, UT, USA, Sep. 11–14 2001, pp. 1515–1521.

[146] ——, "Indoor GPS theory and implementation," in *Proc. IEEE PLANS 2002*, Palm Springs, CA, USA, Apr. 15–18 2002, pp. 240–247.

[147] ——, *A-GPS: assisted GPS, GNSS, and SBAS*. Artech House, 2009.

[148] H. L. Van Trees, *Detection, estimation, and modulation theory – Part I: detection, estimation, and linear modulation theory*. Wiley, 2001.

[149] S. J. Vaughan-Nichols, "Will mobile computing's future be location, location, location?" *IEEE Computer*, vol. 42, no. 2, pp. 14–17, Feb. 2009.

[150] A. Wald, "Sequential tests of statistical hypotheses," *Ann. Math. Statist.*, vol. 16, no. 2, pp. 117–186, 1945.

[151] S. Wallner, J.-Á. Ávila-Rodríguez, G. W. Hein, and J. J. Rushanan, "Galileo E1 OS and GPS L1C pseudo random noise codes - requirements, generation, optimization and comparison," in *Proc. ION GNSS 2007*, Fort Worth, TX, USA, Sep. 25–28 2007, pp. 1549–1563.

[152] S. Wallner, J.-Á. Ávila-Rodríguez, J.-H. Won, G. W. Hein, and J.-L. Issler, "Revised PRN code structures for Galileo E1 OS," in *Proc. ION GNSS 2008*, Savannah, GA, USA, Sep. 16–19 2008, pp. 887–899.

[153] P. W. Ward, "GPS receiver search techniques," in *Proc. IEEE PLANS 1996*, Atlanta, GA, USA, Apr. 22–26 1996, pp. 604–611.

[154] R. Watson, G. Lachapelle, R. Klukas, S. Turunen, S. Pietilä, and I. Halivaara, "Investigating GPS signals indoors with extreme high-sensitivity detection techniques," *Journal of The Institute of Navigation*, vol. 52, no. 4, pp. 199–213, Winter 2005–2006.

[155] L. R. Weill, "Theoretical and practical sensitivity limits for assisted GNSS receivers using legacy and future GNSS signals," in *Proc. ION GNSS 2006*, Fort Worth, TX, USA, Apr. 26–29 2006, pp. 2930–2943.

[156] L. R. Weill, N. Kishimoto, S. Hirata, and K. X. Chin, "The next generation of super sensitive GPS system," in *Proc. ION GNSS 2004*, Long Beach, CA, USA, Sep. 21–24 2004, pp. 1924–1935.

[157] L. R. Welch, "Lower bounds on the maximum cross correlation of signals," *IEEE Trans. Inf. Theory*, vol. 20, no. 3, pp. 397–399, May 1974.

[158] L. Wirola, I. Halivaara, S. Verhagen, and C. Tiberius, "On the feasibility of adding carrier phase -assistance to cellular GNSS assistance standards," *Journal of Global Positioning*, vol. 6, no. 1, pp. 1–12, Winter 2005–2006 2007.

[159] L. Wirola and J. Syrjärinne, "Bringing the GNSSs on the same line in the GNSS assistance standards," in *Proc. ION NTM 2007*, Cambridge, MA, USA, Apr. 23–25 2007, pp. 242–252.

[160] A. S. Zaidi and M. R. Suddle, "Global navigation satellite systems: A survey," in *Proc. IEEE ICAST 2006*, Islamabad, Pakistan, Sep. 2–3 2006, pp. 84–87.

[161] M. H. Zarrabizadeh and E. S. Sousa, "A differentially coherent PN code acquisition receiver for CDMA systems," *IEEE Trans. Commun.*, vol. 45, no. 11, pp. 1456–1465, Nov. 1997.

[162] Q. Zhengdi, *Method of reducing interference, and radio system. US Patent No. US 6,751,247*, June 2004.

[163] Q. Zhengdi and S. Turunen, "Unequal code lenghts in GNSS," in *Proc. of The European Navigation Conference GNSS 2004*, Rotterdam, NL, May 17–19 2004, pp. 167.1–4.

[164] N. Ziedan, "Acquisition and fine acquisition of weak GPS L2C and L5 signals under high dynamic conditions for limited-resource applications," in *Proc. ION GNSS 2005*, Long Beach, CA, USA, Sep. 13–16 2005, pp. 1577–1588.

PUBLICATION 1

S. Turunen, “Acquisition of satellite navigation signals with dynamically chosen measurements,” *IET Radar Sonar Navig.*, vol. 4, no. 1, pp. 49–61, Feb. 2010.

www.ietdl.org

Published in IET Radar, Sonar and Navigation
Received on 25th February 2009
Revised on 28th May 2009
doi: 10.1049/iet-rsn.2009.0037

ISSN 1751-8784

Acquisition of satellite navigation signals using dynamically chosen measurements

S. Turunen

Nokia Corporation, Visiokatu 4, 33720 Tampere, Finland
E-mail: seppo.turunen@nokia.com

Abstract: A new approach to sequential acquisition of satellite navigation signals is presented where the collection of measurement statistics is steered dynamically during the acquisition process. The process consists of a fixed number of operation cycles during which the state of the receiver is maintained as a vector of conditional probabilities of acquisition hypotheses, each hypothesis being associated with a code delay and a Doppler frequency. During each operation cycle, one hypothesis is singled out by applying a suitable policy on the state vector. The down-converted satellite signal is then despread and frequency shifted according to the hypothesis. The resulting signal is integrated and squared to form a statistic that is used to update the state vector according to Bayes' theorem. After completing the cycles, a decision is made in favour of the hypothesis corresponding to the highest posterior probability. Two policies are investigated, one based on the maximisation of one-step posterior probability and the other based on the maximisation of information gain. Simulation results are presented indicating that the proposed approach provides a significant performance advantage over standard techniques for a wide range of signal-to-noise ratios.

1 Introduction

Navigation satellites, or global navigation satellite systems (GNSS) satellites [1], transmit direct sequence spread-spectrum radio signals with low rate data modulation. At receiver input the signals have a wide Doppler frequency range because of satellite movement and a low signal-to-noise ratio (SNR) because of propagation losses. To detect a satellite signal, the receiver must eliminate its Doppler frequency and align a locally generated replica code to its spreading code. The Doppler frequency and the timing of the signal are first coarsely estimated and the estimates then refined using tracking correlators [2]. The coarse estimation step is referred to as signal acquisition.

To acquire a satellite signal, a navigation satellite receiver conducts a search over an uncertainty region in time–frequency domain. The region is usually discretised into cells that correspond to time and frequency shifted copies of the transmitted signal. For each cell the received signal is down-converted, frequency shifted, correlated with the replica code and integrated to yield a complex variate that is then squared to generate a test statistic. If the SNR of the integration result is insufficient, it may be improved by making the integration time longer or by combining several squared integration results additively to generate an alternative test statistic [3]. The former approach is more efficient but not always applicable since the integration time cannot be usefully extended beyond a limit determined by the data modulation, oscillator instability or receiver movement.

The size of the uncertainty region can be very large unless prior information is available about satellite trajectories, time and user location. Such information is available internally for a receiver that has recently been tracking satellite signals or externally for a receiver that has access to acquisition assistance [4] from a cellular telephone network or some other information network. While acquisition under full uncertainty, if possible at all, usually requires a dedicated processing facility for parallel search, acquisition under constrained uncertainty, made possible by the prior information, can be meaningfully accomplished with a low degree of parallelism or purely sequentially. Our discussion below is concerned with sequential acquisition in a situation where the prior information has allowed the size

of the uncertainty region to be reduced to a few tens of cells. This situation is typical for mobile wireless terminals since they often have access to acquisition assistance and frequently need to reacquire satellite signals after short signal outages.

Performance requirements for consumer GNSS receivers are often given under the assumption of a fixed acquisition time. This practice was adopted by the mobile telephone industry in the early 1990s when global positioning system (GPS) receivers were first integrated into telephones for emergency call purposes. For such purposes it is desirable to use an acquisition algorithm with a deterministic stopping time. In this correspondence we propose an algorithm with a predefined execution time and, in contrast with so-called double-dwell strategies, suggest handling both the initial screening and final validation of acquisition results inside the same algorithm.

In a basic sequential acquisition scheme, test statistics are collected cyclically for one time–frequency cell at a time until a cell is found whose statistics meet some predefined criteria [5]. We propose an alternative strategy where the order of collecting test statistics is steered dynamically during the acquisition process. Our proposal is motivated by the observation that sequential acquisition can be viewed as a partially observed Markov decision problem (POMDP) [6] where the state consists of the conditional probabilities of all acquisition hypotheses given past measurements [7]. A vector containing as elements the probabilities of the hypotheses conditioned on earlier measurements thus represents sufficient statistics for the measurements. Keeping to this line of thought, the proposed strategy does not make use of additive combining to improve SNR but instead achieves an equivalent improvement in the probability domain.

Monte Carlo simulations, presented as receiver operating characteristic and detection probability plots, show that the proposed strategy outperforms a reference strategy over a wide range of SNR and false alarm rates for an equal number of coherent integrations.

The remainder of this paper is organised as follows. Section 2 gives an overview of related search theory results. Section 3 describes the channel and receiver models. Section 4 explains the proposed acquisition strategy including two alternative search policies. Section 5 reports the simulation results. In Section 6, receiver implementation is discussed. Some further observations concerning the use of the proposed strategy are presented in Section 7. Section 8 concludes the paper.

2 Search theory background

Wald [8] uses probability as a state variable in his sequential probability ratio test for binary hypotheses. His problem setting is not one of choosing an optimal measurement sequence but rather one of deciding when enough information has been collected so that no further measurements are needed. Baum and Veeravalli [9] provide a generalisation to multihypothesis testing, but their discussion is similarly limited to fixed measurement sequences. Kadane [10] investigates the whereabouts search problem, a multihypothesis search problem where measuring a specific location gives a binary result indicating if an object is present in that location. He assumes that no false alarms occur, which leads to a considerable simplification of the problem and allows him to show that only open-loop strategies have to be considered as candidates for an optimal search strategy. Unfortunately, this simplification does not apply to the satellite acquisition problem where false alarms can occur.

Castañon [11] discusses a more general class of multihypothesis search problems with a fixed number of measurements where the measurements are continuous valued and false alarms are not excluded. He shows that an optimal search strategy has a closed-loop structure where the search order is influenced by previous measurements. If the measurements are symmetrically (e.g. normally) distributed, a simple index rule can be found for choosing a next measurement location based on posterior probabilities derived from accumulated measurement statistics. More specifically, the optimal strategy in this case is to measure either the most likely location or the second most likely location. If the measurement distributions are unsymmetric, no index rule can be found in the general case. There is therefore no guarantee for the existence of an index rule-based optimal strategy for the satellite acquisition problem where the test statistics have unsymmetric distributions. Castañon shows, however, that applying the index rule of the symmetric case to an unsymmetric case often gives close to optimal results. This represents a remarkable simplification since the general test sequencing problem is non-deterministic polynomial time hard (NP-hard) [12] and the optimal solution of a POMDP in particular is computationally expensive owing to its continuous valued state vector [6].

We expand the problem setting in [11] by adding, in likeness to [9, 13], a hypothesis that there is no signal in the uncertainty region. Assuming that squared integration results are available as test statistics, we propose two suboptimal search policies and approximate them with simple index rules. The policies are based on minimising one of two alternative uncertainty functions [14], one being the negative of the largest cell probability and the other being the Shannon entropy of the cell probability vector.

3 System model

This section presents the models used for the propagation channel and for the receiver front-end up to coherent integration stage. The models are basic in that they ignore multipath, data modulation and off-peak sampling effects as well as finite precision effects. These simplifications make the derivations in the next section more tractable.

doi: 10.1049/iet-rsn.2009.0037

Assuming that the propagation channel is free of multipath and fading disturbances, a satellite signal at receiver input can be expressed as [5]

$$r(t) = \sqrt{2U}C(t)D(t)\cos((\omega_0 + \Delta\omega)t + \phi_0) + n(t) \quad (1)$$

where U is the signal power, $C(t)$ is the spreading code modulation, $D(t)$ is the data modulation, ω_0 is the carrier radian frequency, $\Delta\omega$ is the radian frequency offset including Doppler frequency, ϕ_0 is the carrier phase and $n(t)$ is stationary additive white gaussian noise (AWGN) with two-sided power spectral density $N_0/2$. We make the assumption that $D(t) \in \{-1, 1\}$.

In the receiver, the signal is down-converted to baseband, frequency shifted to eliminate a hypothesised frequency offset, and correlated with a replica signal suitably timed to account for a hypothesised delay. A set of complex variates is then formed by repeated integration over a time interval chosen such as to preserve the correlation properties of the spreading code. We assume that the data modulation is constant during each integration period. Using T to denote the length of the integration time, k to index the integration period and j to index the delay-frequency pair, referred to here as a cell, the in-phase and quad-phase components of a noise-normalised integration result can be expressed as (see (2))

where $\Delta\omega_j(k)$ is a residual frequency offset and $\phi_j(k)$ is a residual complex phase. The in-phase and quad-phase noise components are denoted by $\eta_{\mathrm{I},j}(k)$ and $\eta_{\mathrm{Q},j}(k)$, respectively, and the normalised cross-correlation function of the received and replica signals for a mutual code delay $\tau_j(k)$ by $R(\tau_j(k))$. The equation assumes that the time $(\Delta\omega/\omega_0)T$ is much shorter than a spreading code element so that changes in element duration due to satellite movement can be ignored. It is assumed that $R(0) = 1$ and further that either no signal is present in the uncertainty region or that there is a signal present in exactly one cell, and that $\Delta\omega_j(k)$ and $\tau_j(k)$ vanish for that cell.

The noise components in (2) have unity mean square value because of the normalisation. They are assumed to be mutually uncorrelated except when their indices are identical. As for the index j, this idealisation is justified by the fact that GNSS spreading codes are chosen for low autocorrelation side lobes in the time–frequency domain so that the local replica signal effectively decorrelates the noise components.

It is assumed that the integration is followed by squaring to eliminate the unknown residual complex phase and to generate a signal statistic for the procedure described in the next section. The squared magnitude of the noise-normalised complex integration result (2), referred to here as a measurement, can now be expressed as

$$y_j(k) = (I_j^2(k) + Q_j^2(k)) = \left(\sqrt{2\frac{U}{N_0}}T\,\sin(\phi_j(k)) + \eta_{\mathrm{I},j}(k)\right)^2 + \left(\sqrt{2\frac{U}{N_0}}T\,\cos(\phi_j(k)) + \eta_{\mathrm{Q},j}(k)\right)^2 \quad (3)$$

It follows the central chi-square distribution with two degrees of freedom and has the probability distribution function (pdf) [15]

$$f_0(y_j(k)) = \frac{1}{2}\exp\left(-\frac{y_j(k)}{2}\right) \quad (4)$$

for no signal in cell j and

$$g_0(y_j(k)) = \frac{1}{2}\exp\left(-\frac{y_j(k)+2s}{2}\right)I_0\left(\sqrt{2sy_j(k)}\right) \quad (5)$$

for a signal in cell j. In (5), s denotes the post-integration SNR, $s = PT/N_0$ and $I_0(\cdot)$ denotes the modified Bessel function of the first kind of order zero. The mean value of the right-hand side (rhs) of (4) is 2 in representation of the total noise variance of the normalised complex signal.

4 Acquisition strategy

In this section, satellite acquisition is discussed as a multiple hypothesis testing problem where all prior and accumulated information about satellites is contained in a vector of conditional probabilities that represent the current state of belief in the acquisition hypotheses. After introducing some further notation, state update equations are given and a decision rule for acquisition presented. Up to this point, the discussion is in terms of general measurement distributions. The key question of choosing new cells for measurement is then discussed in sub-sections where two alternative search policies are presented. To derive the policies, the measurement distributions obtained in the previous section are invoked.

Let there be N cells in the uncertainty region and consider signal acquisition as a multiple hypothesis testing problem

$$\begin{cases} I_j(k) = \dfrac{\sin(\Delta\omega_j(k)T/2)}{\Delta\omega_j(k)T/2}\sqrt{2\dfrac{U}{N_0}}TR(\tau_j(k))\sin(\phi_j(k)) + \eta_{\mathrm{I},j}(k) \\ Q_j(k) = \dfrac{\sin(\Delta\omega_j(k)T/2)}{\Delta\omega_j(k)T/2}\sqrt{2\dfrac{U}{N_0}}TR(\tau_j(k))\cos(\phi_j(k)) + \eta_{\mathrm{Q},j}(k) \end{cases} \quad (2)$$

where H_j, $j = 1, \ldots, N$, stands for the hypothesis that a signal is present in cell j and H_0 for the hypothesis that no signal is present in the uncertainty region. In accordance with this notation it is assumed that at most one signal is present in the uncertainty region.

We assume that the receiver is provided with a vector $\boldsymbol{\pi}(0)$ of prior probabilities $\pi_j(0)$, $\boldsymbol{\pi}(0) = \{\pi_j(0), j = 0, \ldots, N\}$, so that $\pi_j(0)$ is the prior probability that H_j is true, that is, that a satellite signal is present in cell j. For example, if the receiver has been tracking a satellite and then lost the signal, there is an uncertainty about the signal that can be expressed by including multiple non-zero elements in $\boldsymbol{\pi}(0)$. The probabilities $\pi_j(0)$ are assumed to sum to unity in reflection of the fact that at most one signal is present. It is further assumed that $\pi_0(0) \in [0,\ 1)$, $\pi_1(0),\ \ldots, \pi_N(0) \in (0,\ 1)$ and, in the case where $N = 1$, $\pi_0(0) \neq 0$, because the remaining cases are trivial.

Assume that the receiver is set to execute $K+1$ steps indexed by k, $k = 0, \ldots, K$. At step $k = 0$ one cell is chosen for measurement by subjecting $\boldsymbol{\pi}(0)$ to one of the search policies defined in Sections 4.1 and 4.2 below. The chosen cell is then measured and the measurement used to update the receiver state as is explained below. At each of the steps $k = 1, \ldots, K-1$ a new cell is chosen for measurement based on the receiver state and the state subsequently updated using the measurement result. Finally, at step $k = K$ the acquisition result is declared based on the final value of the receiver state.

Let $i(k)$ denote the cell measured at step k and $y(k)$ the measurement obtained. Let further $J(k) = \{\boldsymbol{\pi}(0),\ i(l),\ y(l),\ l = 0, \ldots, k-1\}$ designate the information available before the measurement at step k. The receiver is assumed to have the necessary processing facilities to make full use of $J(k)$ in choosing what measurement to take at step k, that is, to decide $i(k)$. Finally, assume that the measurements $y(k)$ are independent and identically distributed random variables with pdf $g(y(k))$ if a signal is present in the cell measured and with pdf $f(y(k))$ if no signal is present.

Let $\boldsymbol{\pi}(k)$, $\boldsymbol{\pi}(k) = \{\pi_j(k), j = 0, \ldots, N\}$, denote a vector of conditional probabilities where $\pi_j(k)$ is the probability of H_j being true given $J(k)$. It is shown in Appendix that the posterior probabilities $\pi_j(k+1)$ obtain the expressions

$$\begin{cases} \pi_j(k+1) = \dfrac{\pi_j(k) f(y(k))}{p(y(k)|i(k))}, & j \neq i(k) \\ \pi_j(k+1) = \dfrac{\pi_j(k) g(y(k))}{p(y(k)|i(k))}, & j = i(k) \end{cases} \tag{6}$$

where

$$p(y(k)|i(k)) = (1 - \pi_{i(k)}(k)) f(y(k)) + \pi_{i(k)}(k) g(y(k)) \tag{7}$$

The measurement history on the rhs of (6) is represented solely by $\pi_j(k)$. This is possible since sequential acquisition is a Markov decision problem [6] where the probabilities $\pi_j(k)$ constitute a state vector [7]. It can be noted from (6) that the components of $\boldsymbol{\pi}(k)$ are non-negative and sum to unity for $k = 1, \ldots, K$.

Define a search policy $\boldsymbol{\gamma}$, $\boldsymbol{\gamma} = \{\gamma_k, k = 0, \ldots, K-1\}$, as a sequence of maps γ_k: $J(k) \rightarrow \{1, \ldots, N\}$ that determine $i(k)$. Since, as mentioned earlier, $\boldsymbol{\pi}(k)$ constitutes sufficient measurement statistics, the maps γ_k can be restricted to γ_k: $\boldsymbol{\pi}(k) \rightarrow \{1, \ldots, N\}$ without loss of generality. In other words, $\boldsymbol{\pi}(k)$ represents the receiver state for the needs of acquisition.

Assume that $\boldsymbol{\pi}(K)$ has been obtained by repeated application of (6) on $\boldsymbol{\pi}(0)$ and on a sequence of measurements chosen according to some policy $\boldsymbol{\gamma}$. We declare H_j as an acquisition result if

$$j = \arg\max_{l=0,\ldots,N} \pi_l(K) \tag{8}$$

that is, if H_j is the hypothesis with the highest posterior probability. Fig. 1 illustrates the main steps of the proposed acquisition process.

In order to find a search policy that provides good receiver operating characteristics (ROC) with moderate computational load we investigate two heuristic policies for choosing measurements, one motivated by the optimal index policy for symmetric probability densities suggested in [11] and the other motivated by information theory.

4.1 Probability maximising search policy

We aim to maximise the expectation

$$E_{\boldsymbol{\gamma}}\left(\max_{j=0,\ldots,N} \pi_j(K) | \boldsymbol{\pi}(0) \right) \tag{9}$$

of the probability of the acquisition result as defined in (8) being correct under the assumptions

$$\begin{cases} f(y(k)) = f_0(y(k)) \\ g(y(k)) = g_0(y(k)) \end{cases} \tag{10}$$

To this end, we use the following policy: at step k, $k = 0, \ldots, K-1$, measure the cell associated with the second largest element of $\boldsymbol{\pi}(k)$ unless this element is $\pi_0(k)$, in which case measure the cell associated with the largest element of $\boldsymbol{\pi}(k)$.

To argue that this policy is at least sub-optimal we start from an observation in [11] that expectation (9) is maximised or nearly maximised for several measurement distributions by maximising the one-step expectation

$$E_{\gamma_k}\left(\max_{j=0,\ldots,N} \pi_j(k+1) | \boldsymbol{\pi}(k) \right) \tag{11}$$

doi: 10.1049/iet-rsn.2009.0037

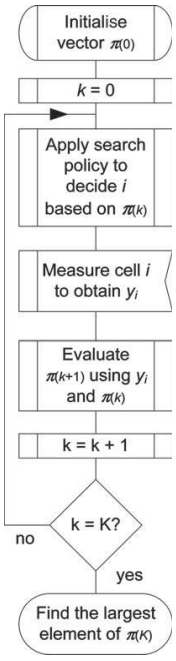

Figure 1 *Main steps of the acquisition process*

We next show that the proposed policy results from the maximisation of (11).

Denote by $S(\boldsymbol{\pi}(k), i(k), y(k))$ the transformation defined by (6) such that $\boldsymbol{\pi}(k+1) = S(\boldsymbol{\pi}(k), i(k), y(k))$. We want to choose $i(k)$ so as to maximise the expectation

$$E_{y(k)}\left[\max_{j=0,\ldots,N}\left(S(\boldsymbol{\pi}(k), i(k), y(k))_j\right)\right] \tag{12}$$

of the largest element of $\boldsymbol{\pi}(k+1)$. The expectation in (12) should be taken with respect to the random variable $y(k)$ conditioned on the search location being $i(k)$ and on the information summarised in the probability distribution $\boldsymbol{\pi}(k)$. Under these conditions $y(k)$ is distributed according to (7).

Assume that $\pi_m(k)$, $\pi_n(k)$ and $\pi_r(k)$ are the largest, second largest and third largest elements of $\boldsymbol{\pi}(k)$, respectively. Observing that the transformation defined by (6) preserves the mutual order of those elements of $\boldsymbol{\pi}(k)$ that are not indexed by $i(k)$, the cell currently being measured, the maximisation in (12) becomes

$$\max_{j=0,\ldots,N} S(\boldsymbol{\pi}(k), i(k), y(k))_j = \max\left[\frac{\pi_m(k)f(y(k))}{p(y(k)|i(k))}, \frac{\pi_{i(k)}(k)g(y(k))}{p(y(k)|i(k))}\right] \tag{13}$$

if $i(k) \neq m$ and

$$\max_{j=0,\ldots,N} S(\boldsymbol{\pi}(k), i(k), y(k))_j = \max\left[\frac{\pi_m(k)g(y(k))}{p(y(k)|i(k))}, \frac{\pi_n(k)f(y(k))}{p(y(k)|i(k))}\right] \tag{14}$$

if $i(k) = m$.

For $i(k) \neq m$, (12) can now be expressed as

$$\begin{aligned} &E_{y(k)}\left[\max_{j=0,\ldots,N}(S(\boldsymbol{\pi}(k), i(k), y(k))_j)\right] \\ &= E_{y(k)}\left\{\max\left[\frac{\pi_m(k)f(y(k))}{p(y(k)|i(k))}, \frac{\pi_{i(k)}(k)g(y(k))}{p(y(k)|i(k))}\right]\right\} \\ &= \int_{-\infty}^{\infty} \max\left[\frac{\pi_m(k)f(y(k))}{p(y(k)|i(k))}, \frac{\pi_{i(k)}(k)g(y(k))}{p(y(k)|i(k))}\right] \\ &\quad \times p(y(k)|i(k))\mathrm{d}y(k) \\ &= \int_{-\infty}^{\infty} \max\left[\pi_m(k)f(y(k)),\ \pi_{i(k)}(k)g(y(k))\right]\mathrm{d}y(k) \end{aligned} \tag{15}$$

and, for $i(k) = m$, similarly as

$$\begin{aligned} &E_{y(k)}\left[\max_{j=0,\ldots,N}(S(\boldsymbol{\pi}(k), i(k), y(k))_j)\right] \\ &= E_{y(k)}\left\{\max\left[\frac{\pi_m(k)g(y(k))}{p(y(k)|i(k))}, \frac{\pi_n(k)f(y(k))}{p(y(k)|i(k))}\right]\right\} \\ &= \int_{-\infty}^{\infty} \max\left[\pi_m(k)g(y(k)),\ \pi_n(k)f(y(k))\right]\mathrm{d}y(k) \end{aligned} \tag{16}$$

It can be seen that choosing $i(k)$ different from n does not make the rhs of (15) larger than choosing $i(k) = n$. This choice with substitutions (10) results in the rhs of (15) being larger than the rhs of (16) for at least all practically important values of s, which can be verified as follows.

We put $q = \pi_m(k)/(\pi_m(k) + \pi_n(k))$ and observe that $q \in (1/2, 1)$. This follows because $\pi_m(k)$ is greater than $\pi_n(k)$ and because both quantities are positive. In fact, if $\pi_m(k)$ were zero, $\boldsymbol{\pi}(k)$ would be a null vector, which contradicts the earlier observation that its components sum to unity. If $\pi_n(k)$ were zero, $\pi_m(k)$ would be the only non-zero component of $\boldsymbol{\pi}(k)$. As can be seen from (6), this is only possible if $\pi_m(0)$ is the sole non-zero component of $\boldsymbol{\pi}(0)$. But it would then have to be unity valued, which contradicts the assumption that none of the components of $\boldsymbol{\pi}(0)$ are unity valued.

The statement that, given (10), the rhs of (15) with $i(k) = n$ is larger than the rhs of (16) can now be expressed in an equivalent form by stating that the integral

$$\int_0^\infty \{\max[qf_0(x), (1-q)g_0(x)] - \max[(1-q)f_0(x), qg_0(x)]\}\mathrm{d}x \tag{17}$$

is positive when $q \in (1/2, 1)$ and $s \in (0, \infty)$. It can be seen that the integral vanishes at the boundaries of this area, that is, when $q = 1/2$, $q = 1$, $s = 0$ or $s = \infty$. We have not been able find a rigorous proof for its positiveness inside the area. Nevertheless, a numerical evaluation showed that it is positive on a dense two-dimensional grid with q evenly distributed between $1/2$ and 1 and s evenly distributed between 0 and 50, the latter range including all values of practical interest.

Since the rhs of (15) with $i(k) = n$ is greater than the rhs of (16), the cell associated with the second largest component of $\boldsymbol{\pi}(k)$ should be measured at step k because measuring this cell gives a higher value for (11) than measuring the cell associated with the highest component or, as shown above, than measuring any other cell. The case where $\pi_0(k)$ is the second largest component is an exception, because H_0 does not correspond to any measurement. An examination of expressions similar to (15) and (16) shows that in this case either the cell associated with $\pi_m(k)$ or the cell associated with $\pi_i(k)$ should be measured. To keep matters simple, our chosen policy is to always measure the cell associated with $\pi_m(k)$ when $\pi_0(k)$ is the second largest component of $\boldsymbol{\pi}(k)$.

4.2 Information gain maximising search policy

Another heuristic suggested for solving search problems is the maximisation of the information gained or, equivalently, the entropy lost because of each measurement. Both Shannon entropy [12–14, 16] and Renyi entropy [17] have been used in earlier work. We elect to use Shannon entropy and set out to find a simple rule for choosing a measurement that minimises the expectation of the Shannon entropy of the receiver state posterior to each measurement. The rule, which we will justify below, is the following: at each step, measure the cell $i(k)$ for which $\pi_i(k)$ is closest to $1/2$.

The Shannon entropy of the probability vector $\boldsymbol{\pi}(k)$ is, by definition:

$$H(k) = -\sum_{j=0}^{N} \pi_j(k) \log(\pi_j(k)) \tag{18}$$

Using (6), the entropy after measuring cell $i(k)$ can be written as

$$H(k+1) = \sum_{\substack{j=0 \\ j \neq i(k)}}^{N} \left[\frac{-\pi_j(k) f(y(k))}{p(y(k)|i(k))} \log\left(\frac{\pi_j(k) f(y(k))}{p(y(k)|i(k))} \right) \right] - \frac{\pi_{i(k)} g(y(k))}{p(y(k)|i(k))} \log\left(\frac{\pi_{i(k)}(k) g(y(k))}{p(y(k)|i(k))} \right) \tag{19}$$

Remembering that the components of $\boldsymbol{\pi}(k)$ sum to unity, (19) can be recast as

$$H(k+1) = \log(p(y(k)|i(k))) - \frac{\left[\begin{array}{c} \pi_{i(k)}(k) g(y(k)) \log(\pi_{i(k)}(k) g(y(k))) \\ + \sum_{\substack{j=0 \\ j \neq i(k)}}^{N} \pi_j(k) f(y(k)) \log(\pi_j(k) f(y(k))) \end{array} \right]}{p(y(k)|i(k))} \tag{20}$$

The expectation of $H(k+1)$ can be taken by multiplying the rhs of (20) with the prior pdf of $y(k)$, given in (7), and integrating over the measurement space

$$\bar{H}(k+1) = \int_{-\infty}^{\infty} p(y(k)|i(k)) H(k+1) \mathrm{d}y \tag{21}$$

By inserting (20) into (21), subtracting the result from (18), applying (7) and using the fact that $f(\cdot)$ and $g(\cdot)$ integrate to unity, the expectation for the information gain $G(k)$ can now be expressed as (see (22))

To decide which cell to measure, one could evaluate (22) for all $i(k)$, $i(k) = 1, \ldots, N$, and choose the value that gives the largest outcome. However, since the integral in (22) is impractical to evaluate for the densities $f_0(\cdot)$ and $g_0(\cdot)$, we proceed as follows. The first and second derivatives of $\bar{G}(k)$ with respect to $\pi_{i(k)}$ are, respectively (see (23))

and

$$\begin{aligned} \bar{G}(k) &= H(k) - \bar{H}(k+1) \\ &= \int_{-\infty}^{\infty} \left\{ \begin{array}{l} (1 - \pi_{i(k)}) f(y) \log(f(y)) + \pi_{i(k)} g(y) \log(g(y)) - [(1 - \pi_{i(k)}) f(y) + \pi_{i(k)} g(y)] \\ \quad \times \log[(1 - \pi_{i(k)}) f(y) + \pi_i(k) g(y)] \end{array} \right\} \mathrm{d}y \end{aligned} \tag{22}$$

$$\frac{\partial \bar{G}(k)}{\partial \pi_{i(k)}} = \int_{-\infty}^{\infty} \{ g(y) \log(g(y)) - f(y) \log(f(y)) - (g(y) - f(y)) \log[(1 - \pi_{i(k)}) f(y) + \pi_{i(k)} g(y)] \} \mathrm{d}y \tag{23}$$

doi: 10.1049/iet-rsn.2009.0037

$$\frac{\partial^2 \bar{G}(k)}{\partial \pi_{i(k)}^2} = -\int_{-\infty}^{\infty} \frac{(g(y)-f(y))^2}{(1-\pi_{i(k)})f(y)+\pi_{i(k)}g(y)}\,\mathrm{d}y \qquad (24)$$

The rhs of (24) can be seen to be negative for all $\pi_{i(k)} \in [0, 1]$ so that a possible maximum of $\bar{G}(k)$ in this range can be found by setting the rhs of (23) to zero. It is easy to see that (23) has a zero at $\pi_{i(k)} = 1/2$ if the distributions $f(\cdot)$ and $g(\cdot)$ are identical or if they have disjoint supports. The distributions $f_0(\cdot)$ and $g_0(\cdot)$ are identical when $s = 0$ and their supports become disjoint when s tends to infinity. Numerical integration shows that when (10) applies, the zero of the rhs of (23) is close to 1/2 also for the practically important intermediate values of s. More specifically, when s ranges from −12 to 12 dB the zero of (23) lies within the range $\pi_{i(k)} \in (0.47, 0.5)$. We therefore venture to define the simplified search policy as that of always measuring the cell $i(k)$ with $\pi_{i(k)}(k)$ closest to 1/2. Note in particular that the probability $\pi_0(k)$ should be excluded from this comparison since it is not associated with any cell that could be measured.

5 Performance evaluation

In this section, simulation results are presented for the two variants of the proposed acquisition strategy and for a reference strategy that represents an upper performance limit for traditional sequential strategies. Both ROC curves and detection probability plots are shown for several sets of parameters. The results indicate that the proposed strategy offers a 3 dB sensitivity advantage over a wide range of parameters.

In order to plot the ROC and detection probability curves, we have to generalise the notions of false alarm and detection from binary hypothesis testing to multiple hypothesis testing. We follow [18] by defining 'system false alarm probability in the absence of signal', $P_{\mathrm{FA}}^{\mathrm{a}}$, as the probability of a detector indicating signal presence when no signal is present and 'system detection probability', P_{D}, as the probability of a detector recognising a signal and correctly identifying the cell where it is present. It may be noted that this generalisation does not make a distinction between the case where the signal is placed in the wrong cell and the case where it is not recognised at all.

5.1 Reference strategy

As a reference strategy we use additive non-coherent combining followed by parallel search to establish an upper performance limit for standard sequential strategies. For each cell an equal number of squared integration results is summed and the largest sum compared with a preset threshold. If the sum exceeds the threshold, a signal is declared present in the corresponding cell while in the opposite case no signal is declared present. To compare the proposed strategy with the reference strategy we set their total number of integration results equal and use the threshold to adjust the sensitivity of the reference strategy. It is shown in [18] that this reference strategy has uniformly better receiver operating characteristics than a standard sequential strategy that evaluates the uncertainty region cell by cell or subset by subset in a predefined order and stops at the first threshold crossing.

To evaluate $P_{\mathrm{FA}}^{\mathrm{a}}$ and P_{D} for the reference strategy we use the formulas [19]

$$P_{\mathrm{FA}}^{\mathrm{a}}(b) = 1 - P\left(l, \frac{b}{2}\right)^N \qquad (25)$$

and

$$P_{\mathrm{D}}(b) = \frac{1}{2}\int_b^{\infty} \left(\frac{x}{2ls}\right)^{(l-1)/2} \mathrm{e}^{-(x+2ls)/2} I_{l-1}\left(\sqrt{2lsx}\right) P\left(l, \frac{x}{2}\right)^{N-1} \mathrm{d}x \qquad (26)$$

where b denotes the detection threshold, l the number of squared integration results per cell, $I_l(\cdot)$ the modified Bessel function of the first kind of order l and $P(\cdot,\cdot)$ the incomplete gamma function as defined in [20]. We set $l = K/N$ to make the total number of squared integration results equal to that in the proposed sequential strategy. The integral in (26) does not have a closed-form expression and we therefore evaluate it numerically.

5.2 ROC

Figs. 2–4 show ROC curves for the reference and proposed strategies for the following choice of parameters: $K = 30$, $N = 10$ and $s = 0$ dB. In order to see the effect of unexpected signal strength variations on performance, ROC curves are also shown for signals that differ by an amount Δs from the design assumption $s = 0$ dB. When plotting these curves, only the signal strength was changed while no change was made to the receiver model. Figs. 5–7

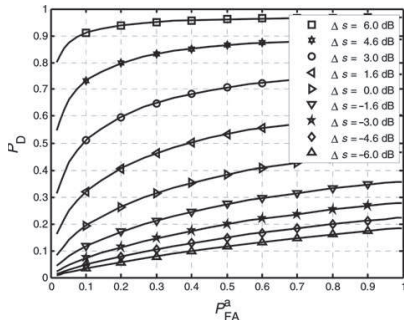

Figure 2 *ROC curves for the reference strategy at different post-integration SNR levels (K = 30, N = 10 and s = 0 dB)*

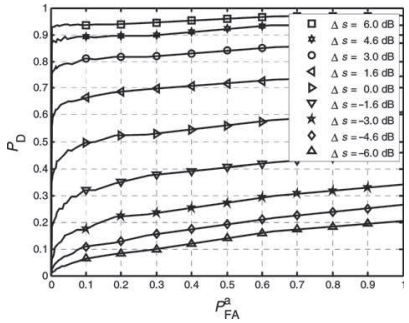

Figure 3 *ROC curves for the probability maximising strategy at different post-integration SNR levels ($K = 30$, $N = 10$ and $s = 0$ dB)*

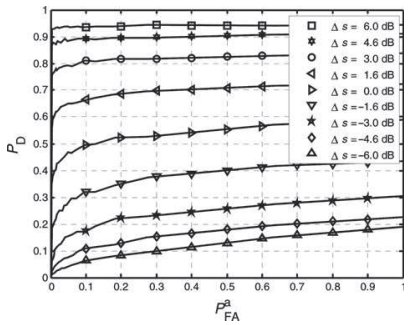

Figure 4 *ROC curves for the information gain maximising strategy at different post-integration SNR levels ($K = 30$, $N = 10$ and $s = 0$ dB)*

show ROC curves for several values of N when $K = 100$, $s = 0$ dB and $\Delta s = 0$ dB.

The ROC curves for the proposed strategy were obtained by Monte Carlo simulation with $\pi_0(0)$ as parameter. The simulation procedure involved the following steps:

Step 1: Set $\pi_0(0)$ to zero.

Step 2: Set $\pi_1(0), \ldots, \pi_N(0)$ to $(1 - \pi_0(0))/N$, thus assuming a uniform prior probability distribution.

Step 3: Fill the search space with complex Gaussian noise.

Step 4: Execute the strategy and register a possible false alarm.

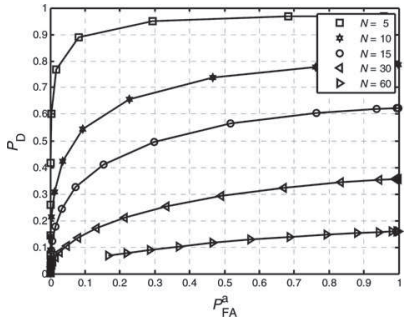

Figure 5 *ROC curves for the reference strategy for different numbers of cells ($K = 100$, $s = 0$ dB and $\Delta s = 0$ dB)*

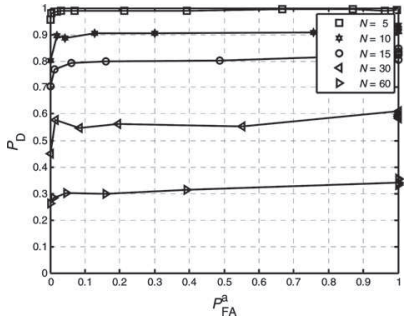

Figure 6 *ROC curves for the probability maximising strategy for different numbers of cells ($K = 100$, $s = 0$ dB and $\Delta s = 0$ dB)*

Step 5: Repeat steps 3 and 4 one thousand times and calculate the percentage of false alarms to obtain an estimate for P_{FA}^a.

Step 6: Fill the search space with complex Gaussian noise and superimpose a signal in a randomly chosen cell.

Step 7: Execute the strategy and register a possible faultless detection.

Step 8: Repeat steps 6 and 7 one thousand times and calculate the percentage of faultless detections to obtain an estimate for P_D.

Step 9: Plot the estimates obtained in steps 5 and 8 in $P_{FA}^a - P_D$ coordinates.

doi: 10.1049/iet-rsn.2009.0037

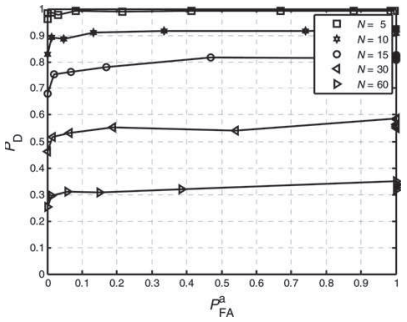

Figure 7 *ROC curves for the information gain maximising strategy for different numbers of cells ($K = 100$, $s = 0$ dB and $\Delta s = 0$ dB)*

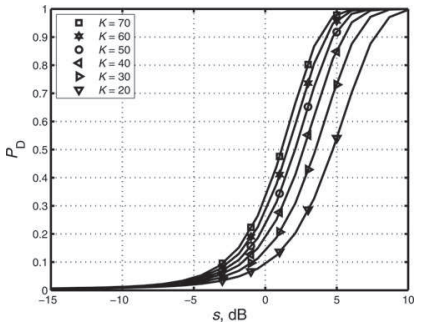

Figure 8 *Detection probability of the reference strategy against post-integration SNR for different numbers of correlation results ($N = 10$, $\Delta s = 0$ dB and $P_{FA}^a = 5\%$)*

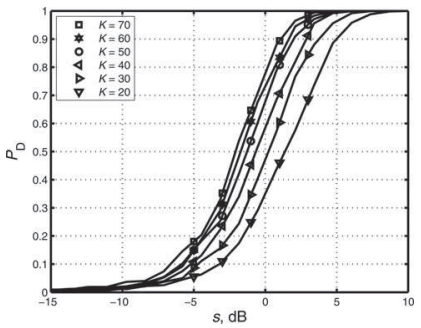

Figure 9 *Detection probability of the probability maximising strategy against post-integration SNR for different numbers of correlation results ($N = 10$, $\Delta s = 0$ dB and $P_{FA}^a = 5\%$)*

Step 10: Increment $\pi_0(0)$ and repeat steps 2–10 until $\pi_0(0) > 1$, then terminate.

The ROC curves for the reference strategy were obtained by numerical evaluation of (25) and (26) using b as parameter.

It is noted from Figs. 2 to 4 that the proposed strategy provides an SNR advantage of at least 1.5 dB over the reference strategy for the whole range of P_{FA}^a values when Δs ranges from -3 to 3 dB. The advantage exceeds 3 dB for the practically important range $0\% \leq P_{FA}^a \leq 5\%$. It can be seen that a positive Δs improves receiver performance despite a mismatch between signal and model. This is due to an improvement of P_D that takes place in spite of the mismatch.

The superiority of the proposed strategy over the reference strategy for the whole range of P_{FA}^a values is also obvious from Figs. 5 to 7. It can be seen that if the proposed strategy is put at a disadvantage by making its uncertainty range two to three times as large as that of the reference strategy, its performance still roughly equals that of the reference strategy. A somewhat unexpected finding is that the performance of the information gain maximising policy is almost identical to that of the probability maximising policy, the latter exhibiting just noticeably weaker performance. It would thus seem immaterial whether one measures cells with a high prior success probability or cells with a high prior uncertainty.

5.3 Detection probability

Figs. 8–10 show the P_D plots of the reference and proposed strategies against post-integration SNR for $N = 10$, $\Delta s = 0$ dB and $P_{FA}^a = 5\%$. Plots are shown for values of K ranging from 20 to 70.

The plots for the proposed strategy were obtained by a Monte Carlo simulation involving the following steps:

Step 1: Set $\pi_0(0)$ to zero.

Step 2: Set $\pi_1(0), \ldots, \pi_N(0)$ to $(1 - \pi_0(0))/N$, thus assuming a uniform prior probability distribution.

Step 3: Fill the search space with complex Gaussian noise.

Step 4: Execute the strategy and register a possible false alarm.

Step 5: Repeat steps 3 and 4 one thousand times and calculate the percentage of false alarms to obtain an estimate for P_{FA}^a.

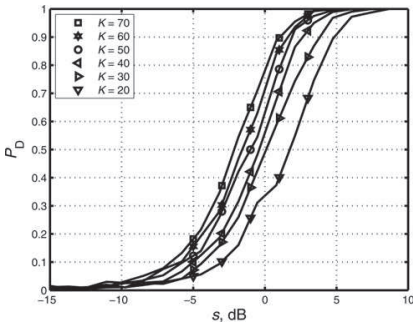

Figure 10 *Detection probability of the information gain maximising strategy against post-integration SNR for different numbers of correlation results ($N = 10$, $\Delta s = 0$ dB and $P_{FA}^{a} = 5\%$)*

Step 6: If the estimate obtained in step 5 is within the range $5 \pm 0.5\%$, continue to step 7. If it is below the range, decrement $\pi_0(0)$ and repeat steps 2–6. If it is above the range, increment $\pi_0(0)$ and repeat steps 2–6.

Step 7: Set s to the lower plotting limit.

Step 8: Fill the search space with complex Gaussian noise and superimpose a signal in a randomly chosen cell.

Step 9: Execute the strategy and register a possible faultless detection.

Step 10: Repeat steps 8 and 9 one thousand times and calculate the percentage of faultless detections to obtain an estimate for P_D.

Step 11: Plot the estimate obtained in step 10 in $s - P_D$ coordinates.

Step 12: Increment s. If s exceeds the higher plotting limit, terminate. Otherwise, repeat steps 8–12.

The plots for the reference strategy were obtained by solving (25) numerically for b and substituting the value so obtained into (26).

The foregoing observations regarding Figs. 2–4 are echoed by the plots in Figs. 8–10 where the 3 dB SNR advantage of the proposed strategy is clearly visible. The advantage would not seem to depend significantly on the number of coherent integration results K. It may also be noted that approximately equal performance is still obtained if the proposed strategy is put at a disadvantage by doubling or tripling the number of integration results available for the reference strategy.

6 Receiver implementation

In this section we analyse the computational load of the proposed strategy and compare it with that of the reference strategy. The proposed strategy executes K cycles with Doppler removal, correlation, integration, squaring, state updating and linear search. Assuming that M complex signal samples are taken during each coherent integration period, the number of multiplications before the integrations is $6KM$. Here, it is assumed that Doppler removal requires four and correlation two real multiplications per sample. The complex squaring operations require a total of $2K$ multiplications. State updates are preceded by the evaluation of the transcendental functions (4) and (5), which is likely to be a table lookup operation in a practical receiver. As a further preparatory step for a state update, the constant terms on the rhs of (6) are calculated, requiring a total of $2K$ multiplications and $2K$ divisions. Finally, the state updates require a total of KN multiplications. There are thus $(6M + N + 4)K$ multiplications and $2K$ divisions in total.

The reference strategy requires the same number of multiplications for Doppler removal, correlation and squaring as the proposed strategy, but it requires only additions for state updates. The number of multiplications is therefore $(6M + 2)K$ and the number of divisions zero.

For a typical GPS receiver with a sampling rate of 2 MHz and a coherent integration time of 10 ms, M has the value of 20 000. Since N is assumed not to be higher than 100, it follows from the preceding formulas that the processing load of the proposed strategy is not more than 0.01% higher than that of the reference strategy. It is assumed here that additions can be ignored and that all multiplications and divisions can be considered equal. Admittedly, the latter assumption could be regarded as an oversimplification since the state updates of the proposed strategy are likely to require higher numerical precision than Doppler removal and correlation.

In absolute terms, the load of the proposed strategy is $(N + 2)K$ multiplications and $2K$ divisions per acquisition. Keeping in mind that the duration of the acquisition process is KT and assuming that $N = 50$, $K = 100$ and $T = 10$ ms, the average load evaluates to 5200 multiplications and 200 divisions per second. This load is not constant, however, since the probability updates only take place between coherent integration periods. In order not to introduce unwanted latencies, the instantaneous processing rate therefore has to be significantly higher than the average processing rate. Assuming that ten times the average is sufficient, an instantaneous processing capacity of 52 000 multiplications and 2000 divisions per second is required. While this is not negligible, it is only a small fraction of the total processing capacity of a mobile handset that typically ranges in hundreds of millions of multiplications per second.

doi: 10.1049/iet-rsn.2009.0037

The foregoing discussion assumes that the number of coherent integrations is the same for both strategies so that the performance advantage of the proposed strategy is fully exploited to improve sensitivity. Another option would be to exploit the advantage to reduce acquisition time and computational load while maintaining the sensitivity unchanged. It was found in Section 5 that the number of coherent integrations required by the proposed strategy to provide a given sensitivity is one-third to one-half of the number required by the reference strategy. This means that the proposed strategy allows acquisition times and computational loads to be reduced by a factor of two to three if sensitivity is kept unchanged.

7 Discussion

The numerical results indicate that the proposed acquisition strategy is superior to the reference strategy over a wide range of parameters and, in particular, at low post-integration SNR levels. The results also indicate that the strategy is insensitive to errors in the assumed SNR despite the fact that the mathematical derivation was made for simple hypothesis testing as opposed to composite hypothesis testing. It would have been interesting to compare the performance with a theoretical upper bound but, unfortunately, no suitable bound was found in the literature.

Probabilities as state and decision variables would seem to have several desirable properties in comparison with raw integration results or their non-coherent combinations that are used in standard acquisition techniques. First, prior information about cell-specific success probabilities can be accounted for in the initialisation. The standard techniques, in contrast, merge prior information into a scalar threshold that does not make a distinction between cells. Second, since the probabilities represent sufficient measurement statistics, there is no need to recall the measurement history when taking a decision. In standard techniques one has to consider noise levels, coherent integration times and the number of correlation results when setting the decision threshold. This is cumbersome especially if the cells have different measurement histories, as is the case in dynamical search strategies. The proposed strategy, being based on state variables that are commensurable, allows the cells to have different measurement histories as long as the prevailing measurement distribution is used in each probability update. Third, probabilities are dimensionless quantities and have a fixed range, which is convenient from implementation point of view.

The time evolution of the probability vector during a typical simulated acquisition run is shown in Fig. 11 to illustrate the dynamic behaviour of the state variables. In this run, the vector components converge to their final values long before the processing is completed, thus suggesting potential for time saving. The saving would seem difficult to achieve in practice, however, since often an apparent convergence to an erroneous state first occurs

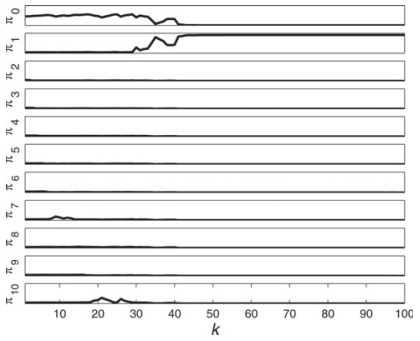

Figure 11 *Sample evolution of probability vector in the probability maximising strategy (vertical range 0–1, signal in cell 1, $s = \Delta s = 0$ dB and $N = 10$)*

and an abrupt transition to the correct state only then takes place. The abruptness of the transition, also visible in Fig. 11, perhaps results from the fact that only one of the components of the probability vector is changed in relation to others at any given probability update. In the initial phase, when measurements are not focused on any particular cell, the signal containing cell is measured infrequently and its corresponding vector component does not stand out. When this later happens, measurements become more focused, which gives rise to positive feedback and leads to rapid convergence.

The proposed acquisition strategy assumes that only one correlator is available. Two obvious approaches offer themselves as ways of extending the strategy to the multiple correlator case and might deserve further evaluation. One approach would be to partition the uncertainty region into as many sections as there are correlators and to apply the single correlator strategy to each of them separately. The probability vectors so obtained could then be concatenated and a decision made as explained above. Another approach would be to have several correlators operate in parallel in the full uncertainty region by using one of the proposed policies to allocate new cells to correlators that become vacant. In this variant both the probability updates and the decision making could be as proposed above. It may be noted that the probability update equations (6) are idempotent so that the order of making probability updates is immaterial in the case where several integration results become available simultaneously.

An important topic for further study would be to evaluate the performance of the proposed strategy in a multipath environment and in the presence of interference. Additional insight could be gained if during such an evaluation the signal models (4) and (5) were varied

according to environment. As a further refinement, adaptive strategies could be considered for this purpose.

8 Conclusion

A fixed sample size sequential acquisition strategy for GNSS signals has been proposed where the order of collecting test statistics is steered dynamically during the acquisition process. The state of the acquisition process is maintained as a vector of probabilities and updated each time a new statistic becomes available. Two policies for collecting the test statistics have been examined and shown to have approximate implementations as index rules. Monte Carlo simulations have been presented that indicate a significant performance improvement over a reference strategy for a wide range of parameters.

9 References

[1] HEGARTY C.J., CHATRE E.: 'Evolution of the global navigation satellite system (GNSS)', *Proc. IEEE*, 2008, **96**, (12), pp. 1902–1917

[2] MISRA P., ENGE P.: 'Global positioning system' (Ganga-Jamuna Press, 2001, 2006, 2nd edn.)

[3] O'DRISCOLL C.: 'Performance analysis of parallel acquisition of weak GPS signals', PhD thesis, National University of Ireland, 2007

[4] MONNERAT M.: 'AGNSS standardization – the path to success in location-based services', *Inside GNSS*, 2008, **3**, (5), pp. 22–33

[5] VAN DIERENDONCK A.J.: 'GPS receivers', in PARKINSON B.W., SPILKER JR. J.J. (EDS.): 'Global positioning system: theory and applications' vol. 1, (American Institute of Aeronautics and Astronautics, 1996, 1st edn.), pp. 329–407

[6] RAGHAVAN V., SHAKERI M., PATTIPATI K.: 'Test sequencing algorithms with unreliable tests', *IEEE Trans. Syst. Man Cybern. A Syst. Humans*, 1999, **29**, (7), pp. 347–357

[7] BERTSEKAS D.P.: 'Dynamic programming: deterministic and stochastic models' (Prentice Hall, 1987, 1st edn.)

[8] WALD A.: 'Sequential tests of statistical hypotheses', *Ann. Math. Statist.*, 1945, **16**, (2), pp. 117–186

[9] BAUM C.W., VEERAVALLI V.V.: 'Sequential procedure for multihypothesis testing', *IEEE Trans. Inf. Theory*, 1994, **40**, (6), pp. 1994–2007

[10] KADANE J.B.: 'Optimal whereabouts search', *Oper. Res.*, 1971, **19**, (4), pp. 894–904

[11] CASTAÑON D.A.: 'Optimal search strategies in dynamic hypothesis testing', *IEEE Trans. Syst. Man Cybern.*, 1995, **25**, (7), pp. 1130–1138

[12] RUAN S., TU F., PATTIPATI R., PATTERSON-HINE A.: 'On a multimode test sequencing problem', *IEEE Trans. Syst. Man Cybern. B, Cybern.*, 2004, **34**, (3), pp. 1490–1499

[13] PATTIPATI K.R., ALEXANDRIDIS M.G.: 'Application of heuristic search and information theory to sequential fault diagnosis', *IEEE Trans. Syst. Man Cybern.*, 1990, **20**, (4), pp. 872–887

[14] DEGROOT M.H.: 'Optimal statistical decisions' (John Wiley & Sons, 1970, 2004, 2nd edn.)

[15] PROAKIS J.G.: 'Digital communications' (McGraw-Hill, 1983, 1995, 3rd edn.)

[16] COX L.A., SUN X., QIU Y.: 'Optimal and heuristic search for a hidden object in one dimension'. Proc. IEEE Int. Conf. Humans, Information and Technology, San Antonio, TX, USA, October 1994, vol. 2, pp. 1252–1256

[17] BEN-BASSAT M.: 'Myopic policies in sequential classification', *IEEE Trans. Comput.*, 1978, **27**, (2), pp. 170–174

[18] BORIO D., CAMORIANO L., LO PRESTI L.: 'Impact of the acquisition searching strategy on the detection and false alarm probabilities in a CDMA receiver'. USA Institute of Navigation, Proc. IEEE/ION PLANS 2006 Conf., San Diego, CA, USA, April 2006, pp. 1100–1107

[19] TURUNEN S.: 'Acquisition performance of assisted and unassisted GNSS receivers with new satellite signals'. USA Institute of Navigation, Proc. ION-GNSS'2007 Conf., Fort Worth, TX, USA, September 2007, pp. 211–218

[20] ABRAMOWITZ M., STEGUN I.A. (EDS.): 'Handbook of mathematical functions' (Dover Publications, 1965, 1st edn.)

10 Appendix: expressions for the posterior probability $\pi_j(k+1)$

In this appendix we obtain the expressions for $\pi_j(k+1)$ in (6) and (7). Bayes' theorem states that if $\mathcal{A}$ is an event and if $B_1, B_2, \ldots, B_n$ are events that are both exhaustive and mutually exclusive, then, for any j,

$$P\{B_j|\mathcal{A}\} = \frac{P\{B_j\}P\{\mathcal{A}|B_j\}}{\sum_{l=1}^{n} P\{B_l\}P\{\mathcal{A}|B_l\}} \tag{27}$$

Denote by C the event that the measurement $y(k) \in [x,\ x+\Delta x]$ for some $x,\ \Delta x \in \Re$. Since the hypotheses $H_0, H_1, \ldots, H_N$ are exhaustive and mutually

doi: 10.1049/iet-rsn.2009.0037

exclusive, it follows from (27) that the equation

$$P\{H_j|C\} = \frac{P\{H_j\}P\{C|H_j\}}{\sum_{l=0}^{N} P\{H_l\}P\{C|H_l\}} \tag{28}$$

holds for any j, $j = 0, \ldots, N$. The value of the conditional probability $P\{C|H_j\}$ depends on whether at step k the cell indexed with j is measured, $i(k) = j$, or whether some other cell is measured. In the former case a signal is present in the cell being measured so that the pdf of the measurement distribution is $g(\cdot)$. In the latter case there is no signal present in the cell being measured and the measurement distribution thus has the pdf $f(\cdot)$. We can therefore write

$$\begin{cases} P\{C|H_j\} = \int_x^{x+\Delta x} f(u)\mathrm{d}u, & j \neq i(k) \\ P\{C|H_j\} = \int_x^{x+\Delta x} g(u)\mathrm{d}u, & j = i(k) \end{cases} \tag{29}$$

Identifying $P\{H_j\}$ with the prior probability $\pi_j(k)$, (28) can now be written as

$$\begin{cases} P\{H_j|C\} = \dfrac{\pi_j(k)\int_x^{x+\Delta x} f(u)\,\mathrm{d}u}{\left[\begin{array}{l}\pi_{i(k)}(k)\int_x^{x+\Delta x} g(u)\,\mathrm{d}u \\ \quad + \sum_{l=0, l\neq i(k)}^{N} \pi_l(k)\int_x^{x+\Delta x} f(u)\,\mathrm{d}u\end{array}\right]}, & j \neq i(k) \\ P\{H_j|C\} = \dfrac{\pi_j(k)\int_x^{x+\Delta x} g(u)\,\mathrm{d}u}{\left[\begin{array}{l}\pi_{i(k)}(k)\int_x^{x+\Delta x} g(u)\,\mathrm{d}u \\ \quad + \sum_{l=0, l\neq i(k)}^{N} \pi_l(k)\int_x^{x+\Delta x} f(u)\,\mathrm{d}u\end{array}\right]}, & j = i(k) \end{cases} \tag{30}$$

Dividing the numerators and denumerators by Δx, noticing that $\sum_{l=0, l\neq i(k)}^{N} \pi_l(k) = (1 - \pi_{i(k)}(k))$, and passing to the limit $\Delta x \to 0$, (6) and (7) follow by identifying $P\{H_j|\mathrm{C}\}$ with $\pi_j(k+1)$ and by putting $x = y(k)$. This concludes the derivation.

doi: 10.1049/iet-rsn.2009.0037

PUBLICATION 2

D. Akopian, P.K. Sagiraju and S. Turunen, "Performance of two-stage massive correlator architecture for fast acquisition of GPS signals," in *Proc. 2006 IEEE Region 5 Technical, Professional and Student Technical Conference*, San Antonio, TX, USA, Apr. 7–9 2006, 4 p.

Performance of Two-Stage Massive Correlator Architecture for Fast Acquisition of GPS Signals

David Akopian, Phani K. Sagiraju
University of Texas at San Antonio, San Antonio, USA

Seppo Turunen
Nokia Corporation, Tampere, Finland

Abstract

A typical operation of GPS receivers assumes a search of the satellites visible on the sky by synchronizing locally generated replica with the transmitted pseudo-random noise (PRN) code sequence. This synchronization is initially performed by finding the highest correlation between the incoming signal and replica, a process known as "acquisition". Highest correlation is observed as a correlator peak response which is compared with a certain threshold to identify availability and values of unknown code phase and frequency of a residual carrier modulation. If the peak is not detected or the decision is wrong then acquisition stage should be repeated many times which is quite a time consuming task. State-of-the-art advanced receivers use massive correlators which parallelize the acquisition process. While massive correlators improve significantly the sensitivity of the receivers, so-called multiple peak selection approach provides an opportunity to save computations by sharing tasks between the massive correlator and validation system [1]. In this paper we study a performance of two stage correlatior consisting of massive and supplementary implementations. The massive correlator is not making firm decisions each time it finds a peak, but provides several possible options (a limited set of highest peaks) to supplementary system.

INTRODUCTION

For a spread spectrum communication in its basic form [2], a data sequence is used by a transmitting unit to modulate a sinusoidal carrier and then the bandwidth of the resulting signal is spread to a much larger value. For spreading the bandwidth, the single-frequency carrier can be multiplied for example by a high-rate binary pseudorandom noise (PRN) code sequence comprising values of –1 and 1, which is known to a receiver. Thus, the signal that is transmitted includes a data component, a PRN component, and a sinusoidal carrier component. A PRN code period comprises a number of so-called chips, the term chips being used to designate the bits of the code conveyed by the transmitted signal, as opposed to the bits of the data sequence.

A well known system which is based on the evaluation of such code modulated signals is GPS (Global Positioning System) [2]. In GPS, code modulated signals are transmitted by several satellites that orbit the earth and received by GPS receivers of which the current position is to be determined. Each of the satellites transmits two microwave carrier signals. One of these carrier signals L1 is employed for carrying a navigation message and code signals of a standard positioning service (SPS). The L1 carrier phase is modulated by each satellite with a different C/A (Coarse Acquisition) code known at the receivers. Thus, different channels are obtained for the transmission by the different satellites. The C/A code, a direct sequence spread spectrum code, which is spreading the spectrum over a 1 MHz bandwidth, is repeated every 1023 chips, the epoch of the code being 1 ms. The carrier frequency of the L1 signal is further modulated with the navigation information at a bit rate of 50 bit/s. The navigation information, which constitutes a data sequence, can be evaluated for example for determining the position of the respective receiver.

A typical operation of GPS receivers assumes a search of the satellites visible on the sky by synchronizing locally generated replica with the transmitted pseudo-random noise (PRN) code sequence. This synchronization is performed by finding the highest correlation between the incoming signal and replica known as "acquisition" using correlators. This may include several stages of coherent and non-coherent integrations and detection decisions. Highest correlation is observed as a correlator peak response which is compared with certain threshold to identify availability and values of unknown code phase and a frequency of a residual carrier modulation. If the peak is not detected or the

decision is wrong then acquisition stage should be repeated many times until a suitable peak is found, which turns out to be a time consuming task. In weak signal conditions the search space is so big that so called massive correlator structures are used with thousands of correlators to accelerate the processing. There are many new acquisition algorithms developed to reduce the acquisition time such as the one presented in [3-5].

The approach presented in this paper is a new acquisition algorithm which uses massive correlator structures with different distribution of initial search and validation tasks [1]. In this work we study the performance improvements with this kind of correlator designs.

DESCRIPTION OF THE SUGGESTED METHOD

The initial acquisition is a two-dimensional search in code phase and frequency. To meet the real time processing and weak signal sensitivity requirements massive correlator banks, capable to check in parallel hundreds and thousands of options, implement the acquisition stage of state-of-the-art receivers.

Each correlator searches for the signal assuming certain signal characteristics (code phase, frequency of modulation). Its performed by (1) multiplying to a compensating sinusoid of assumed frequency, (2) aligning the incoming signal with the replica at given code-phase, (3) multiplying the samples of the signal and replica element by element and integrating (coherent integration). The integration may also include noncoherent stage. At noncoherent stage the consecutive coherent integration results of certain duration are further integrated summing their absolute or squared values. If the alignment and frequency modulation guesses are correct then the correlation results is a bigger response compared with the case of misalignment. Thus detecting the correlation peak and comparing it with certain threshold is the method to find unknown code phase and frequency of modulation.

In order to reduce the complexity of massive correlators, it is suggested to have a small correlator bank in addition to the massive correlator. The idea is that massive correlator is not making firm decisions at each operation cycle but provides several possible options (set of highest peaks). Then these peaks are validated by the supplementary correlator (software or hardware) using possibly more sophisticated algorithms and the massive correlator is assigned to search another set. The specific time durations are defined by the operational conditions. This architecture minimizes the memory usage and provides an optimal workload for the massive correlator as it continuously performs a simple set of tasks.

The rational of this approach is in the fact that a big fraction of search options can be excluded already after short integration lengths. Nevertheless the conventional massive correlator will check all the options thus performing unnecessarily computations. The architecture under study stops the processing stage after the decision can be made for most of the search options and transfers the task to check remaining options to a smaller correlator bank. The massive correlator is then free to check other set of possible (code phase, frequency) pairs. In addition, due to structural separation massive and supplementary correlator banks may use different algorithms and different integration methods and lengths. This processing is shown in Fig 1.

The Massive Correlator Bank (MCB) outputs candidate search options for Supplementary Correlator Bank (SCB) as pairs (τ_i, f_i) of code phase τ_i and frequency f_i with i used for indexing multiple peaks. It can also output integration result, s_i, associated with that peak. After receiving search option parameters from MCB the SCB assigns a correlator to continue the processing with those parameters.

There might be different modes when choosing the number of SCB correlators such as (a) the number of correlators in SCB is taken big enough to process all the options outputted by the massive correlator; (b) a quality is assigned to each search option. If search option parameters are provided by the MCB and all the correlators of the SCB are already assigned then using the qualification grade some of correlators of SCB may stop checking already assigned search option and start checking the other.

Similarly different structural embodiments are possible for SCB depending on parallel processing and integration algorithms. Couple of approaches considered is (a) The MCB integration output may come after coherent integration. In this case it may be saved and included in the following integration performed by SCB correlator as shown in Fig 2.

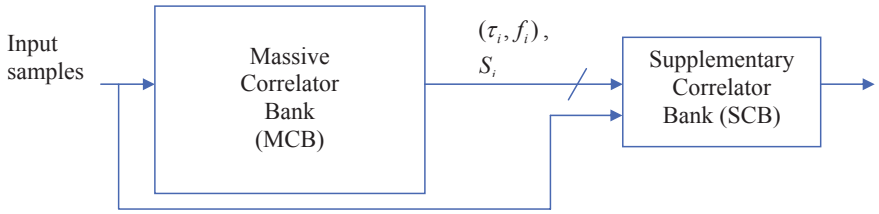

Figure 1. General structure of the Suggested Method. Supplementary correlator bank continues the work of a conventional massive correlator bank [1].

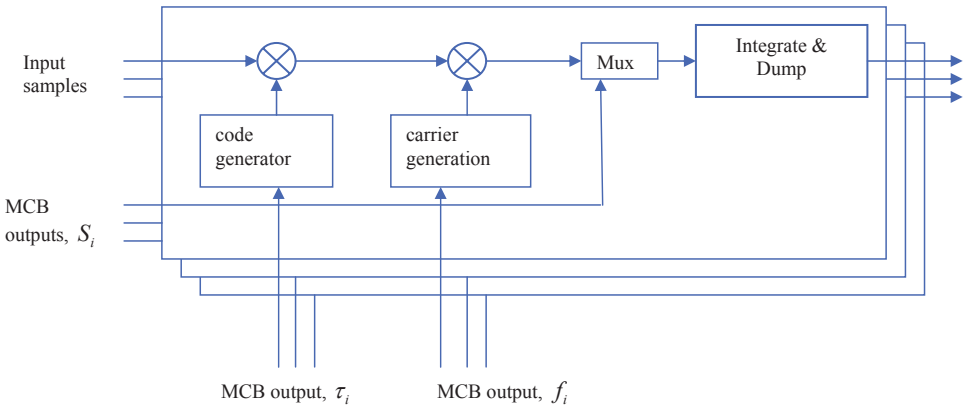

Figure 2. Example of supplementary correlator bank (SCB). Integrate and dump unit may include both coherent and noncoherent integrations [1].

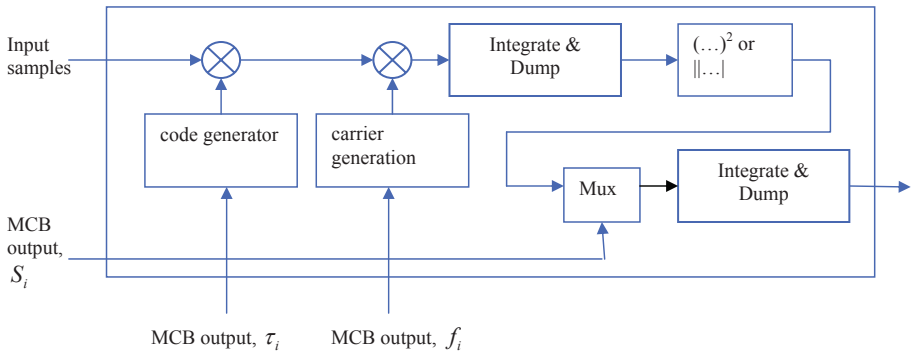

Figure 3. Continuing the noncoherent integration from massive correlator bank [1].

Both coherent and noncoherent accumulation are included in integrate and dump unit. (b) The MCB integration output may come from the noncoherent stage and then included in the noncoherent integration section of the SCB correlator as demonstrated in Fig 3.

SIMULATIONS

In this paper we studied the performance of the two stage correlator. We compared the performance improvement of the conventional correlator where only one peak is outputted, checked and if wrong the whole stage is repeated, where as in the suggested approach multiple peaks are outputted by the MCB and the decision is made in SCB. We considered different cases such as 2, 4, 8 and 12 peaks, and showed the improvement as the number of peaks increased. The performance improvement is illustrated in Fig 4. As can be seen from the figure the improvement is gradually increasing as the number of peaks considered increases, which validates the suggested method.

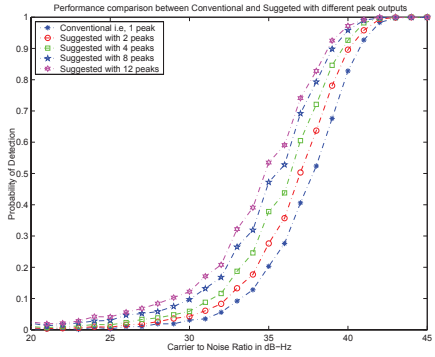

Figure 4. Performance comparison between the conventional and Suggested using different number of peak outputs.

We also considered a structural approach as suggested in Fig 2., where we consider different sets of coherent and noncoherent integration lengths for both conventional and suggested approach. For conventional there is only one peak considered whereas that of the suggested 12 peaks are considered. Their performance improvements are illustrated in Fig 5. As seen from the figure it can be said that for any length of coherent and noncoherent integrations the performance of the suggested is superior to that of the conventional approach which validates the suggested approach.

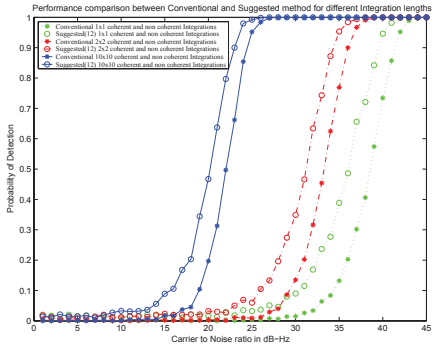

Figure 5. Performance study of two-stage massive correlators. It is clearly observed that for any scenario the performance of using SCB was better than using MCB alone.

CONCLUSIONS

In this paper we studied the performance of a two stage correlator in which the massive correlator is not making firm decisions each time it finds a peak, but provides several possible options (set of highest peaks). The advantage of doing so is even if the peak is not detected once or the decision is wrong then acquisition stage may not be repeated many times, rather other peaks can be checked before the whole acquisition is repeated, which speeds up the acquisition stage. The performance improvements of the suggested approach are illustrated which validate the method.

REFERENCES

[1] D. Akopian, S. Turunen, S. Pietila, H. Valio. Acquisition of code modulated signal. US Patent Application 20050129146, June 16, 2005.

[2] *Understanding GPS: principles and applications.*Edited by Elliott D. Kaplan. Boston, Artech House, 1996.

[3] D. Akopian, "A fast satellite acquisition method,"USA Institute of Navigation, Proceedings of IONGPS' 2001 Conference, Salt Lake City, USA, Sept. 11-14, 2001, pp. 2871-2881.

[4] M. Psiaki, "Block acquisition of weak GPS signals in a software receiver," Proceedings of ION-GPS'2001 Conference, Salt Lake City, USA, Sept. 11-14, 2001

[5] P. K. Sagiraju, D. Akopian, D. Magee , "A Fast Acquisition Algorithm for Indoor Software Receivers", Proceedings of Institute of Navigation 61st Annual Meeting, Cambridge, MA, 2005.

PUBLICATION 3

S. Turunen, "Combinatorial loss in satellite acquisition," in *Proc. ION 18th International Technical Meeting of the Satellite Division (ION GNSS 2005)*, Long Beach, CA, USA, Sept. 13–16 2005, pp. 890–895.

Combinatorial Loss in Satellite Acquisition

Seppo Turunen, *Nokia Corporation*

BIOGRAPHY

Seppo Turunen is a Principal Technologist at Nokia Technology Platforms. He received his M.Sc. in Electrical Engineering in 1979 from the Tampere University of Technology in Finland. From 1979 to 1988, he was involved in the research and development of industrial process control systems at Valmet Process Automation (Finland). He joined Nokia in 1988 and has since held several positions at the Nokia Research Center, Nokia Mobile Phones and Nokia Technology Platforms. His current interests include positioning mobile phones using GPS satellites and cellular base stations.

ABSTRACT

Modern GNSS signal design strives for good cross-correlation and jamming resistance by specifying codes that are one to three orders of magnitude longer than the GPS C/A code. The downside of long codes is that they can be very hard to acquire in indoor areas and other places where satellite signals are heavily attenuated. The longest codes, such as the GPS L2C pilot code, may be infeasible for acquisition with present receiver technology, even in nominal conditions.

It would seem natural to expect that the evolution of receiver technology towards faster parallel processing would eventually solve all acquisition problems. It should be realised, however, that limitations in receiver processing constitute only one part of the problem of acquiring long codes while another part is related to the inherent disadvantage of the long codes themselves. This disadvantage stems from the high false acquisition probability that is caused by a large number of search bins being involved in the acquisition process. The loss of sensitivity related to the false acquisition probability is referred to here as the combinatorial loss.

Combinatorial loss is analysed here in the context of fully parallel acquisition. The analytic expression for false acquisition probability is derived with signal strength, search space size and the number of non-coherent processing steps as its parameters. The expression is then used to derive an approximate closed form functional relationship for the combinatorial loss and the size of the search space. Several numerical examples are given to illustrate the influence that search space size has on receiver sensitivity. The differences in code length are found to account for sensitivity differences of up to 10 dB in theoretical examples and up to 5 dB in practically motivated examples.

INTRODUCTION

The satellite signals planned for GPS modernisation and Galileo are based on spreading codes that are significantly longer than the 1023 long GPS C/A codes; for example, the proposed GPS L2C signal consists of a data code of 10,230 elements and a pilot code of 767,250 elements [4]. Another example, the GPS L5 signal, consists of a data code of 102,300 elements and a pilot code of 204,600 elements [5].

Acquisition is becoming the most computationally demanding function of the modern consumer GNSS receiver due to growing sensitivity requirements. According to mobile telephone standards, a GPS C/A receiver involved in emergency call processing must perform satellite acquisition at a signal level of -140 dBm within a period of a few seconds. Such a low signal level requires a long integration time, which results in narrow frequency search bands. Consequently, a large number of frequency bands have to be scanned for each candidate code phase. These scans already push the present receiver capabilities to its limit with the relatively short code length of the GPS C/A signal; therefore, it is clear that a good deal of receiver development is required before some of the longer codes can be acquired under the same circumstances. Before specifying new receivers, however, it would be good to understand if the new codes change the theoretical limits of acquisition performance and, if so, how.

To assess the effect of code length on acquisition performance apart from any receiver specific limitations, an idealised receiver is assumed where the coherent and non-coherent processing of all time-frequency search bins is first completed, after which a decision is made in favour of the bin with the largest signal value. In order for the scheme to work, exactly one satellite signal must exist in the search space, which clearly does not apply to all

practical situations. Taking a more realistic approach, most practical acquisition algorithms use thresholds in their decision process. The simplification achieved by comparing bins directly with each other is, however, felt to be justified here as it creates results that are independent of any threshold setting conventions.

The discussion below starts with assumptions on signals and receiver operation. An analytic expression for false acquisition probability is then derived using signal strength and the number of search bins and non-coherent processing cycles as parameters. The expression has one definite integral with two transcendental terms. It is further manipulated into the approximate closed form expression by relating the number of search bins to the signal strength at a 50% false acquisition probability. This result is then interpreted as a functional relationship between receiver sensitivity and the size of search space. In the last section, plots are provided to illustrate the analytic results, which turn out to be numerically well behaved for a wide range of parameters. The validity of the approximate expression for receiver sensitivity is also demonstrated numerically, after which the conclusions reached are presented.

SIGNAL AND RECEIVER ASSUMPTIONS

A GNSS parallel acquisition scheme is assumed to divide the search space into N uncorrelated search bins so that N is the number of frequency intervals multiplied by the number of time intervals included in the search. It is further assumed that the bins are uncorrelated and that the bin containing the satellite signal is sampled at its midpoint so that off-peak losses can be ignored.

The signal processing chain is assumed to include down-conversion to a complex base-band signal, coherent integration, squaring, and non-coherent summing. The total reception period is denoted by T and the number of coherent integration periods by m. The base-band signal is assumed to contain AWGN noise at such a power level that the noise variance at both integrator outputs after a T second integration period would be σ^2. The signal amplitude received is assumed to be such that the signal energy, i.e. the sum of the squared signal amplitudes, would be E at the integrator outputs after a coherent integration period T.

If R denotes the ratio of signal power to one-sided noise power spectral density (N_0 in the case of thermal noise) at the receiver base-band input, the equation $E/\sigma^2 = 2RT$ applies.

PROBABILITY OF FALSE ACQUISITION

The amplitude of a noise bin is a central chi-square distributed variable with $2m$ degrees of freedom and a variance parameter $\nu = \sigma^2/m$. The variance parameter is defined as the variance of each of the $2m$ additive terms. The divisor m is required for consistency with the definition of σ above. Using the cdf of the central chi-square distribution [2],

$$F(y)_Y = \frac{1}{\nu^n 2^{\frac{n}{2}} \Gamma\left(\frac{n}{2}\right)} \int_0^y u^{\frac{n}{2}-1} e^{-\frac{u}{2\nu^2}} du \quad , \tag{1}$$

the cdf of a noise bin amplitude can be written as

$$P_0(x) = \frac{1}{\left(\frac{\sigma^2}{m}\right)^m 2^m \Gamma(m)} \int_0^x u^{m-1} e^{-\frac{mu}{2\sigma^2}} du \ , \tag{2}$$

which can be expressed as

$$P_0(x) = \mathrm{P}\left(m, \frac{mx}{2\sigma^2}\right) \tag{3}$$

using the incomplete Gamma function defined as [1]

$$\mathrm{P}(a,x) = \frac{1}{\Gamma(a)} \int_0^x e^{-u} u^{a-1} dt \ . \tag{4}$$

The amplitude of the signal bin is a non-central chi-square distributed variable with $2m$ degrees of freedom, a variance parameter $\nu = \sigma^2/m$, and a sum of squared signal components equalling $m\left(\sqrt{E}/m\right)^2 = E/m$.

Using the pdf of the non-central chi-square distribution [2]

$$p_Y(y) = \frac{1}{2\nu^2} \left(\frac{y}{s^2}\right)^{\frac{n-2}{4}} e^{-\frac{s^2+y}{2\nu^2}} \mathrm{I}_{\frac{n}{2}-1}\left(\frac{s}{\nu^2}\sqrt{y}\right), \tag{5}$$

where ν is the variance parameter and s^2 is the sum of squared signal components, the pdf of the signal bin can be expressed as

$$p_1(x) = \frac{m}{2\sigma^2} \left(\frac{mx}{E}\right)^{\frac{m-1}{2}} e^{-\frac{E+mx}{2\sigma^2}} \mathrm{I}_{m-1}\left(\frac{\sqrt{mxE}}{\sigma^2}\right), \tag{6}$$

where $\mathrm{I}_n(x)$ is the modified Bessel function of the first kind. The mean value of the distribution (5) is $n\nu^2+s^2$ [2],

from which it follows that the mean value of the distribution (6) is $2\sigma^2+E/m$.

A false acquisition occurs whenever the amplitude of at least one of the N-1 noise bins exceeds the amplitude of the signal bin. Its probability P_{fa} can be expressed through its logical complement as:

$$P_{fa} = 1 - \int_0^\infty [P_0(x)]^{N-1} p_1(x)\, dx \quad . \tag{7}$$

By substituting (3) and (6) into (7), the false acquisition probability can be written as:

$$P_{fa} = 1 - \int_0^\infty \frac{m}{2\sigma^2}\left(\frac{mx}{E}\right)^{\frac{m-1}{2}} e^{\frac{E+mx}{2\sigma^2}} \times I_{m-1}\left(\frac{\sqrt{mxE}}{\sigma^2}\right) \mathrm{P}\left(m, \frac{mx}{2\sigma^2}\right)^{N-1} dx \tag{8}$$

or, using the substitution $u = mx/\sigma^2$, as:

$$P_{fa} = 1 - \frac{1}{2}\int_0^\infty \left(\frac{u}{E/\sigma^2}\right)^{\frac{m-1}{2}} e^{-\frac{E/\sigma^2+u}{2}} \times I_{m-1}\left(\sqrt{\frac{uE}{\sigma^2}}\right) \mathrm{P}\left(m, \frac{u}{2}\right)^{N-1} du\,. \tag{9}$$

An equivalent expression would be

$$P_{fa} = 1 - \frac{1}{2}\int_0^\infty \left(\frac{u}{2RT}\right)^{\frac{m-1}{2}} e^{-\frac{2RT+u}{2}} \times I_{m-1}\left(\sqrt{2RTu}\right) \mathrm{P}\left(m, \frac{u}{2}\right)^{N-1} du\,. \tag{10}$$

COMBINATORIAL LOSS

The term $\mathrm{P}(m,mx/2\sigma^2)^{(N-1)}$ in the integrand of (8) corresponds to $P_0(x)^{(N-1)}$ in (7) and represents the cdf of the maximum of the N-1 noise bins. It has been plotted in Fig. 1 for m = 50 and for several values of N. The rest of the integrand represents the $p_1(x)$, the pdf of the signal bin. It has been plotted in Fig. 2 for several values of E. The step function shape of the cdf and the relatively symmetric shape of the pdf would suggest that a 50% false acquisition probability is approximately achieved when the midpoint of the step of the cdf coincides with the mean of the pdf.

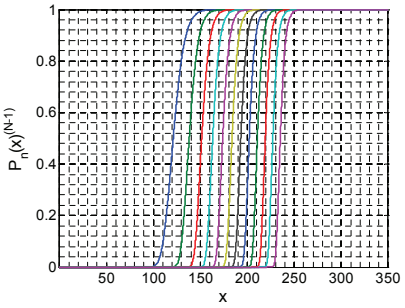

Figure 1. $P_0(m,u/2)^{(N-1)}$ for σ^2/m = 1, m = 50 and $N = 10^1 \ldots 10^{12}$ (from left to right).

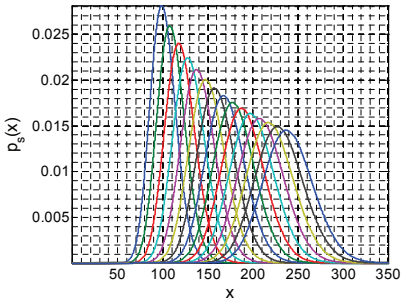

Figure 2. $p_1(x)$ for σ^2/m = 1, m = 50 for E/m = 1, 10, 20, 30, 40, 50, 60, 70, 80, 90, 100, 110, 120, 130, 140 (from left to right).

The midpoint of the step of $P_0(x)^{(N-1)}$ is obviously close to its inflection point, where

$$\frac{d^2}{dx^2} P_0(x)^{N-1} = N\left[(N-1)P_0(x)^{N-2} P_0'(x)^2 + P_0(x)^{N-1} P_0''(x)\right] = 0 \quad , \tag{11}$$

which implies that

$$P_0(x) = -(N-1)\frac{P_0'^2(x)}{P_0''(x)}\,. \tag{12}$$

If N is large, $P_0(x)$ is very close to unity at the inflection point of $P_0(x)^{(N-1)}$. It therefore follows from (2) and (12) that

$$N \approx \left(\frac{2\sigma^2}{m}\right)^m \Gamma(m) \frac{\frac{m}{2\sigma^2}x - m + 1}{x^m} e^{\frac{m}{2\sigma^2}x} + 1 \qquad (13)$$

Equating x in (13) with $E/m + 2\sigma^2$, the mean of the distribution of the signal bin as defined by (6), gives

$$N \approx \left(\frac{1}{\frac{E}{2\sigma^2} + m}\right)^m \Gamma(m)\left(\frac{E}{2\sigma^2} + 1\right) e^{\frac{E}{2\sigma^2}+m} + 1. \qquad (14)$$

Using the Stirling approximation

$$\Gamma(n) \approx \sqrt{\frac{2\pi}{n}}\left(\frac{m}{e}\right)^n \qquad (15)$$

for the gamma function, (14) can be written as

$$N \approx \sqrt{\frac{2\pi}{m}}\left(\frac{1}{\frac{E}{2m\sigma^2} + 1}\right)^m \left(\frac{E}{2\sigma^2} + 1\right) e^{\frac{E}{2\sigma^2}} + 1 \qquad (16)$$

An equivalent expression would be

$$N \approx \sqrt{\frac{2\pi}{m}}\left(\frac{1}{\frac{RT}{m} + 1}\right)^m (RT + 1) e^{RT} + 1. \qquad (17)$$

The signal to noise ratio required to maintain false acquisition probability at a level of 50% is thus determined entirely by the size of the search space and the number of non-coherent integration steps.

For $m = 1$, (14) can be solved for E:

$$E = 2\sigma^2(\ln(N-1) - 1) \quad . \qquad (18)$$

Equivalently,

$$R = \frac{1}{T}(\ln(N-1) - 1) \quad . \qquad (19)$$

For a large N, it follows that the difference on the logarithmic scale between two values of E can be written as a function of the corresponding values of N as

$$\ln(E_2) - \ln(E_1) \approx \ln(\ln(N_2)) - \ln(\ln(N_1)) \qquad (20)$$

or

$$\log_{10}(E_2) - \log_{10}(E_1) \approx \log_{10}(\log_{10}(N_2)) - \log_{10}(\log_{10}(N_1)) \quad . \qquad (21)$$

Associated with an expansion of search space, there is thus a reduction of acquisition sensitivity that is equal to the change of the double logarithm of the number of search bins when the sensitivity is expressed on the logarithmic scale.

NUMERICAL RESULTS

It is assumed in the examples below that the total signal reception time T is one second, which makes the probability of false acquisition a function of R and m only.

Figure 3 shows the probability of false acquisition as a function of R according to (8) for several values of N when $m = 1$. Figure 4 is otherwise similar except that $m = 50$. The integral in (8) was evaluated numerically.

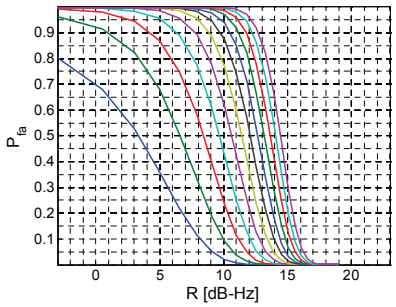

Figure 3. P_{fa} as a function of R for $m = 1$, $T = 1$ s, and $N = 10^1 \ldots 10^{12}$ (from left to right).

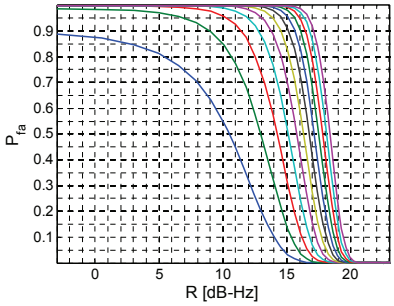

Figure 4. P_{fa} as a function of R for $m = 50$, $T = 1$ s, and $N = 10^1 \ldots 10^{12}$ (from left to right).

The width of a frequency bin is roughly two thirds of the inverse of the coherent integration time [3] so that the number of frequency bands to be searched is 1.5 x BT/m, where B is the total frequency search range. The search space size N thus depends on m since it is the product of code length and the number of frequency bands. Figure 5 shows P_{fa} plots for six pairs of m and N that are related through this dependency so that $N = 1.5$ x 1,023 x 12,000/m. It is assumed that the code length is 1,023 and B is 12 kHz.

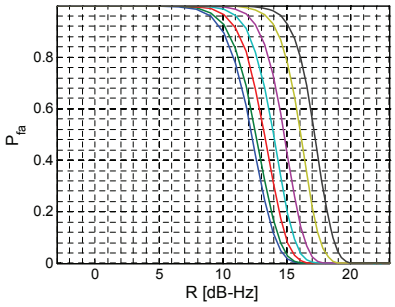

Figure 5. P_{fa} for $m = 1, 2, 5, 10, 20, 50, 100$ (from left to right) and $N = 1.5$ x 1023 x 12,000/m.

Figure 6 shows five P_{fa} plots that were motivated by six existing or proposed signal standards. The parameter assumptions are listed in table 1. It was additionally assumed in all cases that $T = 1$ s and $B = 12{,}000$ Hz. Since the L2C pilot signal is time multiplexed with data and thus has a duty cycle of 50%, the assumed one-second reception time corresponds to two seconds in real time.

Table 1. The GNSS parameters used in Figure 6.

	Code length	Chip rate 10^3/s	Doppler bands	m	N
GPS L2C pilot	767,250	511.5	18,000	1	1.381×10^{10}
Galileo L1 pilot	25x 4,196	1,023	1,800	10	1.888×10^{8}
Galileo E5A pilot	100x 10,230	10,230	1,800	10	1.841×10^{9}
GPS L1 C/A	1,023	1,023	360	50	368,280
GPS L5 pilot	20x 10,230	10,230	360	50	7,365,600
Galileo L1 data	4,196	1,023	72	250	302,112

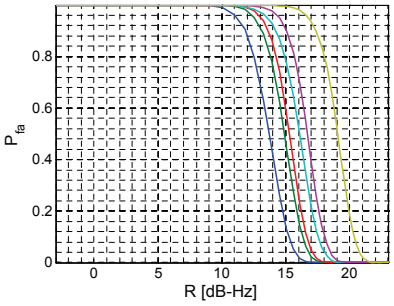

Figure 6. P_{fa} associated with GPS L2C pilot, Galileo L1 pilot, Galileo E5A pilot, GPS L1 C/A, GPS L5 pilot and Galileo L1 data signals (from left to right).

Table 2 shows a comparison of the values of R obtained from the approximate expressions (17) and (19) with those obtained by solving the accurate expression (10) numerically for $P_{fa} = 50\%$ when $T = 1$ s. With these choices, (10), (17) and (19) simplify to

$$P_{fa} = \tfrac{1}{2} = 1 - \tfrac{1}{2}\int_0^{\infty} \left(\frac{u}{2R}\right)^{\frac{m-1}{2}} e^{-\frac{2R+u}{2}} I_{m-1}\left(\sqrt{2Ru}\right) P\left(m, \frac{u}{2}\right)^{N-1} du \quad , \tag{22}$$

$$N = \sqrt{\frac{2\pi}{m}} \left(\frac{1}{\frac{R}{m}+1}\right)^{m} (R+1) e^{R} + 1 \quad , \tag{23}$$

and

$$R = \ln(N-1) - 1 . \quad (24)$$

Table 2. Accurate and approximate values for R when P_{fa}=0.5

R [dB-Hz]	m = 1		m = 50	
N	accurate	approx	accurate	approx
10^1	3.35	5.05	10.49	9.92
10^2	6.62	7.48	12.97	12.60
10^3	8.41	8.98	14.24	13.96
10^4	9.66	10.09	15.11	14.88
10^5	10.63	10.97	15.77	15.58
10^6	11.42	11.71	16.31	16.14
10^7	12.10	12.33	16.76	16.61
10^8	12.68	12.88	17.15	17.02
10^9	13.18	13.37	17.50	17.38
10^{10}	13.64	13.81	17.81	17.70
10^{11}	14.06	14.20	18.09	17.99
10^{12}	14.43	14.57	18.36	18.26

It actually turns out that, for the case $m = 1$, the approximation

$$R = \ln(N) \quad (25)$$

is more accurate than (24).

CONCLUSIONS

The dependence of the sensitivity of an ideal parallel acquisition GNSS receiver on satellite signal code length was analyzed by deriving an analytic expression for false acquisition probability. The expression was used to find an approximate functional relationship between the search space size and acquisition sensitivity for a constant false acquisition probability. In the case of a single coherent integration, the relationship was simplified to a logarithm function.

The false acquisition probability was plotted for several parameter combinations using the signal power to noise density ratio as an independent variable. The approximate functional relationship between search space size and acquisition sensitivity was tabulated and compared with values obtained from the accurate expression. A reasonably good match was found over ten orders of magnitude of search space size.

Numerical examples were analyzed where the differences in the size of the search space were found to account for differences in sensitivity of up to 10 dB. The differences were dependent on the specified false acquisition probability and on the number of non-coherent additions. In the examples motivated by existing and proposed GNSS standards, sensitivity differences of between one and five decibels were found.

REFERENCES

[1] M. Abramowitz and I. A. Stegun (ed.), Handbook of mathematical functions, Dover Publications, 1970.

[2] J.G. Proakis, Digital Communications, McGraw-Hill, 1995.

[3] E.D. Kaplan (ed.), Understanding GPS principles and applications, Artech House Publishers, 1996.

[4] R.D. Fontana, W. Cheung, P.M. Novak and T.A. Stansell, Jr., "The new L2 civil signal," ION GPS 2001, pp. 617–631, 11–14 September 2001.

[5] A.J. Van Dierendonck, and C. Hegarty, "Signal specification for the future GPS L5 Civil signal," ION AM 2000, pp. 232–241, 26–28 June 2000.

PUBLICATION 4

S. Turunen, “Network assistance - what will new GNSS signals bring to it?” *Inside GNSS*, vol. 2, no. 3, pp. 35–41, Spring 2007.

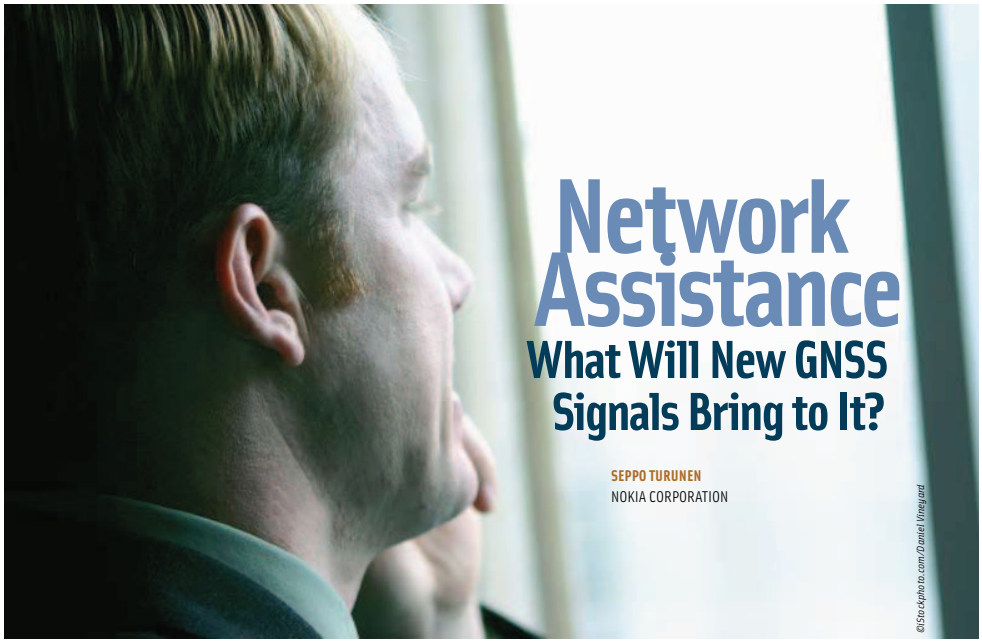

Network Assistance

What Will New GNSS Signals Bring to It?

SEPPO TURUNEN
NOKIA CORPORATION

All GNSS signals are not created equal, and consequently their performance under different kinds of operating environments and using different signal-processing techniques will vary. Rapidly growing GNSS consumer markets are seeing an increase in GNSS receivers that exploit assistance information provided by wireless communications networks to improve performance in challenging environments in cities and indoors. This article by a Nokia senior technologist takes a look at how the many new GNSS signals coming on line might be expected to perform in assisted GNSS and autonomous modes.

Globally GNSS markets are experiencing a sharp growth in sales of consumer products and services. Among these is a cluster of applications known collectively as location based services (LBS), a rapidly evolving field of wireless data services that provide users of mobile terminals with information about their surroundings. As a typical example, travellers can receive directional assistance using downloaded digital maps on which graphical symbols indicate points of interest.

Almost invariably, location based services are delivered using mobile handsets and cellular telephone networks and, ever more often, satellite positioning. Although many LBS applications take place outdoors with unobstructed radiovisibility to GNSS satellites, most will also be used in urban areas and indoors where GNSS signal reception is more problematical. Emergency call positioning is an example of a service that must work both indoors as well as outdoors. However, low-power spread spectrum GNSS satellite signals suffer heavy attenuation in penetrating structures and obstacles.

Due to a strong inverse dependency of dwell time on signal power, traditional sequential-search GNSS receivers have difficulty in acquiring satellite signals if obstructions exist in the signal path. Consequently, assistance techniques that use the wireless communications infrastructure to improve signal acquisition speed and sensitivity are becoming ever more common, and the industry is currently perfecting receiver designs and deploying new network services to exploit these techniques' potential to the full. Moreover, new cellular standards now include stringent sensitivity requirements and test specifications to ensure that the GNSS receivers integrated in mobile phones operate properly under weak signal conditions.

The design of consumer GNSS receivers is still mainly focused on GPS C/A-code reception; however, GNSS providers are envisaging signals with new coding and modulation schemes. These include the new GPS civil signal that transmits on the L2 frequency as well as the new signals that the European Galileo system

now under development will transmit. Because of differences in such variables as frequency allocation, transmission power, and signal structure, these new signals and receiver designs options present a range of possibilities for their practical performance in autonomous and assisted modes.

As is typical of most air interface standards, the related interface control documents (ICDs) focus on the technical specifications of the signals in space and avoid discussing receiver operation and performance. Supplementary analysis is therefore needed in order to set realistic performance targets for future receivers and make informed choices as to which GNSS signals might offer optimal performance.

This article analyzes the expected performance of GPS and Galileo signals in assisted and unassisted modes. It begins with a discussion of state-of-the-art receiver design and signal processing techniques, discusses the assisted GNSS (A-GNSS) mode, and key features of the various GNSS signals.

The article then introduces a numerical scheme for evaluating the theoretical and practical performance of these signals in both assisted and unassisted modes. A key metric introduced in this methodology, attenuation margin, represents the maximum acceptable power loss in a GNSS signal path. The article concludes by assessing the relative performance of GNSS signals in assisted and unassisted mode in terms of the attenuation margin.

GNSS Signal Processing

Typically, GNSS receivers require a reception time of one second or longer in order to detect heavily attenuated GNSS signals, particularly when oscillator instability, signal modulation, or receiver movement preclude the use of long coherent integration times. Under such conditions a serial signal search would proceed extremely slowly, especially when the receiver lacks prior information about code phases or Doppler shifts. As a result, GNSS receivers are ever more often equipped with efficient means of parallel acquisition that allow the processing of the signal search space to be done in a small number of steps or, ideally, in just one step.

A typical parallel acquisition processor consists of a matched filterbank for code phase search and a digital Fourier transformer for frequency domain search. A recent trend is to use software-based acquisition and to perform matched filtering in the frequency domain, which is computationally efficient. The frequency domain processing is typically carried out using data previously sampled into memory, and the required transforms between the time and frequency domains are performed with a fast Fourier transform (FFT).

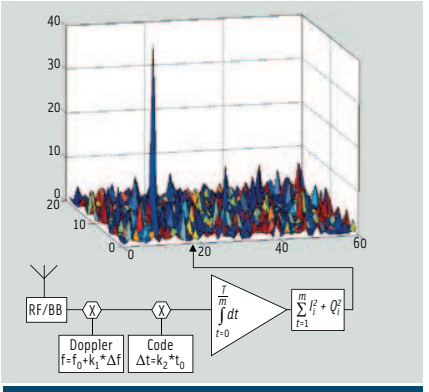

FIGURE 1 Receiver structure for parallel acquisition and signal processing

The processing of one time/frequency bin is shown conceptually in **Figure 1**. A stream of complex baseband samples from the receiver RF section is multiplied with a locally generated replica signal to eliminate Doppler shift and ranging code, leaving a complex DC signal. The signal is then integrated coherently, squared, and added to a memory location dedicated to a specific combination of Doppler shift and code delay.

This sequence of operations, constituting one noncoherent processing step, is performed once or several times for each combination. Finally, some decision strategy is applied to the results to decide whether or not a satellite signal is present and what its parameters are. Any known data modulated on the signal can also be eliminated.

The different eliminations are linear so that their order of execution can be changed without affecting the end result, which can be used to optimize receiver implementation. A wide range of experimental and commercial implementations has been introduced that are functionally equivalent to that shown in Figure 1.

Numerous studies have been published about sequential acquisition strategies that allocate the same processing hardware on different search bins at different instants of time. Sometimes the hardware is allocated repeatedly on the same bin, a procedure called multiple dwelling. Sequential strategies implicitly assume that acquisition performance is limited by receiver processing capacity. The rapid evolution of digital hardware is, however, making this assumption less relevant. In fact, commercial receivers already contain real-time acquisition processors that handle tens of thousands of delay-frequency bins in parallel.

As more processing capacity becomes available, the properties of the satellite signals and the statistics of the parallel acquisition process itself begin to limit receiver performance. This raises the interesting prospect of determining the physical limits of acquisition sensitivity when processing restrictions are left aside entirely. It turns out that the sensitivity then becomes dependent on the dimension of the search space, which, in turn, depends on the ranging code and on the availability of acquisition assistance.

Assisted GNSS. We can reduce the search space and make signal acquisition easier by externally providing direct or

indirect information about code phases, Doppler shifts, and transmitted data bits. When the assistance is indirect, code delays and Doppler shifts are derived from it in the receiver. Indirect assistance typically consists of satellite ephemerides, reference time, reference frequency, and an initial location estimate.

	Data Channel				Pilot Channel		Encoding	Multiplexing
	Code Length	Symbol Length [ms]	Code Rate [kHz]	Data Rate [Hz]	Code Length	Code Rate [kHz]		
GPS L1 C/A	1023	20	-	50	-	-	BPSK(1)	-
GPS L1C	10230	10	1023	50	1800*10230	1023	BOC(1,1)	code+optional phase
GPS L2C	10230	20	511.5	25 or 50	767250	511.5	BPSK(0.5)	code+time
GPS L5	10*10230	10	10230	50	20*10230	10230	BPSK(10)	code+phase
Galileo E1	4092	4	1023	125	25*4092	1023	BOC(1,1)	code
Galileo E5A	20 * 10230	20	10230	25	100 * 10230	10230	Alt-BOC(15,10)	code+phase
Galileo E5B	4 *10230	4	10230	125	100 * 10230	10230	Alt-BOC(15,10)	code+phase
Galileo E6	5115	1	5115	500	100*5115	5115	BPSK(5)	code

TABLE 1. Present and future GNSS signals

AGNSS functionality is included in mobile telephone standards but not yet implemented in all commercial networks. Currently only the GPS L1 C/A signal is covered in the standards but work is going on to extend the coverage to other satellite signals (see the citation, J. Syrjärinne and L. Wirola, referenced in the Additional Resources section at the end of this article).

The reference time and reference frequency could, in principle, be obtained from a local crystal oscillator, but present consumer-grade oscillators are too prone to temperature drift and other instabilities to maintain the required accuracy. Fortunately, cellular base stations have high-quality oscillators and can provide frequency and time references that are accurate enough for Doppler shift estimation. However, the accuracy of absolute time is not always good enough for code phase estimation because the components needed to synchronize the cellular network to the GNSS system time are often missing.

New GNSS Signals

A GNSS signal with ample power and short ranging code can be reliably detected after a reasonably short integration period. Short integration requirements offer the additional benefit of yielding wide frequency-uncertainty bands so that the receiver does not have an excessive number of frequency hypotheses to test. Unfortunately, the planned new GNSS signals have low power and long ranging codes in comparison with the present GPS C/A-code signal and, thus, do not support easy acquisition.

Ranging codes influence signal acquisition mainly through their length, especially if their correlation properties are so good that interference from the signals themselves is insignificant in comparison with the noise component. This influence is twofold. First, a direct linear dependency exists between the search space dimension and the code length. Secondly, the code length may force the receiver to use an otherwise unnecessarily long integration time, thereby narrowing its bandwidth and increasing the number of frequency search bands.

The code length may restrict the choice of integration time if integration over a non-integer multiple of code cycles would undermine the correlation properties of the code. Short codes should present no problem because the integration is, in any case, likely to extend over several code cycles, removing the need to integrate over fractional cycles. Moreover, very long codes may allow termination of the integration phase without needing to complete a full code cycle in order to achieve an acceptable correlation performance.

The original GPS specification dedicated the short C/A code to acquisition and the longer P(Y) code to tracking. No similar distinction is made in the GPS interface specifications for the new L1C [IS-GPS-800], L2C [IS-GPS-200C], and L5 [IS-GPS-705] signals, nor in the Galileo specifications [GAL OS SIS ICD] for the E1, E5, and E6 signals. Instead, all signal components in both systems have relatively long ranging codes, and many of them also have high bit rates. Consequently, their bit energies are lower and search spaces wider than those of the GPS L1 C/A signal and their acquisition, therefore, more difficult.

The new GPS and Galileo specifications introduce pilot signals as a new feature. The specifications do not clearly indicate whether the pilots should be used for tracking, acquisition, or both.

The new signals have long ranging codes, which makes their use for unassisted acquisition more difficult. On the other hand, their lack of data modulation permits coherent integration over multiple bit periods, which yields high processing gain and potentially high receiver sensitivity. However, the actual achievement of higher sensitivity is not immediately evident because the associated search space is large and could give rise to a high false alarm rate that negates the effect of the processing gain.

The dimension of acquisition search space is a product of four factors: length of ranging code, number of frequency search bands, time domain oversampling ratio, and frequency domain oversampling ratio. The number of frequency search bands is proportional to the coherent integration time because the latter is inversely proportional to receiver bandwidth.

The usable coherent integration time of a data signal with unknown content is limited to its symbol length while a pilot signal can, in principle, be integrated indefinitely. In practice, however, coherent integration time is limited to one second or less due to oscillator instability and user movement.

Table 1 shows the code length, symbol length, code rate, and data rate of some freely accessible present and future GNSS signals along with their method of chip encoding and multiplexing. The code lengths of concatenated codes are expressed as the product of the lengths of their constituent codes. Note that the range of code lengths in the table is almost three orders of magnitude.

Noise Bins and Parallel Acquisition

Useful insight into parallel acquisition can be gained by examining the statistics of noise bins in the signal search space. As is well known, the sum of squares of m independent, complex, zero-mean Gaussian random variables of the same variance is non-centrally chi-square distributed with $2m$ degrees of freedom. This is the case with the noise bins when there are m coherent integrations and the receiver input is white noise.

Assume that the noise power and the total reception time are such that the noise variance at both outputs of the complex integrator, when m is taken to be one, is equal to σ^2. In that case, the cumulative distribution function (CDF) of a noise bin, when m is arbitrary, is

$$F(x)=\left(\frac{1}{2\sigma^2}\right)^m \frac{1}{\Gamma(m)}\int_0^{mx} t^{m-1}\exp\left(-\frac{t}{2\sigma^2}\right)dt = \mathrm{P}\left(m,\frac{mx}{2\sigma^2}\right) \quad (1)$$

The expression on the right-hand side is the incomplete Gamma function (discussed in the reference by M. Abramowitz and I. A. Stegun (ed.) cited in Additional Resources), which can be directly evaluated with common numerical software packages. The mean value of the distribution is $2\sigma^2$ which, as could be expected, does not depend on m since it represents the total received energy. The standard deviation (STD), in contrast, depends on m according to the expression $2\sigma^2/\sqrt{m}$.

Parallel acquisition depends on a comparison between the strongest noise bin and the signal bin, and the relevant probability distribution is therefore not that of an individual noise bin but that of the maximum of all noise bins. The CDF of the latter distribution is obtained by raising the CDF of the former distribution to the power of n — n being the total number of noise bins.

Extreme value theory proves that the CDF F_n of the limiting distribution of the maximum of n independent and identically distributed random variables with CDF F, when n tends to infinity, has one of three possible functional forms depending on the tail of the parent distribution F (see the text by E. J. Gumbel in Additional Resources for further discussion of this point). For the chi-square distribution and other distributions with an exponentially decreasing tail, the limiting distribution has the double exponential form

$$F_n(x)=\exp(-\exp(-\alpha_n(x-u_n))), \quad (2)$$

where the coefficients u_n and α_n are defined by the equations

$$F(u_n)=1-\frac{1}{n} \quad (3)$$

and

$$\alpha_n = nF'(u_n) \quad (4)$$

The distribution (2) has the mean value

$$\bar{x}_n = u_n + \frac{\gamma}{\alpha_n} \quad (5)$$

and the standard deviation

$$\sigma(x_n)=\frac{\pi}{\sqrt{6}}\cdot\frac{1}{\alpha_n}, \quad (6)$$

where γ is the Euler constant with the approximate value of 0.5772.

When only one coherent integration step is involved, (1) can be directly substituted into (3) and (4) to yield

$$u_n = 2\sigma^2 \ln(n) \quad (7)$$

and

$$\alpha_n = \frac{1}{2\sigma^2} \quad (8)$$

Using these values in (5) and (6) gives

$$\bar{x}_n = 2\sigma^2(\ln(n)+\gamma) \quad (9)$$

and

$$\sigma(x_n)=\pi\sqrt{\frac{2}{3}}\sigma^2 \quad (10)$$

From (9) and (10), then, we can see that the expected value of the maximum of the chi-square distributed noise bins depends logarithmically on n, while the standard deviation of the maximum is constant. Broadly speaking, the graph of the probability density function (PDF) of the noise maximum retains its shape but shifts horizontally when the size of the search space is changed. This means that signal detection thresholds have to be shifted accordingly in order for error probabilities to remain constant, and a larger search space thus implies lower acquisition sensitivity.

In particular, when there is only one coherent integration step, the signal power required to maintain a constant failure rate is inversely proportional to the logarithm of the search space dimension. In an earlier article in *Coordinates* magazine, January 2007, the author discussed the case in which m is a small integer different from unity and showed that the mean value of the distribution (2) then also has an essentially logarithmic dependency on n and a nearly constant standard deviation.

Borio et al (see Additional Resources) propose the use of so-called system probabilities to characterize parallel acquisition receivers. *System false alarm probability in the absence of signal* is defined as the probability of at least one noise bin in a search space of dimension n exceeding a given detection threshold q. It can be expressed in terms of the false alarm probability P_{fa} of a single time/frequency search cell as

Signal	Nominal Power [dBm]	Coherent Integrations	Unassisted Acquisition Δ f = 10 kHz				Assisted Acquisition Δ f = 100 Hz, Δ t = 10 us				Single Cell Detection	
			Delay Bins	Frequency Bins	E/2σ2 [dB] P_{fa}=0.01 P_d=0.99	Attenuation Margin [dB]	Delay Bins	Fre-quency Bins	E/2σ2 [dB] P_{fa}=0.01 P_d=0.99	Attenuation Margin [dB]	E/2σ2 [dB] P_{fa}=0.01 P_d=0.99	Attenuation Margin [dB]
GPS L1 C/A	-128.50	50	1 023	300	19.06	22.40	10	3	17.45	24.05	16.39	25.10
GPS L1C Data	-133.00	100	20 460	150	20.40	16.60	20	2	18.69	18.31	17.60	19.40
GPS L1C Pilot	-128.25	1	36 828 000	15 000	17.25	23.94	20	150	14.29	26.90	11.49	39.70
GPS L2C Data	-133.00	50	20 460	300	19.42	17.58	5	3	17.45	19.55	16.39	20.61
GPS L2C Pilot	-133.00	1	1 534 500	15 000	16.87	20.13	5	150	14.15	22.85	11.49	25.51
GPS L5 Data	-127.90	100	102 300	150	20.57	21.53	100	2	19.03	23.07	17.60	24.50
GPS L5 Pilot	-127.90	1	204 600	15 000	16.64	25.46	100	150	14.68	27.42	11.49	30.61
Galileo E1 Data	-130.00	250	8 184	60	21.77	17.82	20	1	20.16	19.43	19.27	20.32
Galileo E1 Pilot	-130.00	1	204 600	15 000	16.65	22.94	100	150	14.29	25.29	11.49	28.10
Galileo E5A Data	-128.69	50	204 600	300	19.65	21.66	100	3	17.98	23.33	16.39	24.92
Galileo E5A Pilot	-128.69	1	1 023 000	15 000	16.84	24.47	100	150	14.68	26.64	11.49	29.83
Galileo E5B Data	-128.69	250	40 920	60	21.95	19.36	100	1	20.51	20.80	19.27	22.05
Galileo E5B Pilot	-128.69	1	1 023 000	15 000	16.84	24.47	100	150	14.68	26.64	11.49	29.83
Galileo E6 Data	-128.00	1000	5 115	15	24.18	17.82	50	1	23.06	18.94	22.00	20.00
Galileo E6 Pilot	-128.00	1	511 500	15 000	16.77	25.23	50	150	14.47	27.53	11.49	30.51

TABLE 2. Parameters and results of numerical examples

$$P_{FA}^{a}(q) = 1 - \left[1 - P_{fa}(q)\right]^{n} \quad (11)$$

or in terms of the noise bin CDF F as

$$P_{FA}^{a}(q) = 1 - \left[F(q)\right]^{n} \quad (12)$$

System detection probability, which takes into consideration multiple search bins, is defined as the probability of the signal bin value exceeding both q and all noise bin values. It can be expressed as

$$P_D(q) = \int_{q}^{\infty} \left[1 - P_{fa}(x)\right]^{n-1} f_A(x)\,dx, \quad (13)$$

where $f_A(x)$ is the PDF of the signal bin. In the case of complex Gaussian noise and m coherent integrations the signal bin follows the non-central chi-square distribution and has the PDF

$$f_A(x) = \frac{m}{2\sigma^2}\left(\frac{mx}{E}\right)^{\frac{m-1}{2}} e^{-\frac{E+mx}{2\sigma^2}} \mathrm{I}_{m-1}\left(\frac{\sqrt{mxE}}{\sigma^2}\right) \quad (14)$$

where σ is the noise STD defined earlier, $\mathrm{I}_k(x)$ is the modified Bessel function of the first kind of order k, and E is the squarer output in the absence of noise when m is taken to be one. This point is discussed further in the ION article by this author cited in Additional Resources.

Substituting (1) and (14) into (13) and changing the integration variable to $u = mx/\sigma^2$ gives the system detection probability

$$P_D(q) = \frac{1}{2}\int_{\frac{mq}{\sigma^2}}^{\infty} \left(\frac{u}{E/\sigma^2}\right)^{\frac{m-1}{2}} e^{-\frac{E/\sigma^2+u}{2}} \mathrm{I}_{m-1}\left(\sqrt{\frac{uE}{\sigma^2}}\right) \mathrm{P}\left(m, \frac{u}{2}\right)^{n-1} du \quad (15)$$

When the total reception time T is one second, it follows from the identity

$$E/(2\sigma^2) = PT/(F_N N_0)\,, \quad (16)$$

where F_N is the receiver noise factor, that $E/(\sigma^2)$ in (15) can be interpreted as twice the ratio of signal power P to noise spectral density at receiver baseband input, a quantity customarily measured on a dB-Hz scale.

GNSS Signal Performance

The system detection probabilities for the satellite signals of Table 1 are plotted against the normalized signal energy $E/(2\sigma^2)$ in **Figure 2** (no acquisition assistance) and **Figure 3** (assisted acquisition). The detection threshold q is chosen so that the system false alarm probability as evaluated from (12) and (1) is one percent. The total reception time is taken to be one second.

No acquisition assistance is assumed in Figure 2 so that the search space consists of all code phases and a full frequency uncertainty range, which is taken to be 10 kHz. Acquisition assistance with a time uncertainty of 10 microseconds and a frequency uncertainty of 100 Hz is assumed to be available in Figure 3.

For comparison, the single-cell detection probability P_d is plotted in **Figure 4** using equations (1), (12) and (15) and setting $n = 1$ and $P_{fa} = 0.01$. The numerical evaluation of the equations was done using Matlab standard functions with the exception that the Bessel function, which obtains very large values, was approximated in logarithmic form using a power series described in the previously referenced Abramowitz handbook.

Table 2 gives the receive parameters for Figures 2 and 3. The receiver is assumed to be capable of a one-second coher-

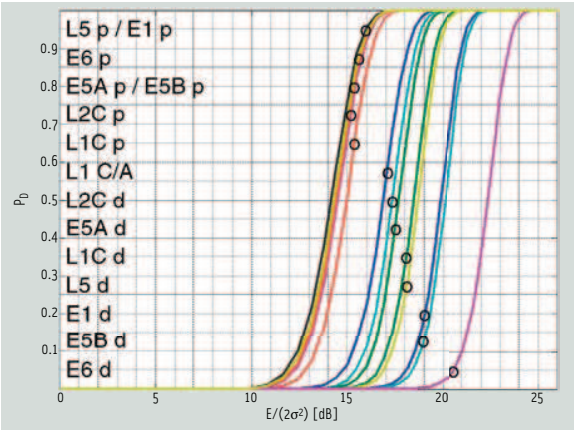

FIGURE 2 System detection probability as a function of normalized signal energy $E/(2\sigma^2)$ in unassisted acquisition (P_{FA} = 0.01)

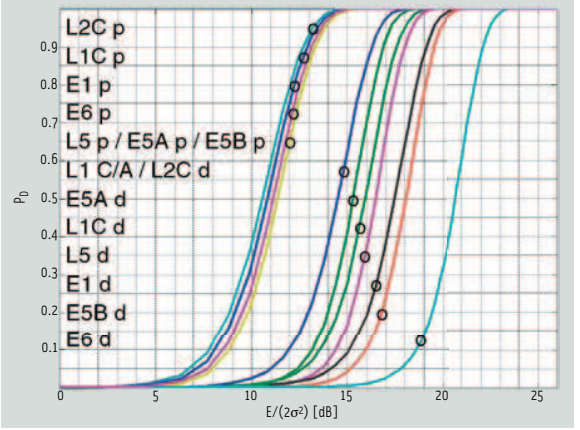

FIGURE 3 System detection probability as a function of normalized signal energy $E/(2\sigma^2)$ in assisted acquisition (P_{FA} = 0.01)

ent integration so that the pilot signals can be processed in a single integration step. The coherent integration time for the data signals is taken to be one bit period. For the BPSK and AltBOC(15,10) modulated signals, one delay bin is assigned for each code element while for the BOC(1,1) modulated signals two bins are assigned.

The number of frequency search bands is calculated from the formula

$$N_f = 1.5 \times BT/m, \quad (17)$$

where B is the frequency uncertainty range. The formula assumes that the width of a frequency search band is two thirds of the inverse coherent integration time. The total number n of search bins is obtained by multiplying the number of delay bins with the number of frequency search bands. Note that the value of n is high, on the order of 10^9, for the unassisted acquisition of pilot signals, but only 15,000 or below when assistance is available.

Table 2 lists the values of $E/(2\sigma^2)$ required to achieve a system detection probability of 0.99 (P_D = 0.99). The table also gives the attenuation margin between the nominal satellite signal power and the required signal power as calculated from (16) when the total implementation loss is 4 dB. The loss is assumed to cover receiver front-end noise, digital processing noise, losses from off-peak sampling, and losses from integrating across bit boundaries.

The nominal satellite signal powers are as specified in the respective ICDs and divided between pilot and data signals as implied by the documents. To account for the constant envelope corrections of the AltBOC(10,15) modulation scheme, 0.69 dB is subtracted from the total power of the Galileo E5 signal.

The L1C pilot signal is assumed to have a high frequency time-multiplexed BOC (TMBOC) signal component that is filtered away, leading to a reduction of power by 4/33. The Galileo E1 data and pilot signals are assumed to have a composite BOC (CBOC) signal component that is likewise filtered away, leading to a reduction of power by 1/11.

The plots show that the unassisted receiver of Figure 2 is significantly less sensitive than the hypothetical single-cell receiver of Figure 4, which is obviously due to the larger search space of the former. For P_D = 0.99 the difference, averaged over all satellite signals, is 4 dB.

The difference in attenuation margins becomes higher the smaller the number of coherent integrations is, as can be seen by comparing the $E/(2\sigma^2)$ values given in Table 2. This can be understood by remembering that a smaller number of coherent integrations results in a larger number of frequency uncertainty bands and, therefore, in a larger search space.

Comparison of Figures 2 and 3 shows that the assisted receiver is more sensitive than the unassisted one. For P_D

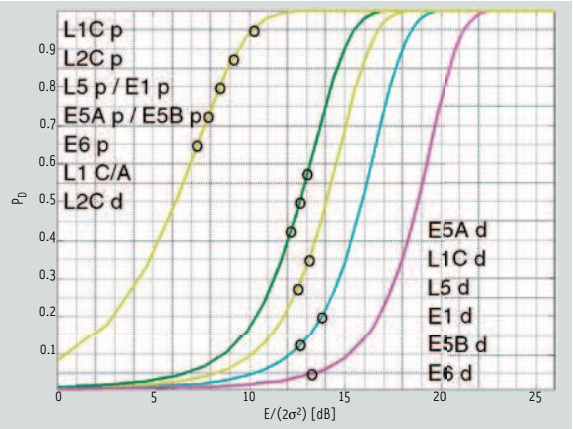

FIGURE 4 Possibility of detection as a function of normalized signal energy $E/(2\sigma^2)$ in single cell acquisition (P_{fa} = 0.01)

= 0.99 the difference, averaged over all satellite signals, is 2 dB. For individual satellite signals the difference can be found by comparing the $E/(2\sigma^2)$ values in Table 2.

The attenuation margins given in Table 2 represent the maximum acceptable loss in signal path. The table reveals that the GPS L1 C/A signal, despite having higher power, has a lower margin than most of the pilot signals. The reason is obviously the shorter coherent integration time of the L1 C/A signal.

The differences between the pilot signals are fairly small and mainly due to different transmission powers. For example, the GPS L5 pilot has a 1.5 dB higher attenuation margin in unassisted mode than the GPS L1C pilot, which is hardly a sufficient reason to convert a receiver to a new band. As can be seen from the table, however, there is the additional motivation that the size of the search space of the L5 receiver is less than one hundredth of that of the L1C receiver.

Conclusion

This article highlights the importance of GNSS acquisition sensitivity for location based services in view of regulations and user expectations. Parallel receiver architectures and terrestrially available assistance were mentioned as means of improving acquisition performance. Extreme value theory was used to gain an insight into the distribution of signals in large search spaces typical of parallel acquisition receivers. The discussion showed that acquisition sensitivity depends approximately on the inverse of the logarithm of the search space dimension.

An analytic expression was derived for system detection probability and used to assess receiver performance in the assisted and unassisted acquisition of several GPS and Galileo signals. The results indicate that while the achievable acquisition sensitivity depends mainly on the length of coherent integration, it is also negatively influenced by the dimension of the search space. The average sensitivity loss attributable to the dimension was 4 dB in unassisted acquisition and 2 dB in assisted acquisition so that an average sensitivity improvement of 2 dB can be attributed to the assistance.

Pilot signals could be acquired at a level 5 dB lower than the corresponding data signals both in the assisted and unassisted cases. However, use of pilots is only practical when assistance is available due to the otherwise extremely high volume of the search space. Taking into consideration the 2 dB improvement from reduction in search space, a total average sensitivity improvement of 7 dB could therefore be achieved by using assistance in the acquisition of the new GNSS signals.

Additional Resources

Abramowitz, M., and I.A. Stegun (ed.), "Handbook of mathematical functions," Dover Publications, 1970.

Borio, D., and L. Camoriano and L. Lo Presti, "Impact of the Acquisition Searching Strategy on the Detection and False Alarm Probabilities in a CDMA Receiver," IEEE/ION PLANS 2006, April 25-27, 2006, San Diego, California.

GAL OS SIS ICD/D.0, Galileo Open Service Signal In Space Control Document, Draft 0, ESA/GJU, May 5, 2006.

Gumbel, E. J., *Statistics of Extremes,* Dover publications, 2004.

IS-GPS-200D, Navstar GPS Space Segment/Navigation User Interfaces, March 7, 2006.

IS-GPS-705, Navstar GPS Space Segment/User Segment L5 Interfaces, January 5, 2005.

IS-GPS-800, Navstar GPS Space Segment/User Segment L1C Interfaces, April 19, 2006.

Kaplan, E.D., and C.J. Hegarty, (ed.) *Understanding GPS Principles and Applications,* Artech House, 2006.

Syrjärinne, J., and L. Wirola, "Setting a New Standard – Assisting GNSS Receivers That Use Wireless Networks," *Inside GNSS*, Vol. 1, Number 7, October 2006.

Turunen, S., "Combinatorial loss in satellite acquisition," ION GNSS 2005, Long Beach, CA, USA, September 13-16, 2005.

Turunen, S., "Acquisition sensitivity limits of new civil GNSS signals," *Coordinates* (cGIT, Delhi, India), Volume III, Issue 1, January 2007.

Author

Seppo Turunen is a principal technologist at Nokia Technology Platforms. He received his M.Sc. in electrical engineering from Tampere University of Technology in Finland. From 1979 to 1988 he was involved in the research and development of industrial process control systems at Valmet Process Automation. He joined Nokia in 1988 and has held several positions at Nokia Research Center, Nokia Mobile Phones, and Nokia Technology Platforms. His current interests include mobile phone positioning techniques based on assisted GNSS, cellular network measurements, and motion sensors.

PUBLICATION 5

S. Turunen, "Acquisition performance of assisted and unassisted GNSS receivers with new satellite signals," in *Proc. ION 20th International Technical Meeting of the Satellite Division (ION GNSS 2007)*, Fort Worth, TX, USA, Sept. 25–28 2007, pp. 211–218.

Acquisition Performance of Assisted and Unassisted GNSS Receivers with New Satellite Signals

Seppo Turunen, *Nokia Corporation*

BIOGRAPHY

Seppo Turunen is a Principal Technologist at Nokia Technology Platforms. He received his M.Sc. in Electrical Engineering in 1979 from Tampere University of Technology in Finland. From 1979 to 1988, he was involved in the research and development of industrial process control systems at Valmet Process Automation. He joined Nokia in 1988 and has held several positions at Nokia Research Center, Nokia Mobile Phones and Nokia Technology Platforms. His current interests include mobile phone positioning techniques based on GNSS, motion sensors and cellular network measurements.

ABSTRACT

Location based services (LBS) are a rapidly evolving field of wireless data services that provide location related information to the users of mobile terminals. The user's position is determined by terrestrial radiolocation or, more and more often, by satellite positioning. The LBS information is almost invariably provided through cellular telephone networks that offer the required availability, mobility and transmission capacity. They also allow assistance information to be downloaded to the GNSS receiver to facilitate satellite acquisition in poor signal conditions.

Some location based services are intended for open-air use while others are meant for use in urban and indoor areas. As satellite signals suffer heavy attenuation in penetrating structures and obstacles, stringent sensitivity requirements and test specifications have been included in mobile telephone standards to make sure that the GNSS receivers integrated in phones operate properly under weak signal conditions.

While the design of consumer GNSS receivers is still mainly focused on GPS C/A reception, satellite operators are envisaging signals with new coding and modulation schemes. The original GPS and Glonass specifications dedicated the short C/A codes to acquisition and the longer P(Y) codes to tracking. No similar distinction is made in the specifications of the new GPS L1C, L2C and L5 signals or in the specifications of the Galileo E1, E5 and E6 signals. Instead, all signal components in both standards have relatively long ranging codes and many of them also have high bit rates. Consequently, their search spaces are wider and bit energies lower than those of the GPS L1 C/A signal so that their acquisition is likely to be more difficult.

The interface control documents of the new GNSS signals do not discuss receiver operation or performance. Supplementary analysis is therefore needed to set realistic performance targets for future receivers. This study analyses the acquisition sensitivity that can be achieved with the new signals when they are combined with various levels of assistance. Special attention is paid to the role of search space dimension under the assumption that processing capacity limitations do not constrain receiver performance.

INTRODUCTION

Weak signal acquisition is problematic in traditional sequential search GNSS receivers due to a strong inverse dependency of dwell time on signal power. Acquisition assistance and parallel acquisition are promising techniques for improving acquisition speed and sensitivity, and the industry is in the process of perfecting receiver designs and deploying new wireless services to exploit their potential to the full.

Acquisition assistance simplifies acquisition by providing direct or indirect code phase and Doppler information from an external source, forming a part of a technique called assisted GNSS (A-GNSS) [1]. A-GNSS functionality is included in mobile telephone standards but not yet implemented in all commercial networks. The standards currently support the GPS L1 C/A signal and work is continuing to extend their coverage to other open GNSS signals.

Parallel acquisition receivers use hardware accelerators or off-line software processing to search satellite signals from the whole uncertainty space in a small number of sequential steps

or, ideally, in just one step. Present GNSS receivers are often equipped with parallel acquisition processors that are capable of testing tens of thousands of frequency-delay hypotheses simultaneously, allowing them to detect heavily attenuated signals that require dwell times of one second or longer.

A typical parallel acquisition processor consists of a matched filter bank for code phase search and a digital Fourier transformer for frequency domain search. Circuitry for eliminating data modulation may also be present if prior information about the modulation is available. As an alternative for time-domain matched filtering it is possible to do matched filtering in frequency domain using the computationally efficient fast Fourier transform (FFT), especially if memory is available for storing long data samples. The order of execution of matched filtering, Fourier transformation and data demodulation is immaterial from a theoretical standpoint, all these operations being linear, but often has implications on practical receiver design.

The result of the linear processing steps is a complex noise signal or, if a satellite signal is present, a near-DC signal superimposed on noise. The next processing steps are typically coherent integration, squaring and non-coherent summation. The final step is to apply a suitable decision policy to conclude if a satellite signal is present in the search space and to provide approximations for its Doppler shift and code delay.

Numerous studies have been published about sequential search strategies where the same hardware is allocated on different frequency-delay bins at different instants of time. It is typical of the strategies that the same bin is visited repeatedly in a procedure called multiple dwelling. All sequential strategies start from the premise that acquisition performance is limited by receiver capacity. For this reason they would be an ambiguous reference framework for comparing the merits of different satellite signals, especially as receiver capacity limitations manifest themselves in different ways and tend to change over time. One possible way to establish a more solid reference framework is to assume that unlimited processing capacity is available.

If receiver processing capacity is unlimited and if all frequency-delay bins are a priori equiprobable, an optimal acquisition strategy obviously utilizes all signal energy available during the observation time and treats all frequency-delay bins symmetrically. This leads one to consider a receiver that first derives a test statistic for each frequency-delay bin in parallel using the procedure described above, then searches for an extremum among of these, and finally decides whether the extremum is strong enough to represent a satellite signal. Since the procedure has few arbitrary parameters and is conceptually simple, we use it below as a reference framework for comparing satellite signals.

Setting aside signal cross-correlation effects, the acquisition performance of the fully parallel receiver depends essentially on signal power and search space dimension. Since the search space contains a large number of identically distributed noise variables and since the main goal of the search obviously is to find the variable with the largest absolute value, the crucial probability distribution is that of the maximum of all noise bins. It was pointed out in an earlier study [2] that according to extreme value theory the cdf of the distribution has the limiting form

$$F_n(x) = \exp\left(-\exp\left(-\alpha_n\left(x-u_n\right)\right)\right) , \quad (1)$$

where n is the search space dimension and α_n and u_n are parameters dependent on n. When there is just one coherent integration step, $F_n(x)$ has the mean value

$$\bar{x}_n = 2\sigma^2\left(\ln(n)+\gamma\right) \quad (2)$$

and the standard deviation

$$\sqrt{\left(x_n - \overline{x_n}\right)^2} = \pi\sqrt{\frac{2}{3}}\sigma^2 , \quad (3)$$

where σ is the noise std after either complex integrator branch and γ is the Euler constant. Expressions (2) and (3) lead to the broad conclusion that the signal power required to maintain a constant failure rate is inversely proportional to the logarithm of the search space dimension, or, in other words, receiver sensitivity has an inverse logarithmic dependency on the dimension of the search space.

Acquisition assistance can dramatically reduce search space dimension and can thus be expected to improve receiver sensitivity. The improvement depends on the dimension of the initial search space that further depends on several characteristics of the satellite signal.

Table 1. Present and future GNSS signals.

	Data channel				Pilot channel		Encoding	Multiplexing
	Code length	Symbol length [ms]	Code rate [kHz]	Data rate [Hz]	Code length	Code rate [kHz]		
GPS L1 C/A	1023	20	1023	50	-	-	BPSK(1)	-
GPS L1C	10230	10	1023	50	1800 * 10230	1023	BOC(1,1)	code+optional phase
GPS L2C	10230	20	511.5	25 or 50	767250	511.5	BPSK(0.5)	code+time
GPS L5	10 * 10230	10	10230	50	20 * 10230	10230	BPSK(10)	code+phase
Galileo E1	4092	4	1023	125	25 * 4092	1023	BOC(1,1)	code
Galileo E5A	20 * 10230	20	10230	25	100 * 10230	10230	AltBOC(15,10)	code+phase
Galileo E5B	4 * 10230	4	10230	125	100 * 10230	10230	AltBOC(15,10)	code+phase
Galileo E6	5115	1	5115	500	100 * 5115	5115	BPSK(5)	code
Glonass L1 C/A	511	10	511	50	-	-	BPSK(0.5)	-

NEW SATELLITE SIGNALS

The new GPS and Galileo signals have two components, data and pilot. Both components have long ranging codes, which makes their use for unassisted acquisition difficult. As a compensating feature, the pilots lack data modulation, which allows coherent integration beyond bit boundaries, thus yielding high processing gain and potentially also high receiver sensitivity. However, it is not immediately evident that the high sensitivity can actually be achieved, because the associated search space is large and could give rise to a high false alarm rate that negates the benefit of the processing gain.

The dimension of the acquisition search space has four factors: length of ranging code, number of frequency search bands, time domain oversampling ratio, and frequency domain oversampling ratio. The number of frequency search bands is proportional to coherent integration time because the latter is inversely proportional to receiver bandwidth. The coherent integration time of a portable receiver seldom exceeds one second due to user movement, clock instability and unknown data modulation.

The symbol lengths, data rates, code rates and code lengths of several present and planned freely accessible GNSS signals [3-7] are shown in Table 1. The table also shows the type of chip encoding, the method of multiplexing and the factorization of the code length into constituent parts in those cases where composite codes are used.

PERFORMANCE MODEL

To compare the satellite signals we assume that the receiver performs m complex coherent integrations, the non-coherent summation is preceded by squaring, and the receiver input is white Gaussian noise such that the noise variance at both real and complex integrator outputs is equal to σ^2 in the case where $m = 1$. Each frequency-delay bin then has a central chi-square distribution with $2m$ degrees of freedom defined by the cdf

$$F(x) = \left(\frac{1}{2\sigma^2}\right)^m \frac{1}{\Gamma(m)} \int_0^{mx} t^{m-1} \exp\left(-\frac{t}{2\sigma^2}\right) dt = \mathrm{P}\left(m, \frac{mx}{2\sigma^2}\right) \quad . \tag{4}$$

The expression on the right-hand side is the incomplete gamma function [8] which can be directly evaluated with common numerical software packages. The mean value of the distribution is $2\sigma^2$ and it represents the total received energy. The standard deviation depends on m and has the expression $2\sigma^2/\sqrt{m}$.

Borio [9] defines *System false alarm probability in the absence of signal* as the probability of at least one noise bin in a search space of dimension n exceeding a given detection threshold q. It can be expressed in terms of the single bin false alarm probability P_{fa} as

$$P_{FA}^{a}(q) = 1 - \left[1 - P_{fa}(q)\right]^n \tag{5}$$

or in terms of the noise bin cdf $F(x)$ as

$$P_{FA}^{a}(q) = 1 - \left[F(q)\right]^n . \tag{6}$$

He also defines *System detection probability* as the probability of the signal bin exceeding both q and all noise bins in value. It can be expressed as

$$P_D(q) = \int_q^{\infty} \left[1 - P_{fa}(x)\right]^{n-1} f_A(x)\, dx \ , \qquad (7)$$

where $f_A(x)$ is the pdf of the signal bin. In the case of complex Gaussian noise and m coherent integrations the signal bin follows the non-central chi-square distribution and has the pdf

$$f_A(x) = \frac{m}{2\sigma^2}\left(\frac{mx}{E}\right)^{\frac{m-1}{2}} e^{-\frac{E+mx}{2\sigma^2}} \mathrm{I}_{m-1}\left(\frac{\sqrt{mxE}}{\sigma^2}\right), \qquad (8)$$

where σ is the noise std defined above, $\mathrm{I}_k(x)$ is the modified Bessel function of the first kind of order k and E is the output of the complex squarer in the absence of noise when m is taken to be one.

Substituting $P_{fa} = 1\text{-}F(x)$ from (4) and $f_A(x)$ from (8) into (7) and changing the integration variable to $u = mx/\sigma^2$ gives

$$P_D(q) = \frac{1}{2}\int_{\frac{mq}{\sigma^2}}^{\infty} \left(\frac{u}{E/\sigma^2}\right)^{\frac{m-1}{2}} e^{-\frac{E/\sigma^2+u}{2}} \mathrm{I}_{m-1}\left(\sqrt{\frac{uE}{\sigma^2}}\right) \mathrm{P}\left(m, \frac{u}{2}\right)^{n-1} du \ . \qquad (9)$$

If the total observation time T is one second, it follows from the identity

$$E/(2\sigma^2) = PT/(F_N N_0) \ , \qquad (10)$$

where F_N is the receiver noise factor, that $E/(2\sigma^2)$ can be interpreted as the C/N_0 ratio at receiver baseband input. The integrand of (9) is therefore determined once C/N_0 is known.

NUMERICAL EVALUATIONS

The ratio $E/(2\sigma^2)$ required to provide a P_D of 0.99 at a P^a_{FA} of 0.01 is shown in Figure 1 for the satellite signals of Table 1. For each signal there is a separate bar for unassisted acquisition, for two levels of assisted acquisition, and for the idealized case of testing signal presence in a single bin at a detection rate of 0.99 and a false alarm rate of 0.01. The signal observation time is one second so that the results are directly interpretable as C/N_0 at receiver baseband input.

Figure 2 shows the margin between the nominal and required signal power as calculated from the $E/(2\sigma^2)$ values of Figure 1 using (10) and assuming a total implementation loss of 4 dB. The loss is assumed to cover receiver front-end noise, digital processing noise, losses from off-peak sampling, and losses from integrating across bit boundaries. The nominal satellite signal powers are as specified in the respective ICD documents [3-7] and they are assumed to divide into pilot and data components as implied by the documents. The Glonass signal power is assumed to divide evenly between the P and C/A components. To account for the constant envelope corrections of the AltBOC(10,15) modulation scheme of the Galileo E5 signal, 0.69 dB is subtracted from the total power.

The parameter assumptions for the calculations are shown in Table 2. The receiver is assumed to be capable of one second coherent integration so that the pilot signals can be processed in a single integration step. The coherent integration time for the data signals is taken to be one bit period. For the BPSK and AltBOC(15,10) modulated signals one delay bin is assigned to each code element while for the BOC(1,1) modulated signals two bins are assigned. The number of frequency search bands is calculated from the expression [10]

$$N_f = 1.5 \text{ x } BT/m, \qquad (11)$$

where B is the frequency uncertainty range. The total number n of search bins is obtained by multiplying the number of delay bins with the number of frequency search bands.

When no assistance is available, the search space consists of all code phases and the full frequency uncertainty range which is taken to be 10 kHz. The term coarse assistance refers to a case where the assistance reduces frequency uncertainty but does not reduce code uncertainty. This is the case in most GSM and WCDMA networks as their base stations provide an accurate frequency reference but only a coarse time reference. The term fine assistance refers to a case where a microsecond level time reference is additionally available. This is typical of CDMA networks that have synchronized base stations.

Two factors contribute to the accuracy of frequency assistance: the accuracy of frequency reference and the accuracy of Doppler estimate. Cellular base station oscillators typically exhibit a frequency bias in the order of ± 0.05 ppm. Assuming that the user is walking at a speed of 5 km/h with respect to the base station, his movement contributes a Doppler error of ± 0.005 ppm. Adding a receiver tracking error of ± 0.075 ppm gives a total worst case error of 0.13 ppm which corresponds to approximately ± 200 Hz at satellite signal frequencies. The Doppler estimate is based on an initial terminal position estimate, satellite ephemeris information and reference time. The initial position estimate is usually the known location of the nearest cellular base station and it is typically accurate to within a couple of kilometers. The time is usually available at an accuracy of 2-3 s in

networks with coarse assistance. With this information the Doppler shift can be estimated to within a few Hz so that the inaccuracy of the frequency assistance is clearly dominated by the error of the frequency reference. We therefore use ± 200 Hz as the frequency uncertainty range for both coarse and fine assistance.

The accuracy of reference time in the case of fine assistance depends on the accuracy of base station clock, on the accuracy of estimating propagation delay, and on the accuracy of signal tracking in the terminal. We use the WCDMA standard test requirement of ± 32 us.

To obtain the values for $E/(2\sigma^2)$, the threshold q was first chosen so that the system false alarm probability as evaluated numerically from (4) and (6) was one percent. The threshold and the required parameters from Table 2 were then substituted into (9) which was solved numerically for E. The numerical calculations were performed using Matlab standard functions with the exception that the Bessel function, which obtains very large values, was approximated in logarithmic form using a power series from [8]. The results for single bin detection were obtained accordingly by setting $n = 1$.

The single bin $E/(2\sigma^2)$ values in Figure 1 depend solely on the number of coherent integrations given in Table 2 and reflect the conventional wisdom that sensitivity in power terms is proportional to the square root of the number of coherent integrations when observation time is given. The unassisted values exceed the single bin values by 2−6 dB, the difference being the wider the larger the search space is.

The most inefficient signaling scheme would seem to be that of the Galileo E6 data channel, its high data rate obviously taking a toll by enforcing a short coherent integration time. The other new data signals are not very efficient, either, and would seem be inferior to GPS C/A when no assistance is available. The unassisted pilot signals provide a couple of decibels more sensitivity than GPS C/A. The pilot signals in general offer a higher sensitivity than their corresponding data signals, the difference being 2–7 dB when no assistance is present and 3–8 dB when fine assistance is available.

Coarse assistance provides 0.5 dB and fine assistance 1–2 dB of sensitivity improvement as compared to unassisted acquisition, the improvement being the higher the larger the original search space is.

It can be seen from Figure 2 that the GPS L5 and Galileo E6 pilot signals in combination with fine assistance provide the highest attenuation margins of all signals, over 4 dB higher than the unassisted GPS L1 C/A signal.

As can be seen from Table 2, the unassisted pilot signals have extremely large search spaces. Assistance would therefore seem to be a precondition for their use in weak signal acquisition at least in the foreseeable future. It may thus be argued that assistance here serves both as an enabler for using the pilot signals and as a means of improving sensitivity. This line of argument would attribute a sensitivity improvement as high as 9 dB to the assistance, 7 dB due to the difference between data and pilot signals and 2 dB due to the improvement resulting from search space reduction.

Table 2. Parameters used in numerical evaluations.

Signal	Nominal power [dBm]	Coherent integrations	No assistance Δ f = ±5 kHz Δ t = ∞		Coarse assistance Δ f = ±200 Hz Δ t = ∞		Fine assistance Δ f = ±200 Hz Δ t = ±32 us	
			Delay bins	Frequency bins	Delay bins	Frequency bins	Delay bins	Frequency bins
GPS L1 C/A	-128.50	50	1 023	300	1023	12	65	12
GPS L1C data	-133.00	100	20 460	150	20460	6	65	6
GPS L1C pilot	-128.25	1	36 828 000	15 000	36828000	600	65	600
GPS L2C data	-133.00	50	20 460	300	20460	12	33	12
GPS L2C pilot	-133.00	1	1 534 500	15 000	1534500	600	33	600
GPS L5 data	-127.90	100	102 300	150	102300	6	655	6
GPS L5 pilot	-127.90	1	204 600	15 000	204600	600	655	600
Galileo E1 data	-130.00	250	8 184	60	8184	2	65	2
Galileo E1 pilot	-130.00	1	204 600	15 000	204600	600	65	600
Galileo E5A data	-128.69	50	204 600	300	204600	12	655	12
Galileo E5A pilot	-128.69	1	1 023 000	15 000	1023000	600	655	600
Galileo E5B data	-128.69	250	40 920	60	40920	2	655	2
Galileo E5B pilot	-128.69	1	1 023 000	15 000	1023000	600	655	600
Galileo E6 data	-128.00	1000	5 115	15	5115	1	327	1
Galileo E6 pilot	-128.00	1	511 500	15 000	511500	600	327	600
Glonass L1 C/A	-134.00	100	511	150	511	6	33	6

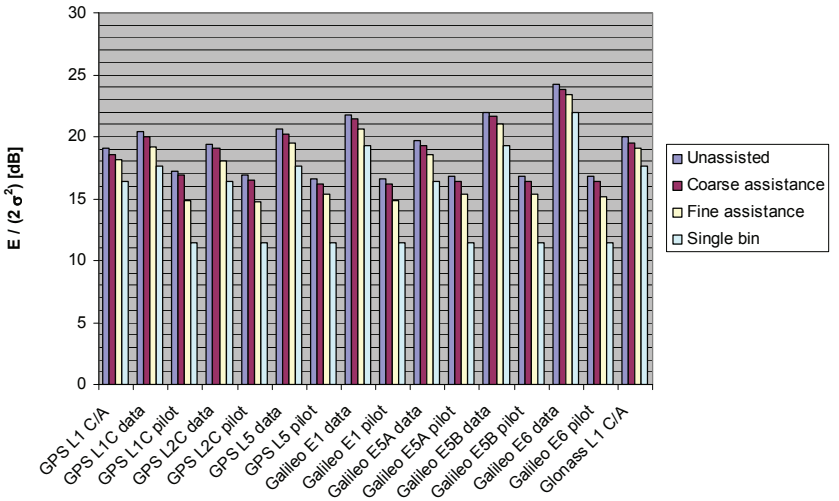

Figure 1. Noise normalized signal energy. $P_D = 0.99$ and $P^a_{FA} = 0.01$.

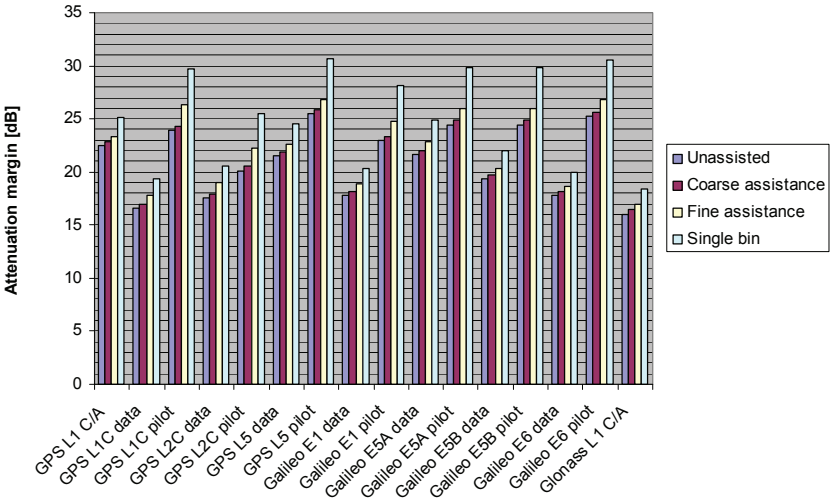

Figure 2. Attenuation margin. $P_D = 0.99$ and $P^a_{FA} = 0.01$.

CONCLUSIONS

The importance of GNSS acquisition sensitivity for location based services was discussed and the status of the related mobile telephone standards briefly explained. Parallel receiver architectures and terrestrial GNSS assistance from mobile telephone networks were mentioned as important means of sensitivity improvement.

Theoretical acquisition sensitivities of present and future freely accessible GNSS signals from the GPS, Galileo and Glonass constellations were evaluated using an analytical model from earlier work. The analysis was performed for unassisted receivers and for receivers with two types of assistance, coarse and fine. The main input parameters were signal power, coherent integration time, and search space dimension. The required C/N_0 at baseband input and the allowable signal path attenuation were reported as results.

The results indicate that terrestrial assistance improves the acquisition sensitivity of both pilot and data signals by decreasing false alarm rate through search space reduction. Since the pilot signals yield very large search spaces, the reduction of search space dimension is also likely to be a precondition for their use in acquisition. The results would further indicate that the pilot signals of the new GNSS services can provide significantly higher acquisition sensitivity than the corresponding data signals. Assistance could therefore serve an important role as an enabler for future receiver sensitivity improvements.

REFERENCES

[1] J. Syrjärinne, L.Wirola: Setting a new standard – assisting GNSS receivers that use wireless networks. InsideGNSS, vol. 1, number 7, October 2006.

[2] Turunen S: Network assistance – what will new GNSS signals bring to it? InsideGNSS, Volume 2, Number 3, Spring 2007, pp. 35-41.

[3] IS-GPS-800, Navstar GPS Space Segment / User Segment L1C Interfaces, GPS Navstar JPO, 19. April 2006.

[4] IS-GPS-200C-005R1, Navstar GPS Space Segment / Navigation User Interfaces, GPS Navstar JPO, 14 January 2003.

[5] IS-GPS-705, Navstar GPS Space Segment / User Segment L5 Interfaces, GPS Navstar JPO, 5. January 2005.

[6] GAL OS SIS ICD/D.0, Galileo Open Service Signal In Space Control Document, Draft 0, ESA/GJU, 2006.

[7] GLONASS interface control document (version 5.0), Coordination Scientific Information Center, Moscow 2002.

[8] M. Abramowitz and I. A. Stegun (ed.), Handbook of mathematical functions, Dover Publications, 1970.

[9] D. Borio, L.Camoriano and L. Lo Presti, "Impact of the acquisition searching strategy on the detection and false alarm probabilities in a CDMA receiver", IEEE/ION PLANS 2006, April 25-27, 2006, San Diego, California.

[10] E.D. Kaplan (ed.), Understanding GPS principles and applications, Artech House Publishers, 1996.

PUBLICATION 6

S. Turunen, “Acquisition sensitivity limits of new civil GNSS signals,” *Coordinates*, vol. 3, no. 1, pp. 14–19, Jan. 2007.

Coordinates
A monthly magazine on positioning, navigation and beyond

E-Zine
Previous Issues
Articles-by-Author

Acquisition sensitivity limits of new civil GNSS signals

SEPPO TURUNEN
JAN 2007 | COMMENTS OFF

The importance of sensitivity for consumer GNSS receivers is discussed in view of location based services and emergency call positioning

Location based services (LBS) are a rapidly growing field of wireless data services that can be accessed through a mobile phone equipped with a GNSS receiver. Some of the services are intended for outdoor use while others are suited for use in urban and indoor areas. It is therefore likely that subscribers will expect these services to be available throughout the coverage area of the mobile telephone network. Regulators, who are mainly interested in the positioning of emergency calls, have likewise established requirements for mobile phones that have a builtin GNSS receiver. According to the requirements, the GNSS receiver must successfully acquire and track satellite signals under measurement scenarios that simulate heavy signal attenuation. Since the processing load for signal acquisition has a strong inverse dependency on signal power, acquisition is rapidly becoming the most demanding task computationally of modern consumer GNSS receivers.

The challenge of signal acquisition does not depend only on the received signal power but also on the availability of reference time, reference frequency, satellite ephemeris information, and an initial location estimate. When available, they allow the receiver to calculate estimates for Doppler shifts and, if sufficiently accurate, for code phases. The estimates allow the receiver to reduce search ambiguity and the time and effort needed for acquisition. The reference time and reference frequency could, in principle, be obtained from a good crystal oscillator. However, the crystal oscillator of a consumer grade receiver is often prone to temperature drift and other instabilities. GNSS receivers that are integrated into a mobile phone have a high-quality frequency reference available from the cellular network. If the so-called assisted GNSS (A-GNSS) functionality is enabled, the receiver can also obtain time, location and satellite ephemeris information from the network. The required transactions are specified in all mobile telephone standards but the functionality has not, unfortunately, been implemented in all networks. The accuracy and content of the information is also dependent on the network.

Trends in receiver architecture

To successfully search and detect a GNSS satellite signal in an area of heavy fading it is often necessary to use an integration time of one second or more. This is true in particular when oscillator instability, signal modulation or receiver movement limits coherent integration time. Under such circumstances, a serial search would proceed extremely slowly except when accurate prior information about the code phases and Doppler frequencies is available. Modern consumer GNSS receivers are therefore more and more often equipped with a means of efficient parallel acquisition. A typical acquisition processor consists of a bank of time-domain matched filters for code phase searching and a digital Fourier transformer for frequency searching.

A recent trend is to use softwarebased acquisition and to perform the matched filtering in the frequency domain, which is computationally efficient. This kind of software acquisition is typically carried out off-line and the required transforms between the time and frequency domain are performed with FFT.

The processing of a delay-frequency bin for satellite acquisition is conceptually shown in Fig. 1. A stream of complex-valued baseband samples from the receiver RF section is multiplied with a locally generated replica signal to eliminate – or wipe off – the Doppler frequency and ranging code, leaving a complexvalued DC signal. The DC signal is then integrated coherently, squared, and added to a memory location dedicated to the specific combination of Doppler frequency and code delay. This sequence of

Interview

"We have just scratched the surface of what photogrammetry will do for all of us in the future" Alexander Wiechert, CEO, Vexcel Imaging

Advertisment

My News

"Bhuvan is a visualisation tool for showcasing India's imaging capabilities and societal applications using remote sensing." says Dr V Jayaraman, Director, National Remote Sensing Centre, Indian Space Research Organisation, in an exclusive interview with Coordinates magazine on 'Bhuvan'

Easy Subscribe

Just Drop your Email Here

Go

Login

Username:

Password:

Remember me

Login »

Register
Lost your password?

Previous Issues

Volume V Issues 11, Nov.2009
Volume V, Issue 10, Oct 2009
Volume V, Issue 9, September 2009
Volume V, Issue 8, August 2009

Links

Ads by Google
Galileo Position
GSM Tracking
GNSS
Galileo Home
GPS Chip

Partnership

Asia Oceania Region Workshop on GNSS
25-26 January 2010
Bangkok, Thailand
ws@multignss.asia

GEOFORM+'2010
March 30 – April 02
Moscow, Russia
dnj@mvk.ru

operations, which constitutes one non-coherent processing step, is performed for each delayfrequency bin in parallel and repeated one or several times. Finally, a decision strategy is applied to the contents of the memory and a conclusion made about the existence of a satellite signal in one of the bins. If there is a known data modulation on the signal, it can also be wiped off. The wipe-off operations are linear so that their order of execution can be freely changed without effecting the end result, which is useful when optimising the HW implementation. Practical considerations, such as the availability of special signal processing elements, have resulted in widely different implementation architectures.

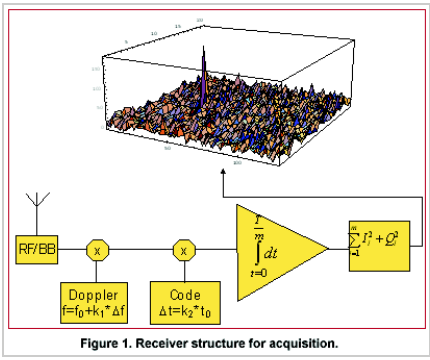

Figure 1. Receiver structure for acquisition.

Numerous studies have been published about sequential acquisition strategies where the same hardware is allocated on different search bins at different times. An element frequently present in sequential strategies is multiple dwelling, where some bins are processed repeatedly to verify the acquisition results. Sequential strategies implicitly assume that acquisition performance is limited by the processing capacity. However, the rapid evolution of digital hardware is making the assumption less relevant. In fact, commercial receivers already contain real-time acquisition processors that can handle tens of thousands of delay-frequency bins in parallel, and SW receivers operating off-line with sample streams stored in memory do not even have strict hardware limitations. It is therefore interesting to know how acquisition performance is bounded when processing restrictions are removed and only physical limitations apply. It turns out that acquisition sensitivity then becomes heavily dependent on the length of the ranging code and on the availability of assistance information, a fact that has not been fully appreciated in the GNSS literature.

New civil GNSS signals and their acquisition strategies

The short C/A code was dedicated for acquisition and the longer P(Y) code for tracking in the original GPS specification. There is no similar division in the newer L1C [IS-GPS- 800], L2C [Fontana] and L5 [ISGPS- 705] civil signal specifications or in the Galileo OS [GJU] signal specification. Instead, all component signals have fairly long ranging codes and some of them also have high bit rates. These characteristics are likely to make acquisition difficult due to the resulting expansion of the search space and reduction of bit energy. The new specifications also include pilot signals that take up a significant fraction of the transmitted power. While it is thinkable that the unmodulated pilots are useful for tracking, it is questionable whether they can be used in acquisition due to their extremely long cycle lengths.

Table 1. shows the code lengths and other parameters of some present and future civil GNSS signals. The shortest ranging code belongs to the GPS L1 C/A signal and the longest to the GPS L2C pilot signal, the difference being approximately three orders of magnitude. Both codes are shift-register generated sequences that do not have a discernible substructure. As another example, the proposed Galileo L1 OS pilot signal has a concatenated ranging code consisting of a primary code with 4092 elements and a secondary code with 25 elements. Its cycle length is the product of the lengths of the component codes, i.e. 102300 elements.

The size of the acquisition search space is the product of four factors: the code length of the ranging code, the number of frequency search bands, the time domain over-sampling ratio, and the frequency domain over-sampling ratio. The number of frequency search bands is proportional to the coherent integration time since the latter is inversely related to the receiver bandwidth. In order to avoid code self-noise, the coherent integration time should normally be an integer multiple of code cycles. In the case of the GPS L2C pilot signal, this means that the shortest possible coherent integration time is 1.5 seconds. The coherent integration time for the GPS C/A signal is limited by data modulation to about 20 ms. It follows that the number of frequency search bands needed for the GPS L2C pilot signal is about 100 times larger than that needed for the GPS C/A signal, and further, that the size of the search space for the GPS L2C pilot signal exceeds that for the GPS L1 C/A signal by five orders of magnitude.

Table 1. Present and future GNSS signals.

	DATA CHANNEL			PILOT CHANNEL	
	Code length [elements]	Symbol length [ms]	Chip rate [10^6/s]	Code length [elements]	Chip rate [10^6/s]
GPS L1 C/A	1023	20	—	—	—
Galileo L1	4092	4	1.023	25*4092	1.023
GPS L2C	10230	20	0.5115	767250	0.5115
Galileo E5B	4*10230	4	10.23	100*10230	10.23
GPS L5	10*10230	10	10.23	20*10230	10.23
Galileo E5A	20*10230	20	10.23	100*10230	10.23

~~~~~~~~~~~~~~~

Theoretical and practical limitations

A useful insight into parallel acquisition can be gained by examining the statistics of noise bins in the search space. It is well known that the squaring and subsequent summing of m independent complex zero-mean Gaussian variables results in a central chi-square distributed variable with 2m degrees of freedom [Proakis]. This is exactly the process that produces the noise bin values when there are m coherent integrations and when the input is thermal noise. Assuming a constant total reception time and an input power that corresponds to a noise variance equal to s2 at both integrator outputs when m is one, the cdf of a noise bin for an arbitrary m is

$$F(x) = \left(\frac{1}{2\sigma^2}\right)^m \frac{1}{\Gamma(m)} \int_0^{mx} t^{m-1} \exp\left(-\frac{t}{2\sigma^2}\right) dt \qquad (1)$$

The related mean value of the distribution is $2\sigma^2$ and the standard deviation is $2\sigma^2/\sqrt{m}$ Since signal detection is critically based on the highest noise bin, the relevant probability distribution is not that of an individual noise bin but that of the maximum of all noise bins in the search space. The cdf of the latter distribution can be written by raising the cdf of the former distribution to the power of n, n being the total number of noise bins:

$$\Pr(x_i \le x, i = 1 \Lambda\ n) = F^n(x). \qquad (2)$$

Extreme value theory (EVT), a branch of mathematics developed by Fisher, Tippett, Gumbel and others during the 20th century, proves that the limiting distribution Fn of the maximum of n i.i.d. random variables, when n tends to infinity, has one of three possible functional forms depending on the tail of the parent distribution. For the chi-square distribution and other distributions with an exponentially decreasing tail, the limiting distribution has the double exponential form

$$\lim_{n\to\infty} F^n(x) = F_n(x) = \exp\left(\exp\left(\alpha_n (x - u_n)\right)\right) \quad , \qquad (3)$$

where the coefficients u_n and α_n are defined by the equations

$$F(u_n) = 1 - \frac{1}{n} \qquad (4)$$

and

$$\alpha_n = nF'(u_n) \qquad (5)$$

The approximation

$$u_n \approx \frac{2\sigma^2}{m}\left(\ln\left(\frac{n}{\Gamma(m)}\right) + (m-1)\ln\ln\left(\frac{n}{\Gamma(m)}\right)\right) \qquad (6)$$

for the chi-square distribution can be obtained from an expression given by Gumbel [Gumbel] for the gamma distribution. Numerical evaluation shows that the approximation is fairly accurate for values of m up to five or six. Substituting (6) and (1) into (5) gives
~~~~~~~~~~~~~~~

$$\alpha_n \approx \frac{m}{2\sigma^2}\left(1+(m-1)\frac{\ln\ln\left(\frac{n}{\Gamma(m)}\right)}{\ln\left(\frac{n}{\Gamma(m)}\right)}\right)^{m-1} \quad . \qquad (7)$$

The double exponential distribution (3) has the mean value

$$\bar{x}_n = u_n + \frac{\gamma}{\alpha_n} \qquad (8)$$

and the standard deviation

$$\sigma(x_n) = \frac{\pi}{\sqrt{6}} \cdot \frac{1}{\alpha_n} \qquad (9)$$

where $\gamma = 0.5772\ldots$ is the Euler constant. Substituting (7) into (8) and (9) gives for the mean

$$\bar{x}_n \approx \frac{2\sigma^2}{m}\left[\ln\left(\frac{n}{\Gamma(m)}\right)+(m-1)\ln\ln\left(\frac{n}{\Gamma(m)}\right)+\gamma\right] \Bigg/ \left(1+(m-1)\frac{\ln\ln\left(\frac{n}{\Gamma(m)}\right)}{\ln\left(\frac{n}{\Gamma(m)}\right)}\right)^{m-1} \qquad (10)$$

and for the standard deviation

$$\sigma(x_n) \approx \pi\sqrt{\frac{2}{3}\frac{\sigma^2}{m}} \Bigg/ \left(1+(m-1)\frac{\ln\ln\left(\frac{n}{\Gamma(m)}\right)}{\ln\left(\frac{n}{\Gamma(m)}\right)}\right)^{m-1} \quad . \qquad (11)$$

When only one coherent integration is involved, (10) and (11) simplify to

$$\bar{x}_n \approx 2\sigma^2(\ln(n)+\gamma) \qquad (12)$$

and

$$\sigma(x_n) \approx \pi\sqrt{\frac{2}{3}}\sigma^2 \, . \qquad (13)$$

It can be seen from (10), (11), (12) and (13) that the mean of the maximum of the chi-square distributed noise bins has a logarithmic or slightly stronger than logarithmic dependency on the size of the search space, while the standard deviation of the maximum is nearly constant. In other words, the graph of the probability density function of the noise maximum maintains its width but is shifted horizontally when n changes. This means that signal detection thresholds also have to be shifted in order for error probabilities to remain constant. The consequence of this is that the receiver acquisition sensitivity is lower when the size of the signal search space is larger, the required signal power being approximately proportional to the logarithm of the size of the space.

In an earlier contribution [Turunen] the author derived an expression for the false acquisition probability in a scenario where a satellite signal is known to be present and the receiver

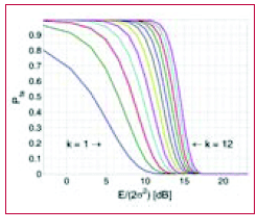

Figure 2. P_{fa} as a function of $E/(2\sigma^2)$ for $m = 1$ and $n = 10^k$.

simply chooses the highest peak in the search space. With the noise power assumption made above and with a signal power such that the squarer output is equal to E when m is one, the false acquisition probability for an arbitrary m was found to be

$$P_{fa} = 1 - \int_0^{\infty} [F(x)]^n g(x)\, dx, \qquad (14)$$

where

$$g(x) = \frac{m}{2\sigma^2}\left(\frac{mx}{E}\right)^{\frac{m-1}{2}} e^{-\frac{E+mx}{2\sigma^2}} I_{m-1}\left(\frac{\sqrt{mxE}}{\sigma^2}\right) \qquad (15)$$

is the pdf of the non-central chi-square distribution obeyed by the signal bin. The last term in (15) is the modified Bessel function of the first kind of order *m*-1. Substituting (1) and (15) into (14) and making the substitution $u = mx/\sigma^2$ leads to

$$P_{fa} = 1 - \frac{1}{2}\int_0^{\infty}\left(\frac{u}{E/\sigma^2}\right)^{\frac{m-1}{2}} e^{-\frac{E/\sigma^2+u}{2}} I_{m-1}\left(\sqrt{\frac{uE}{\sigma^2}}\right) P\left(m, \frac{u}{2}\right)^n du, \qquad (16)$$

where

$$P(a, x) = \frac{1}{\Gamma(a)}\int_0^x e^{-t} t^{a-1} dt \qquad (17)$$

is the incomplete gamma function.

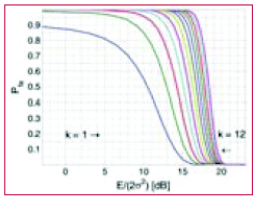

Figure 3. P_{fa} as a function of $E/(2\sigma^2)$ for m = 50 and $n = 10^k$.

~~~~~~~~~~~~~~~

Numerical examples

Fig. 2 shows the probability of false acquisition from (16) as a function of E/(2s2) for several values of n when m = 1. Due to the identity

E/(2s2) = PT/(FN0), (18)

where P is the signal power at baseband input, T is the total reception time and F is the noise figure, E/(2s2>) can be interpreted as the ratio of signal power to noise spectral density at the receiver base-band input when T is one second. Fig. 3 is otherwise similar except that m = 50. It can be seen from the figures that when either m or n varies within the chosen limits, the sensitivity changes by approximately five decibels.

The width of a frequency search band is approximately two thirds of the inverse of the coherent integration time [Kaplan], such that the number of frequency bands is

$$N_f = 1.5 \times BT/m, \qquad (19)$$

where B is the total frequency search range. The size of the search space, which includes the n noise bins and the one signal bin, is the product of Nf and the length of the ranging code when no oversampling is assumed. Due to (19), n and m are therefore inversely related. Fig. 4 shows the Pfa plots for seven pairs of m and n that exhibit this relationship. It is assumed that T is one second, B is 12 kHz and the code length is 1,023 elements. The figure shows that the net effect of increasing the number of coherent integrations is a reduction in sensitivity.
~~~~~~~~~~~~~~~

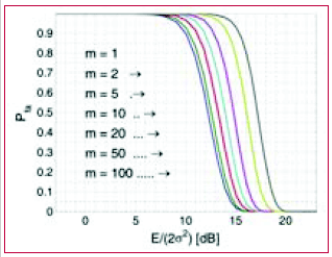

Figure 4. P_{fa} as a function of $E/(2\sigma^2)$ when n = 1.5 x 1023 x 12,000/m-1.

Fig. 5 illustrates the effect of frequency uncertainty on the false acquisition rate when (19) applies. There are two groups of curves, one for m = 1 and another for m = 50, and seven frequency search ranges from 100 Hz to 15000 Hz. The code space uncertainty is 1,023 and T is one second. It may be observed that the sensitivity impact of changing the number of coherent integrations is about 4 dB and that of varying the frequency search range about 2 dB.

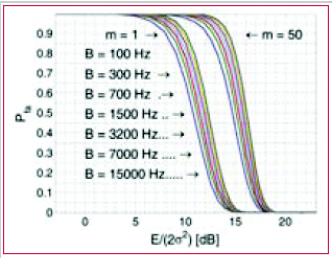

Figure 5. P_{fa} as a function of $E/(2\sigma^2)$ for m = 1 and m = 50 when n = 1.5 x 1023 x B/m.

Fig. 6 shows how sensitivity depends on the code length Nc in an example where the coherent integration length is equal to Nc code elements and the total reception time is a fixed number of code elements, 106 in this case. Taking (19) into account it follows that n = 1.5 BTNc2/106. It is further assumed that there is no oversampling, B is 12 kHz and T is one second. The figure shows that sensitivity becomes higher when the code length is increased. This happens regardless of a simultaneous expansion in the search space.

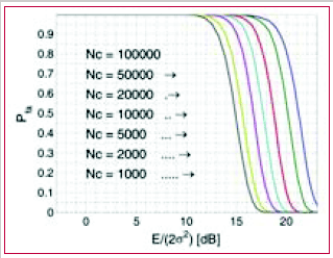

Figure 6. P_{fa} as a function of $E/(2\sigma^2)$ for $m = 10^6/N_c$, n =1.5 $BTN_c^2/10^6$, B=12 kHz and T=1.

Finally, Fig. 7 shows six Pfa plots that are motivated by six existing or proposed GNSS signals. The signals with some of their parameters are listed in Table 2. The number of delay search phases is based on the assumption of taking one sample per code element. For the GPS L2C pilot signal, the correct figure is twice the number of code elements since the signal is timemultiplexed with a data signal. For the Galileo L1 pilot signal, the number of delay search phases is the product of the lengths of a BOC (biphase) code, a primary ranging code, and a secondary ranging code. For all signals, the frequency uncertainty bandwidth B is assumed to be 12 kHz. The reception time T is chosen to be 1.5 seconds

according to the coherence time of the GPS L2C signal which is the longest in the table. The number of coherent integrations was obtained from assuming that the coherent integration time is equal to the coherence time of the signal. The number of frequency search bands is calculated from (19).

Based on the plotted results, the attenuation margin corresponding to a Pfa of 10% and a noise figure of 4 dB is shown in the rightmost column of the table. The margin was calculated by subtracting the required power obtained by solving P from (18) from the nominal signal power. Shown in the table is also the post-detection S/ N ratio, defined here as the difference of the mean value of the signal bin, 2s2+E/m, and the mean value of a noise bin, 2s2, divided by the latter.

Table 2. The GNSS parameters for Fig. 7.

	Delay search phases	Coherence length [chips]	Chip rate [1/s]	Nominal power [dBm]	Coherent integrations	Frequency search bands	Size of search space	E/2σ2 [dB] Pfa=0.1	Post-detection S/N [dB] Pfa=0.1	Attenuation margin [dB] Pfa=0.1
GPS L2C pilot	2*767250	767250	5.12E+05	-133.0	1.00	27000	4.14E+10	15.4	15.4	23.4
Galileo L1 pilot	2*25*4092	102300	1.02E+06	-130.0	15.00	1800	3.68E+08	16.9	5.1	24.9
Galileo E5A pilot	100*10230	1023000	1.02E+07	-128.0	15.00	1800	1.84E+09	17.1	5.3	26.7
GPs L1 C/A	1023	20460	1.02E+06	-127.7	75.00	360	3.68E+05	18.2	-0.6	25.9
GPS L5 pilot	20*10230	204600	1.02E+07	-127.9	75.00	360	7.37E+07	19.0	0.2	24.9
Galileo L1 data	2*4092	4092	1.02E+06	-130.0	375.00	72	5.89E+05	21.2	-4.5	20.6

As seen from Table 2, the required value of E/(2s2) is higher when the number of coherent integrations is larger. This is obviously due to the fact that the length of the coherent integration period is inversely proportional to the number of integrations, which leads to a lower post-detection S/N ratio when the number is larger. The fact that the reduction in the post-detection S/N ratio is not refl ected as a higher false acquisition rate would suggest that the simultaneous reduction in the size of the search space has a compensating effect. It should be kept in mind, however, that the post-detection S/N ratios do not fully characterize the signal distributions in the search space.

Conclusion

The importance of sensitivity for consumer GNSS receivers was discussed in view of location based services and emergency call positioning. The dependence of acquisition sensitivity on the size of signal search space was discussed in the context of an ideal parallel acquisition receiver. The discussion was motivated by the fact that parallel acquisition is gaining popularity in commercial receivers due to growing performance requirements and due to improvements in signal processing electronics. To characterize noise distributions in very large search spaces, results from extreme value statistics (EVT) were used to show, among other things, that the mean of the noise maximum is approximately proportional to the logarithm of the size of the search space. An analytic expression from an earlier publication was used to plot false acquisition probabilities for acquisition scenarios with different numbers of coherent integration steps and frequency search bands. The expression was also applied to analyse the acquisition properties of the chosen GPS and Galileo signals. The results indicate that the best achievable acquisition sensitivity depends not only on signal power and coherence time but also to a signifi cant extent on the size of the search space.

References

IS-GPS-800, Navstar GPS Space Segment / User Segment L1C Interfaces, GPS Navstar JPO, 19. April 2006.

. R.D. Fontana, W. Cheung, P.M. Novak, and T.A. Stansell, Jr., "The new L2 civil signal," ION GPS 2001, pp. 617-631, 11-14 September 2001.

. IS-GPS-705, Navstar GPS Space Segment / User Segment L5 Interfaces, GPS Navstar JPO, 5. January 2005.

. L1 band part of Galileo Signal in Space ICD, http://www. galileoju.com, Galileo Joint Undertaking (GJU), 2005.

. J.G. Proakis, Digital Communications. McGraw-Hill, 1995.

. E.J. Gumbel: Statistics of extremes.375pp. Dover publications, 2004.

• S. Turunen, "Combinatorial loss in satellite acquisition," ION GNSS 2005, Long Beach, CA, USA, 13–16 September 2005.

• E.D. Kaplan (ed.), Understanding GPS principles and applications, Artech House Publishers, 1996.

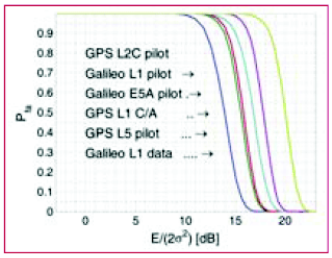

Figure 7. P_{fa} as a function of $E/(2\sigma^2)$ for the examples in Table 2.

Seppo Turunen is a Principal Technologist at Nokia Technology Platforms. He received a M.Sc. in Electrical Engineering from Tampere University of Technology in 1979. From 1979 to 1988 he was involved in the research and development of industrial process control systems at Valmet Process Automation, Finland. He joined Nokia in 1988 and has since held several positions at Nokia Research Center, Nokia Mobile Phones and Nokia Technology Platforms. His current interests include mobile phone positioning techniques using assisted GNSS, cellular network measurements and motion sensors.

Columns

My coordinates	EDITORIAL
News	INDUSTRY | LBS | GPS | GIS | GALILEO UPDATE
Mark your calendar	May 09 TO DECEMBER 2009

«Previous 1 2 3View All| Next»

Pages: 1 2 3

higest rated

- Sustainable Land Governance - 1 votes
- Making of Bandra-Worli Sea Link - 1 votes
- Application of RTK system in railway construction - 1 votes
- Vol 1, Issue 1, Jun05 - 0 votes
- "An extraordinary event in an extraordinary country" - 0 votes

most commented

- Making of Bandra-Worli Sea Link
- GPS equipment accuracy testing

most viewed

- GPS equipment accuracy testing - 316 views
- Practical multivariate statistical multipath detection methods - 314 views
- Sustainable Land Governance - 215 views
- INDUSTRY - 211 views
- The Tellurometer - 184 views

› Coordinates, 2009

PUBLICATION 7

Q. Zhengdi and S. Turunen, “Nearly orthogonal codes in GNSS using unequal code lenghts,” in *Proc. ION 60th Annual Meeting (ION AM 2004)*, Dayton, OH, USA, June 7–9 2004, pp. 666–670.

Nearly Orthogonal Codes in GNSS Using Unequal Code Lengths

Qin Zhengdi, Seppo Turunen, *The Nokia Corporation, Tampere, Finland*

BIOGRAPHY

Qin Zhengdi is a senior research specialist with the Nokia Corporation, Technology Platforms. He graduated from the Department of Physics, Hunan Normal University, China in 1981. He received his M.Sc. in Applied Physics from the Chinese Academy of Science in 1985 and a Ph.D. in Biomedical Engineering from Zhejiang University, China in 1988. He has been with Nokia Corporation since 1993. His current interests include CDMA technology, mobile signal processing and positioning and navigation technologies.

Seppo Turunen is a senior research manager with the Nokia Corporation, Technology Platforms. He received his M.Sc. from the department of Electrical Engineering, Tampere University of Technology, Finland in 1979. He joined the Nokia Corporation in 1988 and has held several managerial positions in research and product development. His current interests include mobile phone positioning techniques based on satellite and network measurements.

ABSTRACT

Signal acquisition in a GNSS receiver is typically based on channel estimation done by correlating the received CDMA signal with a code replica. In order to achieve good sensitivity, the process is usually repeated several times and the results combined. A large number of repeated correlations is needed, especially for weak signal acquisition. The dynamic range for channel separation is, however, limited since co-channel interference cannot be attenuated by means of repeated correlations in a traditional CDMA system that uses short codes of equal length. This results from the fact that the cross-correlation pattern is stationary with respect to the correlation cycles.

A coding method is given that provides an essential reduction of cross-correlation by allocating slightly different code lengths to different channels. The cross-correlation can drop to zero if the code lengths and the integration time in the receiver are carefully chosen and if data modulation is absent, as is the case with the pilot signals now being planned for both GPS and Galileo. Under these assumptions it looks as if the coded channels were orthogonal to each other. Theoretical analysis and simulations show that a group of short codes with unequal lengths can provide better cross-correlation distances than a group of longer codes with equal code length if the distances are calculated over several consecutive cycles of the short codes.

INTRODUCTION

The basic principle of UCL-CDMA (Unequal Code Length CDMA) was first introduced at the GNSS 2004 conference [1]. In this paper, the correlation properties of the method are discussed and some guidance is given for selecting code families for good performance.

In a traditional CDMA system with a single code length, the cross-correlation pattern remains stationary in relation to the channel delay profile from one code cycle to another. This may lead to an interference-limited situation where it is difficult to suppress co-channel interference by continued integration. For example, in the GPS C/A signalling where all satellites share the code length of 1023, the average cross-correlation distance between two channels is –23.9 dB [2]. While the resulting co-channel interference is low enough for open-air reception, it is not sufficient for all indoor or shadowing environments where satellite signals are asymmetrically attenuated.

The normal way to reduce cross-correlation in a CDMA system and hence to improve channel separation is to use longer codes. The price to be paid for this is an increase in receiver complexity, which can be exponential to the code length if signal acquisition is done by parallel search. A related disadvantage is the longer time for signal acquisition. For practical reasons, it may also be difficult to fully utilize the cross-correlation properties of the longer codes because the receiver may not be able to process full code cycles and because the partial correlation properties of algebraic codes are often poor.

The idea behind UCL-CDMA is to use different code lengths for different channels. The difference can be one or several chips, or a fraction of a chip. The purpose is to make the cross-correlation patterns non-stationary with respect to the channel delay profile so that they are

eliminated by averaging when the results of repeated correlations are combined.

We show theoretically and by simulations that if the code lengths are slightly different from channel to channel and if the acquisition process is extended over several consecutive code cycles, it is possible to obtain significantly lower co-channel interference values than by using fixed length codes of comparable length.

SIGNAL MODEL

We denote the unmodulated baseband signal of channel *n* by

$$s_n(t) = \sum_{i=0}^{L_n-1} c_i^n f_n(t - iT_c) \qquad (1)$$

where T_c is the chip length, c_i^n is a sequence of chips belonging to the alphabet {-1,1}, L_n is the length of the sequence c_i^n and f_n is a baseband pulse waveform. The received signal can then be expressed as

$$g_n(t) = \exp(j\omega_n t) \sum_{k=-\infty}^{\infty} s_n(t - kL_nT_c), \qquad (2)$$

where ω_n is the Doppler shift specific to the channel *n*. It is assumed that the effects of code Doppler can be neglected. It is additionally assumed that the pulse waveforms fulfil the following orthonormality requirement:

$$\int_{-\infty}^{\infty} f(t + mT_c) f^*(t + nT_c)dt = \delta(n - m) \qquad . \qquad (3)$$

We define continuous time autocorrelation and cross-correlation functions as

$$R_n(t) = \lim_{T\to\infty} \frac{1}{T} \int_{-T/2}^{T/2} g_n(u) g_n^*(u + t)du \qquad (4)$$

$$R_{m,n}(t) = \lim_{T\to\infty} \frac{1}{T} \int_{-T/2}^{T/2} g_m(u) g_n^*(u + t)du \qquad (5)$$

In the absence of a Doppler shift, the orthonormality of the pulse waveforms and the cyclic nature of the signals allow us to express (4) and (5) at discrete time events in terms of the circular correlations of the codes:

$$\theta_n(l) = \sum_{i=0}^{L_n-1} c_i^n c_{(l+i) \bmod L_n}^{n*}, \qquad (6)$$

$$\theta_{n,m}(l) = \sum_{i=0}^{L_{nm}-1} c_{i \bmod L_m}^m c_{(i+l) \bmod L_n}^{n*} \qquad (7)$$

where L_{nm} is the period of concern. For simplicity, the normalization factor is omitted.

We use the term balanced to indicate that the sum of code elements is zero or, when the code length is odd, it differs from zero by one, i.e.:

$$\sum_{i=0}^{L_n-1} c_i^n = \begin{cases} 0 & (L_n \text{ is even}) \\ \pm 1 & (L_n \text{ is odd}) \end{cases} \qquad (8)$$

CROSS-CORRELATION BETWEEN TWO CHANNELS

The frame length of a pair of channels is defined as

$$L_{frame} = \Psi\{L_m, L_n\} \qquad , \qquad (9)$$

where L_m and L_n are the code lengths in chip units and Ψ denotes the least common multiple. If L_m and L_n are relatively prime to each other, the minimum frame size is $L_m \times L_n$. If Doppler effects can be ignored and chip synchronism between channels is assumed, the two channels have a joint period of length L_{frame}.

If one chip is divided into several samples, the code length difference can be adjusted to a fraction of a chip. L_{frame} can then be counted in samples and the same discussion applies. For example, if we have a sample rate of four samples per chip, the minimum code length difference can be a quarter of a chip. For simplicity, we only discuss integer chip counts in this paper.

We first assume that L_n and L_m are relatively prime to each other. The periodic cross-correlation function can then be expressed as

$$\theta_{n,m}(l) = \sum_{i=0}^{L_nL_m-1} c_{i \bmod L_m}^m c_{(i+l) \bmod L_n}^{n*} \qquad (10)$$

According to the Chinese remainder theorem [3] there exists for each $i \in \{0, L_nL_m - 1\}$ a unique pair of integers $j \in \{0, L_n - 1\}$ and $k \in \{0, L_m - 1\}$ such that $i = j + \xi L_n = k + \zeta L_m$ for some integer ξ and ζ. It follows that $\theta_{n,m}$ can be written as:

$$\theta_{n,m}(l) = \sum_{j=0}^{L_n-1}\sum_{k=0}^{L_m-1} c^m_{(j+\xi L_m) \bmod L_m}\, c^{n*}_{(k+l+\xi L_n) \bmod L_n} = \sum_{j=0}^{L_m-1}\sum_{k=0}^{L_n-1} c^m_{j \bmod L_m}\, c^{n*}_{(k+l) \bmod L_n} \tag{11}$$

Making use of the cyclic and balanced nature of both sequences we have:

$$\theta_{n,m}(l) = \sum_{j=0}^{L_m-1} c^m_j \sum_{k=0}^{L_n-1} c^{n*}_k = \begin{cases} 0 & \text{if one of the code lengths is even} \\ \pm 1 & \text{if both of the code lengths are odd} \end{cases} \tag{12}$$

This means that there is almost no interference between the two channels if the time period under consideration has a duration of one frame. It appears as if the two code sequences were orthogonal to each other. The same is true for any multiple of the frame length.

So far, we have discussed binary sequences that are balanced but otherwise arbitrarily chosen. This means that the orthogonality of the sequences is independent of the content of the codes and of the timing relationship between the codes.

If the code lengths are not pairwise relatively prime, the conclusion above does not hold. Nevertheless, there are several code cycles in a frame for each of the binary sequences and the cross-correlation pattern changes from cycle to cycle due to the code length differences. The changes in the pattern appear as if the cross-correlation peaks were sliding with respect to the primary correlation pattern. It is thus conceivable that when the results of consecutive code cycles are added together, the highest peaks are suppressed more strongly than in a case where the patterns are stationary or random. It can be expected that the full advantage be achieved when the integration time is a full frame cycle or a multiple thereof.

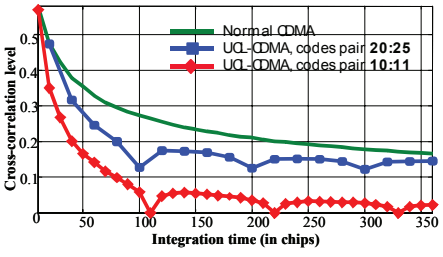

Figure 1: Simulation results.

Figure 1 shows some simulation results. First, we consider a pair of code sequences with lengths of 10 and 11. The lengths are relatively prime and the frame length is thus 110. We can see from the simulation result (red line) that the cross-correlation becomes zero when the integration time approaches a multiple of the frame length. Secondly, we consider a pair of code sequences with lengths of 20 and 25. The lengths are not relatively prime and the frame length is 100. Also, in this case, we see from the simulation result (blue line) that the cross-correlation falls steeply and reaches a minimum when the integration time approaches a multiple of the frame length. In both cases, the cross-correlation level is below that of a CDMA sequence with a code that extends over the total integration time (green line).

DOPPLER SHIFT

The Doppler-shifted case can be analyzed by observing how the frequency components in the Fourier series of the cross-correlating signals overlap.

We denote two pilot signals by $g_m(t)$ and $g_n(t\text{-}t_0)$, where t_0 is an arbitrary delay, and their code lengths by L_m and L_n. We assume that the code lengths are relatively prime numbers and, to simplify expressions, we additionally assume that they are odd numbers. The complex Fourier series representations of the signals, assuming Doppler frequencies f_m and f_n, can be written as

$$g_m(t) = \exp(j2\pi f_m t) \sum_{k=-\infty}^{\infty} d^m_k \exp\left(j2\pi \frac{kt}{L_m T_c}\right) \tag{13}$$

and

$$g_n(t) = \exp(j2\pi f_n t) \sum_{l=-\infty}^{\infty} d^n_l \exp\left(j2\pi \frac{l(t-t_0)}{L_n T_c}\right), \tag{14}$$

where the coefficients are given by

$$d^m_k = \frac{F\left(j2\pi \frac{k}{L_m T_c}\right)}{L_m T_c} \sum_{l=0}^{L_m-1} c^m_l \exp\left(-j2\pi \frac{kl}{L_m}\right) \tag{15}$$

for $g_m(t)$ and similarly for $g_n(t)$.

$F(j\omega)$ denotes the Fourier transform of the chip waveform $f(t)$:

$$F(j\omega) = \int_{-\infty}^{\infty} f(t)\exp(-j\omega t)dt\,. \tag{16}$$

Since the main focus of this work is on codes and not on pulse shaping, it is assumed that the pulse waveform has a flat frequency spectrum with a sharp cut-off at $f = 1/2T_c$:

$$F(j\omega) = \begin{cases} T_c, & |\omega| \le \dfrac{\pi}{T_c} \\ 0, & |\omega| > \dfrac{\pi}{T_c} \end{cases} \tag{17}$$

The spectrum amplitude chosen according to (17) normalizes the pilot signal power to unity. While (17) corresponds to a smooth function in the time domain, it should be possible to make a similar calculation for any of the rectangular waveforms proposed for satellite navigation and to take bandwidth limitations into account by constraining $F(j\omega)$ appropriately. It may be noticed that the time domain waveform corresponding to (17) fulfils the orthonormality requirement (3).

Substituting (13) and (14) into (5), it can be observed that only product terms with identical frequency components in (13) and (14) contribute to the cross-correlation function. But there is at most one such product term, which can be established as follows. Equating the frequency of an arbitrary term in (13) with that of an arbitrary term in (15) results in

$$\frac{k}{L_m T_c} + f_m = \frac{l}{L_n T_c} + f_n, \tag{18}$$

where $|k| \le \dfrac{L_m - 1}{2}$ and $|l| \le \dfrac{L_n - 1}{2}$ due to (17).

Substituting

$$r = k + \frac{L_m - 1}{2} \text{ and } s = -l + \frac{L_n - 1}{2} \tag{19}$$

yields

$$L_n r + L_m s = L_m L_n [1 + T_c(f_n - f_m)] - (L_m + L_n)/2 \tag{20}$$

where $0 \le r < L_m$ and $0 \le s < L_n$.

Equation (20) can have at most one solution (r, s), for if (t, u) were another solution, we would have

$$L_m(s-u) = L_n(t-r), \tag{21}$$

which is impossible since L_m and L_n do not have common factors and since $|t-r| < L_m$ and $|s-u| < L_n$.

Denoting the largest Fourier coefficient of $g_m(t)$ with d_k^m and the largest Fourier coefficient of $g_n(t)$ with d_l^n, the worst-case cross-correlation magnitude of the two signals can now be expressed using (5) as

$$\left|R_{m,n}(t)\right| \le \left|d_k^m d_l^{n*} \exp(j2\pi(f_m - f_n))\right| = \left|d_k^m d_l^n\right|. \tag{22}$$

This is also the amplitude ratio of the maximum cross-correlation component to the signal component in a perfect tracking situation where the desired and disturbing signals have equal power. This follows from the fact that both signals are normalized so that $R_m(0) = R_n(0) = 1$. A lower limit for the magnitude of $R_{m,n}(t)$ is obtained when the spectrums of both signals are flat:

$$\left|R_{m,n}(t)\right| \ge \frac{1}{\sqrt{L_m L_n}} \quad . \tag{23}$$

Assuming that $L_m = 1024$ and $L_n = 1027$, two values close to the GPS C/A epoch length, (23) gives a cross-correlation distance of 60.2 dB. For a set of 40 computer-generated sequences with lengths in the range of 1024–1229, the authors obtained a worst-case cross-correlation distance of 47.7 dB. The figure may be contrasted with the worst-case cross-correlation distance of the GPS C/A codes, which is 21.6 dB [2].

COMPARISON WITH GPS C/A CODE

A simulation was performed to verify the theory with a two-satellite system. The GPS C/A code was used as a reference. The GPS C/A codes are Gold codes with a length of 1023 for all satellites and the chip duration is about 1 μs [2]. For simplicity, we assume that the input signals to the receiver from the satellites have equal signal power. We consider two different situations; one with zero Doppler difference and another with a Doppler difference of 1 kHz.

We configure a UCL-CDMA system with a basic code length of 102 that is about one tenth of the C/A code length. The chip rate is identical to the C/A code. The code sequences are random selected balanced binary codes. One satellite uses the code length of 102, while another 101. The integration for the signal acquisition is done over several consecutive code-cycle intervals.

Table 1: Two satellites with equal power.

System	Integration time	Co-channel interference	
		$\Delta f = 0$	$\Delta f = 1$ kHz
GPS C/A	**≥ 1 ms**	**-23.9 dB**	**-21.2 dB**
UCL-CDMA random selected binary codes (101: 102)	**1 ms**	**-24.2 dB**	**-24.0 dB**
	2 ms	**-28.0 dB**	**-28.1 dB**
	5 ms	**-35.9 dB**	**-33.7 dB**
	10 ms	**-51.4 dB**	**-37.6 dB**

The simulation results are shown in the table above. As can be expected, the co-channel interference of the GPSC/A code remains constant after 1 ms. For UCL-CDMA, it drops rapidly when the integration time increases especially when the integration time approaches the frame length. In this example, the frame length is about 10 ms.

Improvement is also achieved when the Doppler frequency is present. It is remarkable that the better performance is achieved with significantly shorter codes and potentially simpler receiver structure.

CONCLUSION

An Unequal Code Length CDMA (UCL-CDMA) coding technique was proposed for GNSS pilot channels. The idea behind the technique is to use slightly different code lengths in all channels. Analytic expressions for worst-case cross-correlation were derived for the cases of zero and non-zero Doppler difference. Simulation results agree with the theory.

The advantage of the method is the possibility to significantly reduce co-channel interference without using longer codes. The relative advantage is preserved also in the case of a Doppler shift, which is important for the GNSS application.

More work is needed to incorporate the different waveforms proposed for GNSS signals into the analysis and to design codes for data channels. The impact of different code lengths on data frame structure should also be investigated.

REFERENCES

[1] Q. Zhengdi and S. Turunen, "Unequal code lengths in GNSS," Proc. GNSS 2004, Rotterdam, NL, May 2004.

[2] E. Kaplan, editor, "Understanding GPS – Principles and Applications," Artech House Publishers 1996.

[3] W.E. Deskins, "Abstract algebra," Dover publications, 1995.

PUBLICATION 8

S. Turunen and Q. Zhengdi, "Shift register generated pilot codes with good cross-correlation properties," in *Proc. 2004 International Symposium on GNSS/GPS*, Sydney, Australia, Dec. 6–8 2004, Article ID 22, 8 p.

Presented at GNSS 2004
The 2004 International Symposium on GNSS/GPS

Sydney, Australia
6–8 December 2004

Shift register generated pilot codes with good cross-correlation properties

S. Turunen
Nokia Corporation, P.O. Box 68, FIN-33721 Tampere, Finland
Tel: +358 7180 08000, Fax: +358 7180 46953, Email: seppo.turunen@nokia.com

Q. Zhengdi
Nokia Corporation, P.O. Box 68, FIN-33721 Tampere, Finland
Tel: +358 7180 08000, Fax: +358 7180 46953, Email: zhengdi.qin@nokia.com

Seppo Turunen

ABSTRACT

Unmodulated pilot signals are being proposed for future Galileo and GPS services. With proper design, the signals will allow receivers to acquire and track satellite transmissions in areas of heavy signal attenuation. One of the challenges of pilot signal design is to control cross-correlation that can lead to false acquisition especially if weak and strong satellite signals are concurrent. The usual approach to reducing cross-correlation is to use longer codes but this has the disadvantage of significantly increasing the demand for processing resources and memory space in the receiver.

It was shown in an earlier paper that low cross-correlation can be achieved with a set of short codes if all of them are of slightly different length. The concept, Unequal Code Length Code Division Multiple Access (UCL-CDMA), was verified with computer-generated random codes. In this paper a method of generating such codes using truncated shift-register sequences is presented. A set of 40 codes with lengths in the range of 1024-1229 is designed and shown to have a cross-correlation distance of 47 dB at worst-case Doppler difference, which exceeds the 21 dB reported for the GPS C/A codes and the 45 dB reported for the much longer GPS L2C pilot codes.

KEYWORDS: Pilot code, cross-correlation, code design, code generation, Galileo

1. INTRODUCTION

The planned GPS L2C and L5 services and the Galileo L1 and E5 open services will provide unmodulated pilot signals to allow receivers to perform coherent integration across data bit boundaries. The main advantages in comparison with the GPS C/A service will be a better

tracking stability and a potentially higher acquisition sensitivity. The GPS L2C pilot code has 767,250 elements that are time multiplexed with data on a chip by chip basis (Fontana *et al.,* 2001). The Galileo L1 signal specification has not been finalized but a 204,600 long code has been proposed consisting of a primary code of 8184 elements and a secondary code of 25 elements (Mattos 2004).

Some of the properties of good pilot codes are low cross-correlation, robustness to narrow-band interference, simple generation, and ease of acquisition. Depending on the transmission chain the codes may have to be balanced. It is also desirable that the pilot signals support bit synchronization by having a predictable timing relationship with data bit transitions.

New applications such as indoor positioning of mobile phones require reliable acquisition of signals that are 20 dB or more below their nominal level, which leads to a longer integration time and an increased computational load in receivers. In order to keep the load within reasonable limits it is desirable to limit the size of signal search space by using relatively short codes. Short codes also have inherently better acquisition characteristics than long codes since their probability of false acquisition is lower.

The GPS C/A codes have a cross-correlation distance of 21.1 dB at worst-case Doppler difference (Ward 1996). While the distance is sufficient in nominal conditions, it is not long enough to protect high sensitivity receivers from false acquisition in a situation where both weak and strong satellite signals are present. To provide enough margin against noise fluctuations for receivers operating under such conditions a cross-correlation distance of 40 dB or more would be desirable. Fontana *et al.* (2001) report a cross-correlation distance of 45 dB for the GPS L2C pilot codes but do not clearly state their assumptions about Doppler difference.

The usual way to reduce cross-correlation is to use longer codes. Unfortunately, this approach is not very effective (Zhengdi and Turunen 2004a) and can lead to a code length increase of several orders of magnitude. The planned GPS L2C and Galileo pilot codes are examples of code design where acquisition requirements have been compromised in favour of cross-correlation performance. The longer codes in combination with a 20 dB sensitivity improvement could increase receiver complexity by five orders of magnitude (Mattos 2004).

Civil receivers are not normally subjected to high levels of narrow-band interference since it is not allowed to operate other radio transmitters in GNSS bands. It is therefore not always clear how much in-band interference a GNSS system should tolerate. If the interference is a problem, longer codes could be used since the power of their spectral components is lower and the distortion caused by the interferer therefore likely to be less severe. However, this approach is only useful as long as the separation of the spectral components is wider than the bandwidths of the interfering signal and the receiver tracking loops. A disadvantage of longer codes is that the probability of spectral overlap with a narrow-band interferer is higher due to narrower separation of spectral components.

A technique for avoiding long pilot codes, Unequal Code Length Code Division Multiple Access (UCL-CDMA), was recently proposed by Zhengdi and Turunen (2004a). It was shown that good cross-correlation performance can be achieved with codes only a few hundred elements long if their lengths differ from each other. To maximally suppress cross-correlation, the code lengths should be pairwise relatively prime numbers. The good cross-correlation performance is preserved at all Doppler differences, which is in sharp contrast

with single-length codes such as the Gold codes of the GPS C/A signal. Particularly low cross-correlation can be achieved at zero Doppler difference if balanced codes are used.

A theoretical lower limit for UCL-CDMA cross-correlation was derived by Zhengdi and Turunen (2004b), but no practical method was suggested for code design. It was shown, however, that optimal codes have their signal power evenly distributed among spectral components. It is proposed in this contribution to use a long linear shift register sequence as a starting point for code set design and to do a computer search to identify those partial sequences that best satisfy the requirement for spectral power distribution.

The rest of this paper is organized as follows. In section 2 a signal model is presented. In section 3 cross-correlation results concerning UCL-CDMA are reviewed. In section 4, the code set design method is introduced, and in section 5, a design example is given for a set of 40 codes. In section 6, a conceptual proposal is made for data channel coding. Section 7 concludes the paper.

2. SIGNAL MODEL

Denote one code epoch of pilot signal *n* by

$$s_n(t) = \sum_{i=0}^{L_n-1} c_i^n f_n(t - iT_c) \quad , \tag{1}$$

where T_c is chip length, c_i^n is a sequence of code elements belonging to the alphabet {-1,1}, L_n is the length of the sequence c_i^n and f_n is a baseband pulse waveform. It is assumed that the code lengths L_n are relatively prime odd numbers. The full pilot signal at the receiver can be expressed as

$$g_n(t) = \exp(j2\pi f_n t) \sum_{k=-\infty}^{\infty} s_n(t - t_n - kL_nT_c) \quad , \tag{2}$$

where f_n is a Doppler shift and t_n is a channel-specific time delay. It is assumed that the effects of code Doppler can be ignored and that the pulse waveforms fulfil the orthonormality requirement

$$\int_{-\infty}^{\infty} f(t + mT_c) f^*(t + nT_c) dt = \delta(n - m) T_c \quad . \tag{3}$$

The complex Fourier series representation of the signal can be written as

$$g_n(t) = \exp(j2\pi f_n t) \sum_{k=-\infty}^{\infty} d_k^n \exp\left(j2\pi \frac{k(t - t_n)}{L_n T_c} \right) \tag{4}$$

with coefficients given by

$$d_k^n = \frac{F\left(j2\pi \frac{k}{L_n T_c} \right)}{L_n T_c} \sum_{l=0}^{L_n-1} c_l^n \exp\left(-j2\pi \frac{kl}{L_n} \right) \quad . \tag{5}$$

$F(j\omega)$ denotes the Fourier transform of the chip waveform $f(t)$:

$$F(j\omega) = \int_{-\infty}^{\infty} f(t) \exp(-j\omega t) dt \quad . \tag{6}$$

It is finally assumed that the chip waveform has a flat frequency spectrum with a sharp cut-off at $f = 1/2T_c$:

$$F(j\omega) = \begin{cases} T_c, & |\omega| \le \frac{\pi}{T_c} \\ 0, & |\omega| > \frac{\pi}{T_c} \end{cases} \tag{7}$$

Assumption (7) leads to a particularly simple expression for cross-correlation. It also follows from (7) that the signal has unity power and that the time-domain pulse waveform $f(t)$ fulfils the orthonormality requirement (3).

The definition used for the continuous time cross-correlation function is

$$R_{m,n}(t) = \lim_{T \to \infty} \frac{1}{T} \int_{-T/2}^{T/2} g_m(u) g_n^*(u+t) du \quad . \tag{8}$$

3. CROSS-CORRELATION IN THE PRESENCE OF DOPPLER SHIFT

The cross-correlation between two UCL-CDMA coded pilot signals was analysed by Zhengdi and Turunen (2004b) in the case where the signals comply with the definitions of section 2 above. The analysis was based on the observation that two pilot signals have at most one pair of overlapping frequency components independent of Doppler difference. As a consequence, the maximum cross-correlation magnitude can be obtained as the absolute value of the product of the largest Fourier components of the signals:

$$\max \left| R_{m,n}(t) \right| = \max_{k,l} \left| d_k^m d_l^n \right| \quad . \tag{9}$$

In a tracking situation, (9) can be interpreted as the amplitude ratio of cross-correlation components and signal components after code wipe-off in a situation where the powers of the desired and disturbing satellite signals are equal. A lower limit is obtained by assuming that both signals have a flat spectrum:

$$\left| R_{m,n}(t) \right| \ge \frac{1}{\sqrt{L_m L_n}} \quad . \tag{10}$$

4. PROPOSED CODES

In order to minimize cross-correlation the following strategy is proposed for designing a set of N pilot codes. First, N pairwise relatively prime numbers, n_i, i=1…n, are chosen. The numbers should represent a feasible range of code lengths satisfying, e.g., some specific requirements for spectral smoothness. Secondly, a maximum length linear shift register sequence of sizeable length is generated. Finally, a set of N shorter sequences of length n_i is formed by splitting the shift register sequence into non-overlapping parts that are chosen so as to minimize the spectral maximum of the whole set. It may further be required that the sequences are balanced. At present, the only suitable minimization procedure known to the authors is an exhaustive computer search.

According to equation (9), the worst-case cross-correlation reaches its minimum when the product of the two strongest frequency components is minimized. Although the proposed strategy does not directly minimize the product, it can be expected to give good results when the shift register sequence is long so that the individual codes can be chosen from a large number of alternatives. The fact that the spectral maximum of the resulting set of codes is minimized has the additional advantage of providing protection against narrow band interference.

5. DESIGN EXAMPLE

A set of 40 balanced codes was generated using the code generator of Figure 1. The generator is based on the primitive polynomial $x^{24}+x^7+x^2+x^1+x^0$ (Peterson and Weldon 1972) and has a cycle length of 2^{24}-1. It was required that the codes be longer than the GPS C/A codes to have at least the same level of spectral smoothness. It was further required that the shortest and longest code length should differ as little as possible. A computer search for pairwise prime numbers resulted in 40 integers ranging from 1024 to 1229. The integers and their prime factors are shown in the second and third columns of Table 1.

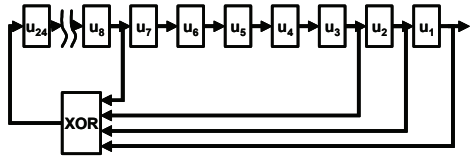

Figure 1. Code generator

Using the 40 integers as code lengths, a code search was performed with a Matlab® program written to minimize the spectral criterion of section 4 above. It was required that the codes be balanced. The procedure was to cyclically decrement a temporary upper limit for spectral component power and to use a sequential search to check during each cycle if 40 codes that do not exceed the limit can be found. To simplify the procedure, the search was only done in ascending order of code length. The fourth column of Table 1 shows the starting point indexes of the codes obtained in relation to the full code generator sequence. The generator was

initialized to all 1s and index 1 was assigned to the value of register u1 in the initial state of the generator. The power of the strongest spectral component as obtained from (5) and (7) and the mean power of all spectral components are shown for each code in the fifth and sixth columns of the table.

The average distribution of the circular autocorrelation function values of the codes is given in Table 2. For comparison, the distribution is also given for the GPS SV1 C/A code.

CODE NUMBER	LENGTH	FACTORS	STARTING POINT	SPECTRAL MAX. [dB]	SPECTRAL AVE. [dB]
1	1024	2^10	676167	-24.02	-30.10
2	1027	13*79	1033171	-23.88	-30.12
3	1031	1031	1291816	-23.85	-30.13
4	1033	1033	1588787	-23.87	-30.14
5	1039	1039	3058396	-24.06	-30.17
6	1041	3*347	4344606	-23.87	-30.17
7	1043	7*149	4394065	-23.88	-30.18
8	1049	1049	4811410	-23.85	-30.21
9	1051	1051	4850102	-23.94	-30.22
10	1055	5*211	5065441	-23.98	-30.23
11	1061	1061	5373691	-23.85	-30.26
12	1063	1063	5476947	-23.97	-30.27
13	1067	11*97	5645593	-23.87	-30.28
14	1069	1069	5645594	-24.05	-30.29
15	1081	23*47	5862857	-23.94	-30.34
16	1087	1087	6276054	-23.94	-30.36
17	1091	1091	6414333	-23.86	-30.38
18	1093	1093	6460906	-24.08	-30.39
19	1097	1097	6483964	-23.93	-30.40
20	1103	1103	6484020	-23.87	-30.43
21	1109	1109	6542651	-23.95	-30.45
22	1117	1117	6564729	-23.95	-30.48
23	1121	19*59	6566385	-24.05	-30.50
24	1123	1123	6775507	-23.85	-30.50
25	1129	1129	6775612	-23.89	-30.53
26	1139	17*67	6839363	-23.94	-30.57
27	1147	31*37	6882127	-23.95	-30.60
28	1151	1151	6890902	-23.92	-30.61
29	1153	1153	6996831	-23.96	-30.62
30	1163	1163	7009574	-23.89	-30.66
31	1171	1171	7075322	-23.87	-30.69
32	1181	1181	7075418	-24.08	-30.72
33	1187	1187	7075432	-23.96	-30.74
34	1189	29*41	7075453	-23.87	-30.75
35	1193	1193	7075454	-24.24	-30.77
36	1201	1201	7087988	-24.00	-30.80
37	1213	1213	7097313	-23.86	-30.84
38	1217	1217	7102659	-23.88	-30.85
39	1223	1223	7102770	-24.09	-30.87
40	1229	1229	7121862	-24.07	-30.90
GPS C/A	1023	3*11*31		-20.6	-30.10

Table 1. Code parameters

	0-19	20-39	40-59	60-79	80-99	100-119	>119
Example	544	354	160	47	7	1	1
GPS C/A	764	0	0	258	0	0	1

Table 2. Distribution of autocorrelation values

According to (9), the worst-case cross-correlation magnitude of a set of codes is the product of the two strongest frequency components belonging to two different codes. In Table 1, the value of the strongest component is -23.85 dB and it is present in four codes (codes 3, 8, 11 and 24). The worst-case cross-correlation distance of the code set is therefore 47.7 dB, a value more than twice as high as that of the GPS C/A codes and higher than that of the GPS L2C pilot codes. A theoretical lower limit according to (10) is 60.2 dB, as can easily be checked by adding the two largest values of the rightmost column of Table 1.

6. PROPOSAL FOR DATA CHANNEL CODING

One of the proposed data symbol rates of Galileo is 250 bits/s. It can be approximately achieved by using the pilot codes of the example above and by using data codes that are four times as long as the corresponding pilot codes. One data code epoch would then correspond to one bit period. The resulting synchronism between the pilot and data codes would allow bit boundaries to be detected with a maximum of four trials after pilot signal acquisition. It is likely that cross-correlation between the data signal and any of the remote satellite signals would remain low due to differences in code length, although a more thorough analysis would be needed to account for bit modulation effects. Choosing a data code with a sufficient cross-correlation distance from the local pilot code would not seem a difficult problem since the distance requirement is not particularly high and since the data code is fairly long.

7. CONCLUSION

A method for planning and generating sets of GNSS pilot signal codes based on Unequal Code Length CDMA (UCL-CDMA) was presented. The method is based on splitting a maximal length shift register sequence into parts that minimize a spectral norm. The minimization is performed by an exhaustive computer search. The coding of related data signals was also briefly discussed.

A set of 40 codes with lengths in the range of 1024-1229 was designed and shown to achieve a cross-correlation distance of 47.7 dB at worst-case Doppler difference, a value more than twice as high as that of the GPS C/A codes and higher than that of the GPS L2C pilot codes.

More research is needed to understand the effect of different pulse waveforms and data modulation on UCL-CDMA signals. The system level impact of unequal code lengths on data frame structure also requires investigation.

REFERENCES

Fontana RD, Cheung W, Novak PM, and Stansell TA (2001) ***The New L2 Civil Signal,*** Proceedings of the 14th Int. Tech. Meeting of the Satellite Division of the U.S. Inst. of Navigation, Salt Lake City, Utah, 11-14 Sept., 617-631

Mattos P (2004) ***Acquiring sensitivity,*** GPS World, 5(15):28-33

Peterson WW, and Weldon EJ (1972) ***Error-correcting codes,***The MIT Press, Cambridge, Massachusetts, U.S.A.

Ward P (1996) ***GPS satellite signal characteristics, in: Kaplan E*** (ed), Understanding GPS – Principles and Applications, Artech House Publishers, Norwood, MA, U.S.A. 83-117

Zhengdi Q, and Turunen S (2004a) ***Unequal code lengths in GNSS***, Proceedings of European Navigation Conference GNSS 2004, Rotterdam, NL, 17-19 May

Zhengdi Q, and Turunen S (2004b) ***Nearly orthogonal codes for GNSS by using unequal code lengths***, Proceedings of the ION 60th annual meeting, Dayton, Ohio, 7-9 June

PUBLICATION 9

S. Turunen, “A robust time labeling mechanism for GNSS data frames,” in *Proc. European Navigation Conference GNSS 2005*, Munich, Germany, July 19–22 2005, Session: Software and Algorithms 1, 5 p.

A robust time-labeling mechanism for GNSS data frames

Seppo Turunen *Nokia Corporation, Tampere, Finland*

ABSTRACT

In this contribution a time-labeling mechanism is proposed that allows a high sensitivity receiver to extract absolute time directly from a GNSS satellite data signal that is not strong enough for bit detection. Carrier, bit, and word synchronisation are assumed to be available from a pilot signal or by some other independent means. The time is then determined using a correlation process from a bit pattern embedded in the data signal. The pattern is constructed so that it can be decoded rapidly when the satellite signal strength is nominal while more time is needed when the signal is weak.

The proposed mechanism makes receiver operation possible in a situation where satellite orbit parameters are provided by an external source but absolute time is not available with sufficient resolution to identify the individual words and frames in a satellite transmission. This is a frequent condition in assisted GPS operation when an asynchronous cellular network, such as a GSM or a WCDMA network, transmits satellite ephemeris information but does not provide accurate time.

KEYWORDS: Synchronisation, Timing, Signal design, Time of week, Galileo

INTRODUCTION

Weak signal operation is required of GNSS receivers designed for use in mobile telephony. All major cellular telephone standards specify reception of GPS signals that are attenuated by 15 decibels or more by buildings or other obstacles. From such heavily attenuated signals, it is possible to extract only code phase and Doppler frequency information while all other signal components lie below detection thresholds and are useless or even harmful to receiver operation.

A terrestrial data channel is needed in weak signal GNSS operation to provide orbit parameters and preferably also approximate initial position and satellite system time to the receiver. The concept is called Assisted GPS, or AGPS, and the terrestrial channel most often used is a cellular telephone network. The slowly changing orbit parameters can be easily transmitted in current cellular networks, using either network internal or end-user accessible transmission channels. However, the transmission of time is more problematic since many networks are neither internally synchronised nor tied to the GPS reference time.

If a GNSS system could transfer absolute time autonomously in both nominal and weak signal conditions, it would serve better the growing number of wireless terminals being operated in urban and indoor areas. The dependency of the GNSS receiver on a terrestrial signal channel would be reduced to infrequent orbit parameter updates at intervals of a few hours. In cases where weak signal operation is required only temporarily, the need for a terrestrial channel could be totally obviated.

The GPS C/A signal is not suited for the transfer of absolute time in a weak signal environment. The subframes are numbered with 17-bit time-of-week words that are transmitted as ordinary data at 6-s intervals. The information does not tolerate bit errors so that it can only be used if satellite signal strength exceeds the threshold of data bit detection. Even when the signal strength is adequate, the added latency from the 6-s transmission interval is problematic for applications such as emergency call positioning.

The planned GPS L2C and L5 services and the Galileo L1 and E5 open services provide data-free pilot signals that allow receivers to use narrow bandwidth carrier tracking loops capable of operating at low signal levels. The stable phase reference thus obtained can be used to enable coherent processing of the data modulated part of the satellite transmission. If a known bit sequence is present in the data modulation, the coherence can be used to reliably detect the timing of the sequence by correlating it with a local replica sequence and integrating the result until a signal-to-noise ratio sufficient for the detection is achieved.

In addition to providing a carrier phase reference, the new pilot signals provide code and data bit timing. If a very long code is used, a pilot signal can also provide word and frame synchronisation. As another alternative to word and frame synchronisation, one could use frame structures with delimiters that are uniquely distinguishable from data [1, 2]. Such structures in combination with the stable phase reference obtained from the pilot signal would allow the receiver to detect word and frame boundaries even when individual data bits are not detectable.

A number of so-called rapid acquisition sequences have been proposed for the synchronisation of noisy signals. Such sequences are typically based on component sequences that are much shorter than the full sequence. Titsworth [3] suggests combining pseudorandom sequences with relatively prime periods T_1, T_2, .. T_m using majority logic to obtain a composite sequence that has a period of lcm(T_1, T_2, … T_m). By correlating the composite sequence with the local replicas of the component sequences a receiver can determine the phases of the component sequences. The phase of the composite sequence is then obtained algebraically. Stiffler [4] proposes using the output bits of a binary ring counter instead of pseudorandom sequences. Bluestein [5] suggests using pseudorandom sequences but, unlike Titsworth, interleaving them rather than combining them.

In this study, the applicability of a Bluestein type of rapid acquisition sequence for GNSS time transfer is analysed. The idea here is to embed the sequence into the data words of the satellite signal as constant length bit fields. The data words are also assumed to be of constant length. The analysis follows the general pattern outlined by Bluestein but includes modifications to accommodate two differences in problem setting. The first difference is that Bluestein assumes a separate channel for time information while it is assumed here that the time information and payload data are transmitted in the same channel. The second difference is that in the Bluestein analysis the component pseudorandom sequences are detected one at a time while it is assumed here that they are detected simultaneously.

In the next section, an ad-hoc design example is given with an error analysis. The bit rate for the example is chosen with the Galileo L1 open service in mind. The analysis is then generalised and expressions are derived for the relationships between failure rate, system clock period, clock detection time, transmission power allocation, and sequence lengths. The relationships are illustrated with diagrams and the results are referred back to the ad-hoc example. Finally, a conclusion is given.

DESIGN EXAMPLE

Consider a pilot-assisted GNSS data channel with a bit rate of 250 bits/s and a data word length of 15 bits and assume that a Bluestein type of rapid acquisition sequence with three component sequences, $c_1(i)$, $c_2(i)$ and $c_3(i)$, is applied as shown in Figure 1. Let the sequence $c_1(i)$ be a pseudorandom sequence of cycle length 127, initialised to a known phase at the beginning of the clock cycle of the satellite system. Similarly, let $c_2(i)$ and $c_3(i)$ be pseudorandom sequences of cycle lengths 255 and 511. It may be observed that the fraction of transmission power allocated to the three sequences is 10% if power is equally divided between the pilot and data signals.

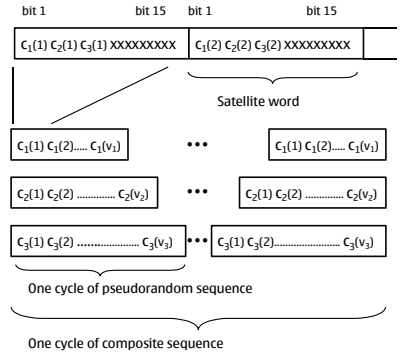

Figure 1. Design example.

The cycle lengths of the component sequences are relatively prime numbers so that the cycle length of the composite sequence [$c_1(i)$, $c_2(i)$, $c_3(i)$] is, according to the Chinese remainder theorem [6], the product of the lengths of the component sequences, or 16,548,735. The cycle time of the composite sequence when embedded in the data stream is 11.5 days.

If the satellite signal is strong enough for reliable detection of data bits, it is sufficient to collect nine consecutive data words to determine the phases of the sequences $c_1(i)$, $c_2(i)$ and $c_3(i)$. This follows from the fact that the phase of a pseudorandom sequence generated by an n-bit shift register is fully determined as soon as n consecutive bits are known. An n-bit shift register creates a sequence of 2^n-1 bits so that the largest value of n is nine, corresponding to the sequence $c_3(i)$. As a result, the phase of the composite sequence can be determined as soon as signal reception has continued for 0.54 s.

If the satellite signal is so weak that bits cannot be detected, several bit samples have to be collected to determine the phase of a component sequence reliably. In order to avoid self-noise effects when correlating the sequence with a local replica, it makes sense to always process an integer number of complete cycles of the sequence. It follows that the minimum reception time, determined by one complete cycle of the sequence $c_3(i)$, is 30.7 s. During this time, it is possible to collect two cycles of the sequence $c_2(i)$ and four cycles of the sequence $c_1(i)$ so that the signal reception time for all three sequences falls between 30.4 and 30.7 s.

The probability of false detection can be approximated with reasonable accuracy by summing the false detection probabilities of the component sequences $c_1(i)$, $c_2(i)$, $c_3(i)$, provided that the latter probabilities are low. Under the same assumption, it is further possible to apply the union-bound approximation [5] to the false detection probabilities of the component sequences, which involves summing the probabilities of all possible false outcomes. Due to the nearly perfect orthogonality of pseudorandom sequences, each false outcome is equally probable so that the sum can be obtained by multiplying the probability of a single false outcome by the total number of different false outcomes. This number is equal to the sequence length less one. By using the exact sequence length for simplicity of expression, the approximate probability of failure can be written as

$$P_e = \sum_{i=1}^{n} \frac{v_i}{\sqrt{2\pi}} \int_{\sqrt{\frac{E_b}{N_0} A_i v_i}}^{\infty} e^{x^2/2} dx \quad , \qquad (1)$$

where v_i is the length of sequence $c_i(j)$, A_i is the number of cycles of sequence $c_i(j)$ that are received, E_b is bit energy and N_0 is the double-sided thermal noise density.

Figure 2 shows the probability of failure P_e as a function of E_b/N_0. It may be noted that P_e is below 5% for an E_b/N_0 of -15.4 dB or higher, which corresponds to a signal level of 8.6 dB-Hz or higher. This performance is likely to be sufficient for any weak signal situation where signal tracking, in general, is possible.

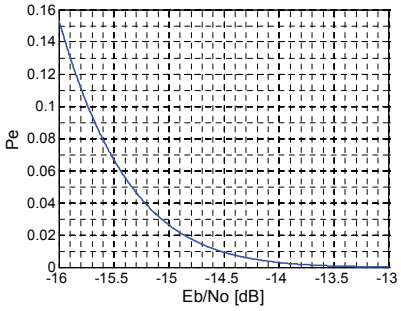

Figure 2. Probability of timing failure as a function of normalised bit energy.

THEORETICAL LIMITS

Let the length of the satellite system clock cycle be p bit periods and the maximum allowed clock detection time be q bit periods. To decide what the number n of component sequences c_i should be, what the lengths v_i of the sequences should be, and what fraction h of transmitted data bits should be allocated to time transfer to achieve a given probability of failure P_e, it is first assumed that v_i are not very different and can be approximated with a single variable v. Assuming further that the same number A of cycles of each component sequence is received, the error probability (1) can be written as

$$P_e = \frac{nv}{\sqrt{2\pi}} \int_{\sqrt{\frac{E_b}{N_0} Av}}^{\infty} e^{x^2/2} dx \quad . \qquad (2)$$

As was discussed in the design example above, the number of elements in the composite timing sequence is the product of the lengths v_j of the individual sequences $c_j(i)$. Each element is of the form $[c_1(i), c_2(i), \ldots, c_n(i)]$ and thus reserves n bits in each data word. Dividing n by h gives the data word length which, when multiplied by the length of the composite sequence, gives the length of the longest possible satellite system clock cycle in bits. Setting this equal to or greater than p results in

$$p \le \frac{n}{h} \prod_{j=1}^{n} v_j = \frac{nv^n}{h} . \qquad (3)$$

Assuming that the n synchronisation sequences are processed simultaneously, the number of words required for time detection is A times v. Since the maximum time allowed for the reception of the words is q bit periods,

$$q \geq \frac{Avn}{h} \quad . \tag{4}$$

Using (3) and (4) interpreted as equalities the probability of failure (2) can be expressed as

$$P_e = \left(\frac{ph}{n}\right)^{\frac{1}{n}} \frac{n}{\sqrt{2\pi}} \int_{\sqrt{\frac{E_b}{N_0}\frac{qh}{n}}}^{\infty} e^{x^2/2} dx \, . \tag{5}$$

This equation can be solved for h with n as a parameter when E_b, p, q and P_e are given. The value so obtained can then be substituted in (3) and (4) to obtain

$$v = \left(\frac{hp}{n}\right)^{\frac{1}{n}} \tag{6}$$

and

$$A = \left(\frac{h}{n}\right)^{1-\frac{1}{n}} qp^{-\frac{1}{n}} \, . \tag{7}$$

It can be seen from (5) that P_e is a growing function of n, suggesting that n should not be unnecessarily large. On the other hand, n is limited from below by (7) and by the requirement that A should have a positive integer value. Thus, for example, $n = 1$ is not acceptable since it would lead to $A = q/p << 1$.

If the satellite signal is strong enough for bit errors to be ignored, $\log_2(v)$ synchronisation bits are sufficient to detect all code phases. The total number of bits to receive in this case is

$$r = \frac{n}{h} \log_2 v \, . \tag{8}$$

NUMERICAL RESULTS

Figure 3 shows P_e as a function of h according to (5) for several values of n when $E_b/S_0 = -10$ dB, $p = 151{,}200{,}000$, and $q = 7{,}500$. At a data rate of 250 bits/s, these values correspond to a 7-day system clock period, a 30-s maximum clock detection time, and a signal level of 14 dB-Hz. Figures 4 and 5 show v and A as functions of h for several values of n as calculated from (6) and (7).

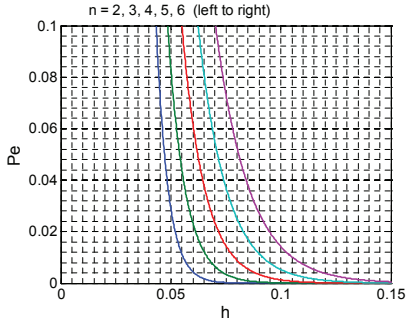

Figure 3. Probability of failure P_e as a function of h for $n = 2$ to 6, $E_b/S_0 = -10$ dB, $p = 151{,}200{,}000$, and $q = 7{,}500$.

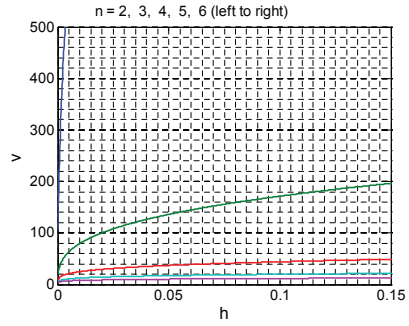

Figure 4. Sequence length v as a function of h for $n=2..6$, $E_b/S_0 = -10$ dB, $p = 151{,}200{,}000$, and $q = 7{,}500$.

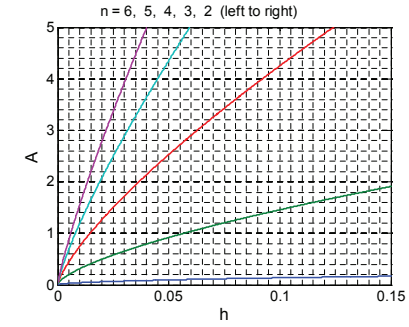

Figure 5. Sequence repetition count A as a function of h for $n=2..6$, $E_b/S_0 = -10$ dB, $p = 151{,}200{,}000$, and $q = 7{,}500$.

Figure 3 shows that it is possible to meet an error probability requirement of 5% by choosing $n = 3$ and $h = 0.054$, i.e. by using three component sequences and by reserving 5.4% of data bits for the sequences. According to Figures 4 and 5, the corresponding value for the average length of the component sequences is 140 and the number of complete cycles to be received is 1. According to (8) the strong signal clock detection time is 396 bits, or 1.58 s.

In the design example given earlier, the same detection time was achieved with a 5.4 dB lower E_b/S_0 ratio. This is obviously due to the fact that the signal power allocation was 5.6 dB higher. The sequence lengths in the example were of the same order of magnitude as obtained here, although an accurate comparison is not possible since the code lengths in the design example are widely spread and thus only very approximately represented by a single variable.

CONCLUSION

A time-transfer mechanism was proposed for GNSS data channels that makes it possible for a receiver to retrieve absolute time when the satellite signal is so heavily attenuated that data bits cannot be detected. The proposed mechanism is based on interleaving of a set of short pseudorandom sequences.

Analytic expressions were derived for relationships between probability of failure, E_b/N_0 ratio, satellite system clock cycle, lengths of the pseudorandom sequences, and the time needed to retrieve absolute time from a satellite signal. A numerical evaluation of the expressions for a 250 bits/s channel indicated that time transfer should be possible at a signal level of 14 dB-Hz if 5.4% of channel capacity is reserved for the proposed mechanism.

The proposed mechanism could be used to extend the coverage of pilot-assisted GNSS signals into indoor spaces and other areas where satellite signals are heavily attenuated. Continuous operation in such areas could be achieved by using a terrestrial radio channel, such as a mobile telephone network, to provide orbit parameter updates.

REFERENCES

[1] E.N. Gilbert, Synchronization of binary messages. IRE Transactions on Information Theory. September 1960, p. 470-477.

[2] A.J. van Wijngaarden, Partial-Prefix Synchronizable Codes. IEEE Transactions on Information Theory, vol. 47, No. 5, July 2001, pp. 1839-1848.

[3] R.C. Titsworth, Optimal Ranging Codes. IEEE Transactions on Space Electronics and Telemetry, vol. SET-10, March 1964, pp. 19-30.

[4] J.J. Stiffler, Rapid Acquisition Sequences. IEEE Transactions on Information Theory, vol. IT-14, March 1968, pp. 221-225.

[5] L.I. Bluestein, Interleaving of Pseudorandom Sequences for Synchronization. IEEE Transactions on Aerospace and Electronic Systems, vol. AES-4, July 1968, pp. 551-556.

[6] W.E. Deskins, Abstract Algebra. Dover Publications, N.Y., U.S.A., 1995, 624 p.

.

Corrections

- p. xvii, line 2: ”Ordered” should be ”Observed”
- p. 15, line 7: ”[79,99]” should be ”[80,99]”
- p. 30, line 9: ”ordered” should be ”observed”
- p. 54, line 9: ”Gold codes” should be ”m-sequences”
- p. 60, line 27: ”L5 signals [50]” should be ”L2 signals [65]”

This thesis was typeset in LaTeX 2_ε. The figures were prepared with Microsoft PowerPoint.